ADDITIVE MANUFACTURING (POTTING) OF FIBER-REINFORCED THERMOSET SANDWICH COMPOSITE STRUCTURES – FABRICATION, NUMERICAL SIMULATION, AND STRUCTURAL OPTIMIZATION

By

RIZWAN QUADRI SYED

A thesis submitted to the

School of Graduate Studies

Rutgers, The State University of New Jersey

In partial fulfillment of the requirements

For the degree of

Master of Science

Graduate Program in Mechanical and Aerospace Engineering

Written under the direction of

Professor Aaron D. Mazzeo

And approved by

_____

_____

_____

_____

New Brunswick, New Jersey

October 2020

ABSTRACT OF THE THESIS

ADDITIVE MANUFACTURING (POTTING) OF FIBER-REINFORCED THERMOSET SANDWICH COMPOSITE STRUCTURES – FABRICATION, NUMERICAL SIMULATION, AND STRUCTURAL OPTIMIZATION

by RIZWAN QUADRI SYED

Thesis Director:

Dr. Aaron D. Mazzeo

Sandwich composite structures are a distinct category of laminated composite materials with extensive applications in the aeronautical, civil, marine, and automotive industries. A sandwich structure constitutes a set of two stiff external face skins bonded to a thick central core of low density. Fiber-reinforced composites are the choice of materials for face skins while the core material comprises foam, honeycomb, or balsa wood. This thesis depicts an eccentric nozzle-based additive manufacturing (AM) technique based on potting to fabricate fiber-reinforced thermoset sandwich specimens. The conventional methods of manufacturing sandwich composites induce significant manual labour. These processes render high cost of fabrication, material waste, and restricted tailoring of designs. Recently, the infusion of additive manufacturing (AM) has garnered widespread attention for its potential to produce high-strength composites. This influx of AM can be attributed to its unprecedented attributes of tailorable design and flexible mechanical properties to produce functional components at a rapid pace and reduced cost. The objective of this thesis is to

utilize the potential of AM to produce fiber-reinforced thermoset sandwich structures for high-strength applications. The research task comprises a sequential approach of initially developing 3D models of two sandwich mold specimens for mechanical characterization (a dog-bone and a rectangular bar). In this work, we adopted a commercial slicer software to develop a unique G-code generating the toolpath for extruding carbon fiber and epoxy face skin materials from a dispensing medium into the cured mold. The original framework of the thesis was then to bond commercially available foam to the face skin. We presented a proposed plan of action for performing 3-pont bending tests and tensile tests of sandwich structures to evaluate load-displacement data, tensile strength, etc. As a means to efficiently transition from manufacturing experiments to numerical simulation, the next part of this thesis presents Finite Element Analysis (FEA) studies to conduct numerical simulation and design optimization of sandwich-shaped structures for the aerospace industry. We performed numerical simulation of a 3-point bending test on a sandwich composite beam in ANSYS to evaluate the load-deflection behavior. Next, we used the built-in optimization module in ANSYS to perform design optimization of three novel structural designs for potential applications in the aerospace industry. The results yielded significant mass savings for all three configurations. Finally, the thesis presents comparative single-objective weight and cost-optimization studies of sandwich composites, carbon-epoxy, and aluminum alloy beams using the interior-point algorithm in MATLAB. The study yielded optimum cost and weight values for these beams within specified constraints. Overall, this work aims to manifest the significance of nozzle-based AM and Finite Element Analysis (FEA) to fabricate and optimize sandwich composite structures for the aerospace industry. Principal benefits include reduced cost, faster production, and improved fuel efficiency.

ACKNOWLEDGEMENTS

With profound admiration, I would like to take this opportunity to express my deepest gratitude to my advisor Dr. Aaron Mazzeo for his invaluable support and enlightenment throughout my research project. As an incoming student with passable experimental expertise, he encouraged me immensely to persevere in my research experiments. His constant guidance has motivated me to develop my skills as an experimentalist and to learn diligently from the outcomes of my research activities. He was always open to listen to my research ideas, and his indispensable suggestions resulted in the successful progress of this novel project. I feel privileged to have worked under the tutelage of such an accomplished instructor.

I am grateful to Professor Jerry Shan and Professor Yuebin Guo for serving as the committee for my thesis defense. Their insightful reviews have equipped me with unique resources to enhance my skills as a researcher. I am confident in utilizing these traits to be a successful engineer.

I would also like to express my gratitude to my labmate Michael Vinciguerra for his extensive contributions to the project, particularly his expertise in setting up the programming aspect of 3D printing. I would like to thank former Rutgers students Bobby Randolph and Jingjin Xie for their previous contributions to this project's framework. I would also like to thank Ali Ashraf for assisting me in analyzing 3D printing material properties, which were a crucial factor in the execution of experiments.

Finally, I would like to thank my fellow lab members Ramendra Pal, Xiyue Zou, and Tongfen Liang, for their guidance. Their continuous support and efforts helped me in having a fruitful experience working in the lab.

DEDICATION

To my beloved parents, Anjum and Farha, my brothers, Shoaib and Noman and to my sister-in law and niece, Afrah and Yumna

TABLE OF CONTENTS

LIST OF FIGURES

LIST OF TABLES

CHAPTER 1 – INTRODUCTION

1.1. Sandwich Composite Structures

An exigent engineering task in the aerospace industry is the design and manufacturing of lightweight, functional components. Lightweight structures provide the legion benefits of increased strength, fuel efficiency, environmental sustainability, and low production cost. It is well established that the aerospace, automotive, and construction industries predominantly use composite materials (composed of a blend of fiber and matrix constituents) in manufacturing critical structural parts. Within these materials, there exists a special class of laminated composites, known as 'sandwich structures.' These unique composites are employed mainly to achieve the fundamental engineering goal of lightweight design and structural integrity.

Typically, the sandwich composite's structural assembly consists of two stiff exterior face skins (also known as face sheets) attached to a core material of high thickness placed in the center (Figure 1). The core exhibits low stiffness, and an adhesive joint bonds the two constituents firmly. This novel structural arrangement of a thick core sandwiched between two outer face skins provides the structure with high stiffness/weight, bending strength/weight ratio, and excellent bending rigidity [1]. By increasing the core thickness, the face skins can be placed further apart. This placement results in further improvement of the characteristics mentioned above, resulting in overall lower density than conventional composites and lightweight construction.

The sandwich structure's face skins serve the purpose of sustaining the majority of the tensile and compressive loads occurring in the sandwich composite. Their high strength

provides the ability to transfer bending stresses in the structure. There are a variety of materials used in the fabrication of skins. The most commonly used materials are Fiber-Reinforced Polymer Composites (FRPCs), in addition to metals, steel, and aluminum. On the other hand, the core of a sandwich structure holds stringent structural applications. It provides structural support to the stiff face skins so that they are evenly placed at the outer portion. More importantly, the core transfers the shear loads in the sandwich structure and requires high shear strength to prevent instability and stiffness reduction in the sandwich composite. Open and closed-cell polymer foams (Polyurethane, PVC, etc.), Nomex, honeycomb, and balsa wood are some of the prevalent materials adopted in manufacturing the core of sandwich structures. [2]

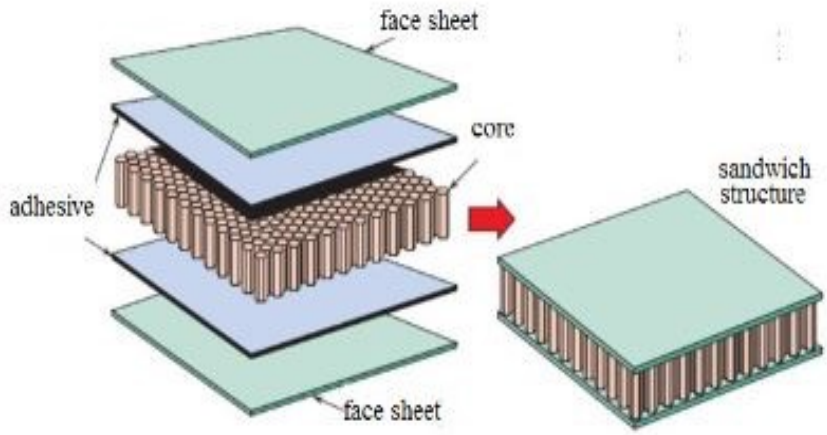

Figure 1. The basic structure of a sandwich composite. Image from Sivak et al. [3]

The selection of robust materials, along with the layered design concept of a sandwich, provides the structure with the inherent advantage of refined mechanical features at a lesser weight. Moreover, sandwich composites exhibit excellent corrosion, damping, and fatigue characteristics and are also employed for thermal insulation. The materials used in the construction of sandwich composites are cost-effective and have minimal impact on

the environment. These attributes render the extensive use of sandwich structures in diverse engineering disciplines where saving weight is of paramount importance. Some of the most notable ones include the aerospace industry (for aircraft control surfaces and interiors), automotive sector, marine engineering (for boats and hulls), and the construction industry (for improved structural integrity and insulation).

1.2. Principle of a Sandwich Construction – Bending Theory of Beams

The principle of a sandwich beam design is homologous to an engineering I-beam where the face skins of the sandwich structure correspond to the flanges, and the core geometry represents the web of the I-beam [3-5]. As shown in Figure 2, the sandwich structure's response to bending loads can be explained based on the fundamental Euler-Bernoulli beam theory, termed as 'sandwich theory.' According to this principle, the application of bending loads on a sandwich structure induces a bending moment on the structure. The sandwich composite endures this moment, thereby generating a stress variation throughout its thickness.

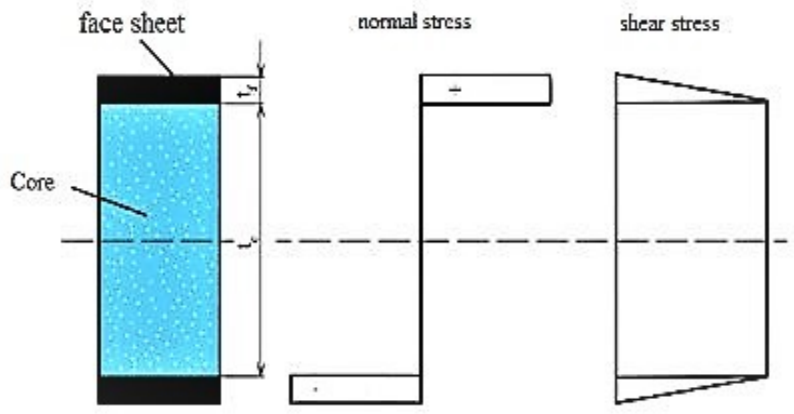

Figure 2. Stress distribution in a sandwich structure. Image from Sivak et al. [3] and inspired by Rikards [5]

As shown in Figure 2, the bending stress distribution develops as tensile stress over the top face skin while compressive stress acts on the lower skin. Essentially, increasing the core thickness results in the face skins being further away from the center of the beam. This corresponds to a surge in the value of the moment of inertia (directly proportional to thickness) [6]. As a result, the bending rigidity of the overall structure increases with a minimal increase in weight. Moreover, to support the stiff face skins far away from the center and prevent failure due to inefficient stress distribution, the core material must possess adequate shear strength. Thus, eventually, the bending of a sandwich beam generates a set of bending and shear stresses in the face skins and core of the composite structure.

By simplifying assumptions, particularly the face skins being of superior Young's modulus and much thinner than the low-density core, the linear sandwich beam theory of stresses postulates that the face skins only generate bending stresses. In contrast, the shear stresses act predominantly on the core of the sandwich composite beam.

1.3. Traditional Manufacturing Processes of Sandwich Composites

Copious methods of conventional manufacturing are available for fabricating sandwich composite structures. Traditionally, this encompasses manual placement of fiber skins, bonding with the core, and physical application of pressure and heat to regulate temperature. These processes exhibit a collective characteristic of involving a significant number of physical tasks. Consequently, the success and efficiency of these techniques depend upon the skill of labor. Based on Karlsson et al.'s work [7], we have described some of the most common mechanisms to produce sandwich structures in the following sections.

1.3.1. Wet-Layup

The process of wet-layup typically involves the deposition of fiber material into an individual mold. Before the application of fiber layer, the placement of an adequate quantity of resin into the mold takes place. The next step is to deposit the reinforcing fibers in the dry state into the resin and pattern with a roller equipment. The sequential iteration of the process results in a layered mixture of fiber and resin. Depending on the deposition method, there are two types of wet-layup - hand layup and spray layup. As the names suggest, hand layup involves the manual application of fibers into the mold. In contrast, spray layup utilizes a spray gun to deposit the blend of fiber and resin, thereby reducing the laborious deposition task. Wet layup manufacturing is optimally suited to produce sandwich structures for moderate structural requirements and prototype applications.

1.3.2. Prereg-Layup

In this process, the impregnation of fiber-reinforcements and resin occurs beforehand (known as preregs) to yield superior mechanical attributes and efficient fiber-resin ratio. Analogous to hand-layup, the production of prereg material involves material deposition into the mold. The preregs may then be laid directly on the core. Alternately, a disparate process utilizing an adhesive material may be employed to bond the fiber-resin mixture and the core. This category of layup involves stringent temperature requirements for the resin material. Thus, special equipment such as vacuum bags and autoclaves facilitate bonding of fiber and resin at the required temperature and pressure.

1.3.3. Adhesive Bonding

Adhesive bonding, a subset of prereg layup, involves the comprehensible positioning of adhesive layers between the face sheets (skins) and core of the sandwich

structure. The bonding between the constituents of the sandwich structure takes place. By rigorously subjecting the structural assembly to the desired temperature and pressure. As with the lay-up method, vacuum bagging or autoclave provide the application of heat and pressure. Adhesive bonding renders improved mechanical properties for the sandwich structure, making them suitable for manufacturing in the aerospace industry.

1.3.4. Liquid Molding

In this manufacturing technique, a mold encloses the blend of fiber-reinforcement skins and the core material. By proper application of pressure, the resin material deposits in this enclosure to achieve impregnation. Liquid Molding may be further categorized into Resin Transfer Molding (RTM), Vacuum-Assisted RTM, Vacuum Injection molding, and Structural Reaction Injection molding (SRIM). This distinction depends on the mechanical characteristics of resin and molds employed for manufacturing, such as reactivity, materials, lead time, and size of components.

1.3.5. Filament Winding

In the filament winding process, filaments of sandwich face skins (reinforcing fibers) weave on a rotating device (mandrel). This arrangement is followed by the concurrent application of resin to the surfaces while it revolves around the mandrel. In this manner, an alternating pattern proceeds to fabricate the outer face skins, followed by bonding the wound material with the core. The process concludes with the repetition of the outer skins to construct the composite sandwich structure.

1.4. Additive Manufacturing (AM) of Sandwich Structures – Background

A notable inference from the description of standard manufacturing methods of sandwich structures is the significant labor required. This aspect has the manifold effect of the surge in fabrication costs, excess material consumption, and increased lead time. Additionally, it significantly limits the design freedom of the structural parts.

Over the past few years, the emergence of Additive Manufacturing (AM), commonly known as 3D printing has revolutionized the manufacturing industry. This novel technology efficiently fabricates structural 3D objects from a digital CAD model by depositing material in a layer-by-layer manner [8]. A G-code program dictates the sequential deposition of the materials. A slicer software generates the program by slicing the model into several layers. The remarkable features of AM, such as tailorable design, rapid production, and minimal environmental impact, have rendered this technique successful in manufacturing composite structures, ranging from the prototype to functional applications. However, there has been limited work documented for the production of sandwich composites by applying AM.

Sugiyama et al. demonstrated the AM of continuous carbon fiber-reinforced Polylactic Acid (PLA) sandwich structures on a commercial 3D printer based on Fused Deposition Modeling (FDM) [9]. Particularly, they fabricated four different core designs were (honeycomb, rhombus, rectangle, and circle). Utilizing the bridge spacing technique, they manufactured the entire structure incessantly. The researchers performed mechanical characterization (bending tests) over these specimens and concluded the best performance (flexural modulus) for the rhombus-shaped core. Additionally, the fiber-reinforced sandwich structure exhibited superior roughness characteristics compared with pure PLA

equivalents. Brischetto et al. employed FDM technology to adopt 3D printing of polymer-filled sandwich specimens and conducted comprehensive mechanical testing [10]. They adopted several AM permutations based on the face skin material and the extruders. Precisely, the authors fabricated eight specimens with Polylactic Acid (PLA) as the common core material, either in the homogenous or honeycomb form. For the face skins, the samples encompassed PLA and Acrylonitrile Butadiene Styrene (ABS) as the preferred material. The researchers implemented the 3D printing technique via single and multiple extruders, followed by conducting a 3-point bending test to evaluate their mechanical properties. Homogenous PLA samples reinforced by ABS samples showed superior elastic modulus and flexural stiffness compared with the honeycomb counterparts. One of the specimens with homogenous core demonstrated poor performance than the rest of the samples, and this was attributed to poor adhesion of the skin and core. This work presented an extensive analysis of the sandwich specimens' failure modes and the effects of using multiple extruders, providing scope for further evaluation. Azzouz et al. presented a novel research work wherein they developed three internal lattice configurations (based on strut arrangements) for the core material [11]. The idea was to embed these configurations to 3D print sandwich structures composed of polypropylene-flax face skins and PLA core material. With the aid of tensile, flexural, compressive, and shear testing, the authors deduced optimal compressive and tensile performance for lattice 1 and 3, respectively. They presented various failure interactions in the core based on loading conditions and the work aptly justified the capability of AM to produce sandwich-structured panels for the aerospace industry.

Similarly, Li et al. designed sandwich structures composed of additively manufactured core materials. The researchers employed three different core arrangements - truss, standard honeycomb, and re-entrant honeycomb [12]. Carbon fiber-reinforced samples in the woven and unidirectional form were bonded with vinyl ester polymer, and the authors 3D printed sandwich structures corresponding to these topologies. They conducted an extensive characterization based on bending and compression tests. Truss and conventional honeycombs displayed superior properties, while the re-entrant configuration exhibited an uncharacteristic response (auxetic) to bending and compression. The researchers also presented numerical simulation (Finite Element Analysis) findings of testing parameters, such as flexural strength, modulus, and stiffness which showed excellent agreement with experimental values.

Hou et al. depicted the 3D printing of a spline-shaped corrugated sandwich structure to manufacture continuous carbon fiber-reinforced thermoplastic composites [13]. This study evaluated the toolpath methodology of 3D printing and its effect on the mechanical attributes of the structural parts. The researchers adopted two path strategies termed as panel-core lap and cross lap for additive manufacturing of specimens. They conducted a compression test and presented a detailed analysis, demonstrating the effect of process variables and printing parameters. For an optimal amount of 11.5 vol% carbon fiber, the authors achieved a compressive strength of 17.17 MPa. This research work widened the horizon of 3D printing to produce structural parts with intricate geometries.

Dikshit et al. adopted inkjet printing technology to produce Acrylonitrile Butadiene Styrene (ABS) rubber-filled core material in two different configurations - vertical pillared sine wave corrugated structure (VPSC) and trapezoidal equivalent abbreviated as ‘VPTC’

[14]. Further, they utilized a Markforged 3D printer to 3D print Kevlar and nylon reinforced face skins. They adhesively bonded the obtained face skins and core structures to obtain a sandwich structure. The researchers conducted an out of plane compression test to evaluate ultimate compression strength, compressive strength, and modulus. The results showed dominant values for sine-wave structured core geometries, while the trapezoidal configuration experienced significant loading.

Galatas et al. proposed the AM of carbon fiber-reinforced polymer (CFRP) sandwich structures with ABS core material to improve the shortcomings of pure thermoplastics composites manufactured by Fused Deposition Modeling (FDM) technology [15]. The authors used an unconventional back propagation method based on an Artificial neural network (ANN) to input parameters and yield output results. This resulted in the evaluation of the composite specimens' specific strength and elastic modulus and its variation based on the number of CFRP layers applied and the density of ABS-filled core material. The tensile test results depicted remarkable improvement in ultimate strength and Young's modulus by augmenting CFRP layers (9 and 16 times, respectively) compared with pure ABS samples. The core density depicted a negligible effect on the strength values. Furthermore, the researchers validated these trends with the help of the ANN technique to reinforce the experimental findings.

1.5. Thesis Motivation and Overview

As described earlier, the mainstream manufacturing systems of sandwich composite structures incur high costs and significant material wastage and constrict the design complexity of structural parts. Nevertheless, they are still predominant in the engineering industry. Additive manufacturing (AM) has supplied a unique opportunity to

supplant these laborious production methods by offering countless benefits such as rapid manufacturing, enhanced mechanical properties at a reduced cost. Up to date, there has been limited research documented for the AM of sandwich composite structures. In this finite literature, the AM of sandwich composites with either pure thermoplastic or fiber-reinforced thermoplastics as the choice of materials has been the primary research area. To the best of our knowledge, there have been no attempts to incorporate thermoset polymer systems as the matrix for reinforcing the fibers. Conceptually, thermoplastic polymers (such as ABS, PLA, Nylon, PP, and PVC) can be reshaped and re-melted at high temperatures, providing excellent flexibility and resistance being used in the manufacturing of high strength parts [16]. However, the application of large heat softens these materials, and these reversible systems are thus unsuitable for high-stress applications like the aerospace industry. On the other hand, thermoset polymers (like epoxy resin, vinyl ester) possess the unique characteristic of irreversible curing [16]. The chemical bond formed permits these materials to withstand melting and reshaping at enormous temperatures, thus rendering them excellent materials for high-temperature applications such as the aerospace and automotive industry. While thermoplastic materials offer the benefit of sustainable manufacturing, their usage incurs a high cost of production.

The objective of this thesis is to consolidate the myriad merits of additive manufacturing and thermoset-based polymer systems to fabricate carbon fiber-reinforced thermoset composite sandwich structures. We will characterize these structures to assess

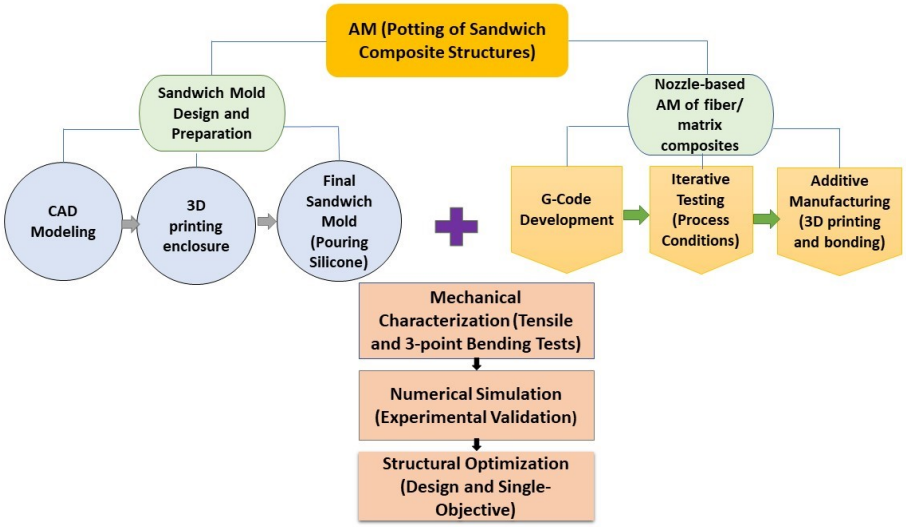

Figure 3. Framework of the thesis

their mechanical performance. The AM technique employed in this thesis project is an eccentric nozzle-based extrusion 3D printing determined by the principle of potting materials. The experimental setup utilized in this work is based on Xie et al.'s research on nozzle-based additive manufacturing [17, 18]. The framework of the thesis, as shown in Figure 3, constitutes a successive process of producing composite sandwich specimens. First, we develop three-dimensional CAD models of two molds enclosing different structural geometries for 3D printing sandwich specimens. The two configurations are dog-bone and rectangular-shaped specimens for performing tensile and 3-point bending tests, respectively. We will adopt a commercial 3D printer to manufacture the thermoplastic enclosure. Next, silicone (Ecoflex^{TM} 0050) is cast into the mold and allowed to cure

sufficiently. Upon demolding the material, we obtain the tensile and bending test molds for 3D printing sandwich specimens.

We would succeed this work by developing the toolpath for extruding composite materials into the sandwich mold. This task involves the conventional AM process of generating a G-code from the STL format of the mold geometry in commercial slicer software. Depending on the complexities of the 3D printing setup, we will implement appropriate adjustments to the G-code. Then, the work involves using the G-code composed of the toolpath for manufacturing for potting (extruding) lower composite face skins from a dispensing medium (nozzle) into the mold, which rests on a metal platform. The materials employed for the construction of face skins are a blend of milled carbon fibers and epoxy systems (G/flex). Commercially available polyurethane foam is selected as the core material and we would bond this foam to the face skins with the aid of an epoxy adhesive. After allowing the assembly to cure, nozzle-based potting would be repeated above this structure to extrude the upper face skins, resulting in the construction of a layered sandwich composite. Thus, we would achieve the manufacturing of tensile and bending test specimens (dog-bone and rectangular bars) for mechanical testing in this organized manner. To simplify the representation of nomenclature for material compositions and manufacturing process, Table (i) lists the essential abbreviations frequently used in this thesis.

Table (i). Important material composition representations used in the thesis

Terms or Material Composition	Abbreviation (Representation)
Additive Manufacturing	AM
Carbon fiber and G/flex epoxy mixture	CF-GF
Carbon fiber – G/flex and Polyurethane foam	Sandwich structure materials

This thesis aimed to demonstrate that 3D-printed composite structures with thermoset matrix systems yield comparable performance with thermoplastic polymers-based structures. Due to unforeseen circumstances surrounding the pandemic (COVID-19), the next part of the thesis entails applying numerical simulation and Finite Element Analysis (FEA) to perform structural and objective-focused optimization. For this purpose, we will present a detailed original plan of potting sandwich specimens. Furthermore, a we also depict a proposed scheme of subjecting the fabricated sandwich specimens to 3-point bending and tensile tests. The values of output parameters such as bending stress and total deformation would serve as an indicator of the sandwich composites' mechanical performance and the feasibility of the proposed AM process.

The second part of the thesis will depict the implementation of numerical simulation of a 3-point bending test of sandwich beams in commercial FEA software (ANSYS) to obtain computational values of the equivalent stresses and the load-deflection data. The goal of the simulation results is to validate the experimental data and detect potential shortcomings in the fabrication conditions. Next, we conduct design optimization experiments of three eccentric aerospace structures that are best fabricated by additive

manufacturing. Finally, we will perform cost-optimization and weight-optimization analysis in MATLAB to evaluate the most efficient mass and cost of producing rectangular geometries comprised of sandwich materials, composite materials, and aluminum alloy. Overall, this work aims to provide a distinctive platform for nozzle-based AM (potting) and its tailorable printing conditions for its application in the manufacturing of sandwich composite structures. Potential applications include the production of high-strength parts for the aerospace industry with the principal advantages such as lightweight design, remarkable fuel efficiency, and structural resilience.

CHAPTER 2 – EXPERIMENTAL DESIGN

2.1. Design of Sandwich Specimens

As the initial step in the construction of sandwich composites, we designed CAD models of two enclosures, each for tensile tests and bending tests. For tensile testing of the parts, we designed a dog-bone-shaped specimen in conformance with the ASTM D638 standard [19]. As shown in Figure 4, the specimen's overall length and width were 63.5 mm and 9.53 mm, respectively, with an extrusion depth of 4 mm. The fillet radius was 12.7 mm, and the width of the narrow section being 3.18 mm. We designed an outer rectangular box enclosing the tensile specimen. We set the dimensions of the box at 70 x 30 x 10 mm. We arbitrarily selected minimal dimensions of the enclosure primarily to avoid material wastage when pouring Ecoflex silicone and to accommodate smooth printing on the heating plate of the 3D printing platform.

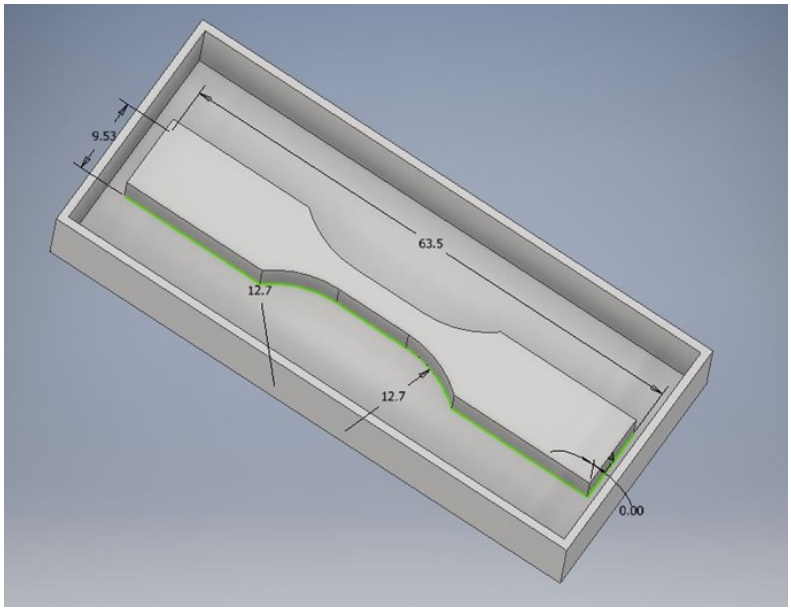

Figure 4. CAD model of the enclosure for tensile test specimen (dimensions are in mm)

Similarly, we designed the second specimen as a rectangular bar representing the sample for 3 point-bending tests (Figure 5). The samples were designed by following the ASTM C393 standard for the bending test of sandwich structures [20]. Again, the selection of dimensions involved meticulous consideration of the testing conditions for the bending test. According to ASTM C393 standard, the non-standard configuration of specimens requires adherence to the following design criteria:

$$2d < b < 6d$$

$$L = S + 50$$

where:

b = width of specimen

d = thickness of specimen

L = length of specimen

S = support span of 3-point bending test

Figure 5. CAD model of the enclosure for bending test specimen (dimensions are in mm)

Based on these equations, we designed a rectangular-shaped bar with an overall length of 100 mm, a width of 12 mm, and a thickness of 6 mm. We restricted the length to 100 mm to accommodate the mold's placement on the extrusion plate of the 3D printing platform (120 mm long). Like the tensile specimen, we designed an outer box enclosing the bending specimen with measurements of 110 x 35 x 10 mm. The difference in thicknesses of the box and specimen facilitates the formation of a rigid base for the 3D-printed sandwich mold.

2.2. Manufacturing of the Sandwich Molds

After developing 3D models of the sandwich molds comprising the specimen geometry and the enclosure, the next step was to fabricate the enclosure molds. We achieved this with the aid of a commercial 3D printer (Lulzbot Mini). After exporting the CAD model as an STL format, the slicer software generated the G-code for additive manufacturing. The material employed was standard PLA material.

We successfully fabricated the initial enclosures for casting polymers for the sandwich mold. (tensile and bending specimens respectively). Next, we cast silicone rubber (Ecoflex^{TM} 00-50 from Smooth On, Inc) into the tensile specimen enclosure [21]. As depicted in Figure 6, we cast up the material to the surrounding enclosure's entire thickness. The same method was adopted for casting Ecoflex into the bending test mold. We allowed the pattern with the poured Ecoflex to cure at room temperature for 24 hours.

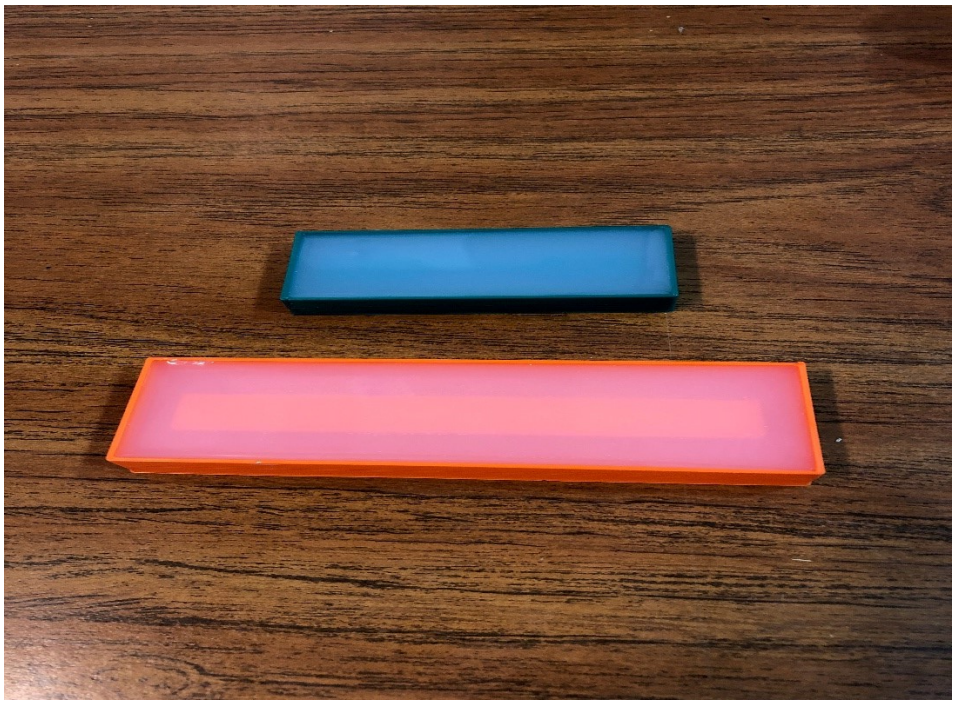

Figure 6. Pouring of silicone (Ecoflex 00-50) into the sandwich molds

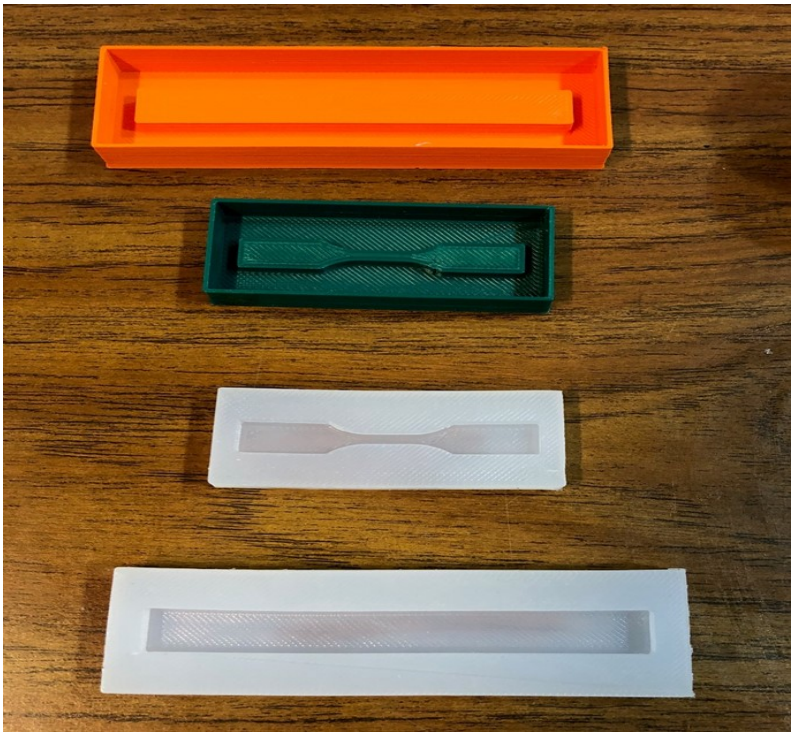

Figure 7. Cured sandwich molds for potting tensile and bending test specimens

Upon sufficient curing, we de-molded the silicone-filled material from the enclosure. As shown in Figure 7, we successfully achieved the sandwich molds for potting fiber-reinforced skins and foam core.

A critical phenomenon during casting of the tensile test mold was the curing discrepancy of thermoplastic polymer. Initially, after pouring Ecoflex into the tensile mold, we placed the model in an oven for an hour and then allowed to cure at room temperature for 24 hours. This resulted in substantial shrinkage of the material along the narrow width of the section. To overcome this, we implemented the tensile mold's fabrication again without the utilization of oven curing. As shown in the image, there was no apparent shrinkage, we produced the mold successfully.

2.3. Bending Tests - Analytical Calculations of Shear and Compressive Strength

The application of a high concentrated load on a sandwich beam during flexural (bending) tests actuates the structure's potential failure. Depending on the materials employed for the face skins and core of the beam, various forms of failure are viable for the sandwich structure. In a critical study, Traiantafillou et al. devised an extensive set of equations depicting the failure loads acting on a sandwich structure. They presented a failure mode map of the sandwich beam, comparing variables of core density and beam dimensions to describe six different modes of failure, as demonstrated in Figure 8 (a) to (f) and their prevalence for a particular set of loads [22]. Furthermore, Kim et al. investigated three failure systems occurring in the face skin and the core by conducting a 3-point bending test and applying a concentrated load on the structure. The researchers evaluated the failure loads as a function of the core density and thicknesses (Figure 9 (a) to (b)) [23].

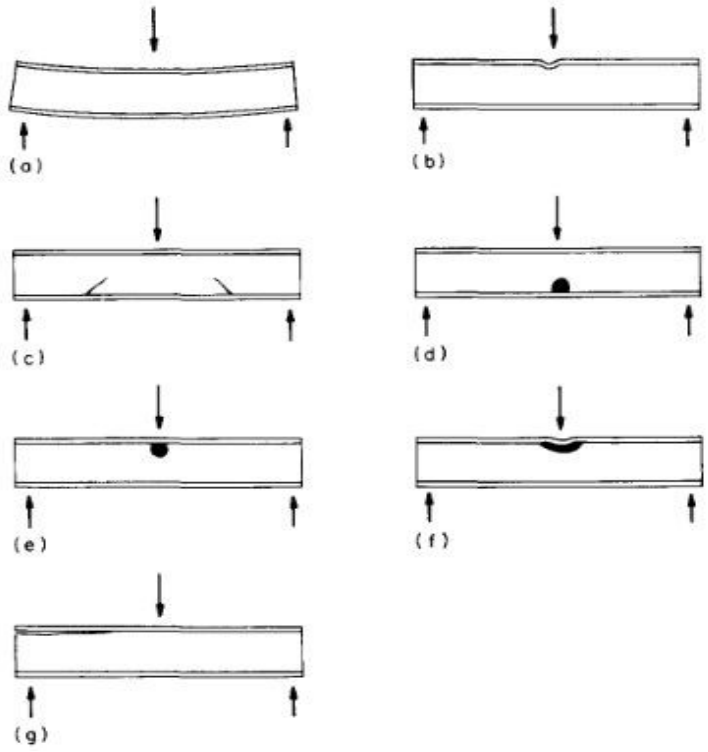

Figure 8. Failure modes in a foam core sandwich beam: (a) face yielding (b) face wrinkling (c) core shear (d) core tensile yield (e) core compressive yield (f) core indentation (g) debonding. Image from Traiantafillou et al. [22]

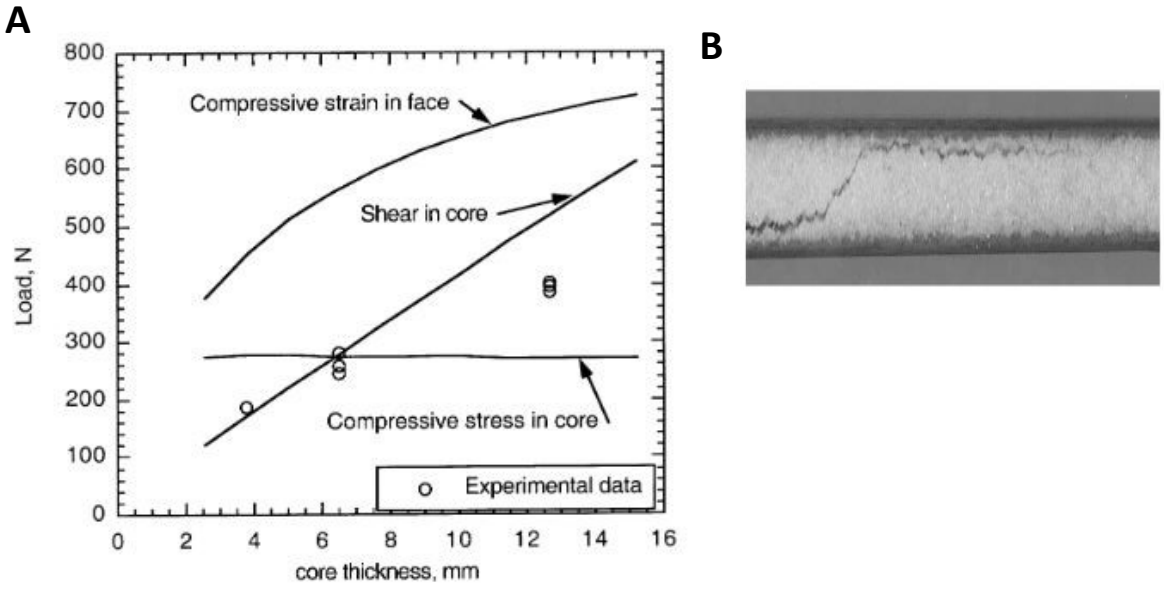

Figure 9. (a) Plot showing core shear failure at low thickness (b) Shear failure in the core of sandwich beam – polyurethane foam. Image from Kim et al. [23]

Table 1 aptly summarizes the six most common failure modes acting on a sandwich structure with their description.

Table 1. Description of the six major failure modes in a sandwich structure

Failure Mode	Description
Face yielding	Equivalent normal stress in face equals the yield stress of the face material
Face wrinkling	Normal stress in the face reaches the critical buckling stress
Core shear failure	Maximum shear stress in the core reaches the shear strength of the core material
Core tensile yield failure	Maximum principal tensile stress of core equals yield strength of core in tension
Core compressive yield failure	Maximum principal compressive stress of core equals yield strength of core in compression
Indentation	Yielding of the core in the loading section, due to local loads

Additionally, the ASTM C393 standard for the flexural test of sandwich structures identifies several failure modes acting on the specimen. These are primarily the core failure, facing skin failure, and delamination of the core-face layer. According to the standard, a stringent requirement for a successful bending test is that the sandwich structure's failure occurs only in the core of the specimen. The standard considers the failure eventuating due to maximum stress in the face skin before the core as inadmissible.

To adhere to this criterion, there are two critical stress equations for the core material strength provided in the standard that dictate the design of the specimen with appropriate dimensions [20].

$$Fs \leq \frac{2k\sigma t}{(S-L)}$$

$$Fc \geq \frac{2(c+t)\sigma t}{(S-L)lpad}$$

where:

S = support span length (mm)

L = loading span length (mm) (L = 0 for 3-point bending test)

σ = expected facing ultimate strength (MPa)

t = facing thickness (mm)

c = core thickness (mm)

Fs = estimated core shear strength (MPa)

k = facing strength factor (k = 0.75 as per standard recommendations)

l_{pad} = dimension of the loading pad in specimen lengthwise direction (mm)

Fc = core compression allowable strength (MPa)

Table 2. Analytical calculations of core shear and compression strength

Length (mm)	**Support Span (mm)**	**Specimen width (mm)**	**Core thickness, c (mm)**	**Facing thickness, t (mm)**	**Core shear strength, F_s (MPa)**	**Core compression strength, F_c (MPa)**
110	60	12	5	0.5	1.46	0.89
100	50	12	5	0.5	1.76	1.07
90	40	12	5	0.5	2.20	1.34
110	60	15	6	0.6	1.76	1.03
100	50	15	6	0.6	2.11	1.24
90	40	15	6	0.6	2.64	1.55
110	60	17	7	0.7	2.05	1.24
100	50	17	7	0.7	2.46	1.49
90	40	17	7	0.7	3.08	1.86
110	60	20	8	0.8	2.34	1.37
100	50	20	8	0.8	2.81	1.65
90	40	20	8	0.8	3.51	2.06
110	60	22	9	0.9	2.64	1.58
100	50	22	9	0.9	3.16	1.90
90	40	22	9	0.9	3.95	2.37
110	60	24	10	1	2.93	1.79
100	50	24	10	1	3.51	2.15
90	40	24	10	1	4.39	2.68

Based on these equations, we performed analytical calculations to determine the shear and compression strength of the sandwich structure's core. As described in Table 2, we calculated these values for three different sets of lengths (90, 100 and 110 mm) and three corresponding span lengths (40, 50, 60 mm) for varying dimensions of the specimen.

We obtained the ultimate tensile strength of the face skins (carbon fiber and epoxy) from the manufacturer's data [24]. We set the dimensions of the loading pad supporting the loading bar equal to the width of the specimen in each case. From the information in the table, and after careful consideration of the 3D printing operating parameters (such as extrusion plate width and operating temperature), we selected a sandwich specimen of measurements 100 x 12 x 6 mm. Based on these dimensions, we deduced the allowable values of shear strength and compression strength, which allowed us to select the appropriate material for the core of the sandwich structure.

2.4. Selection of Materials

For fabricating face skins of the sandwich specimens, we prepared a mixture of reinforcing fibers and a polymer matrix. The fiber material adopted for this research were polyacrylonitrile (PAN)-based, milled carbon fibers (CM150-3.0/200UN, SGL Group, Germany) [25]. The thermoset polymer matrix employed was a two-part toughened, liquid epoxy (G/flex 650 by West System, MI). The epoxy system possesses excellent adhesion characteristics and has an ultimate glass transition temperature of about 67.8 °C [26]. Additionally, for the preceding task of preparing sandwich molds, we utilized a silicone elastomer (Ecoflex^{TM} 00-50 by Smooth-On, PA) to cast the mold enclosure with the material [21]. Table 3 lists the key characteristics of the selected milled carbon fibers and the two thermoset polymer systems.

Table 3. Essential material properties of carbon fibers and thermoset polymers obtained from materials' technical data [21], [25], and [26].

Material Properties	**Carbon fibers**	**G/flex**	**Ecoflex™ 00-50**
Young's Modulus (MPa)	200,000	992.84	0.082
Tensile Strength (MPa)	3000	23.71	2.171
Material Density (kg/m^3)	1800	1110	1070
Elongation at Break (%)	1.5	32.7	980

The core material employed in the sandwich construction was a closed-cell polyurethane foam (RF-2206) from General Plastics Co., possessing a density of 6 lb/ft^3 and a maximum temperature of 171 °C [27]. We deduced the selection of this core material after rigorous analysis of the analytical calculations listed in Table 2 and the mechanical characteristics. Specifically, the foam material chosen satisfies the compressive strength and shear strength requirements for the bending test standards. It adheres to the high-temperature requirements dictated by the nozzle-based additive manufacturing machine.

CHAPTER 3 – ADDITIVE MANUFACTURING OF SANDWICH SPECIMENS

3.1. Experimental Arrangement

The experimental apparatus of the custom 3D printer for potting of composite sandwich specimens consists of a profusion of equipment, ranging from material extrusion mediums, instruments for regulating processing conditions, and hardware components for implementing the AM program [17]. Figure 10 depicts the major components of the experimental setup.

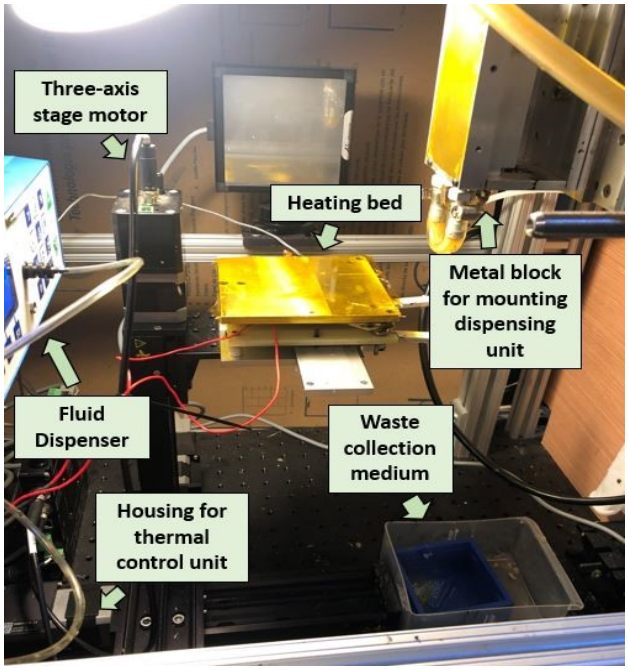

Figure 10. Experimental setup of potting (nozzle-based 3D printing)

As shown, a temperature control device (EZ-ZONE, Watlow, MO) regulates the extrusion plate's temperature for operating it at higher temperatures. For extruding composite materials on the bed (plate), we adopt a pressure-based pneumatic system. It

consists of a pre-mixing and dispensing tool (2K equalizer, Nordson EFD, RI) for extruding the blend of carbon fiber and two-part epoxy onto the heating plate. The materials are initially in their undistributed state in the dual cartridge, wherein the pressure is applied to transfer these materials into a static mixer and the nozzle tip. A high-precision fluid dispenser (Ultimus V, Nordson EFD, RI) controls the application of pressure into this dispensing medium and is housed at the opposite end of the dispensing tool. Figure 11 (a) shows the dispensing device. It provides critical information on dispensing parameters for facilitating smooth extrusion from the dispensing medium into the heating plate. As the material extrudes out of the nozzle, the dispensing assembly remains static. At the same time, the heating plate advances along three axes as dictated by the stream commands generated from the G-code.

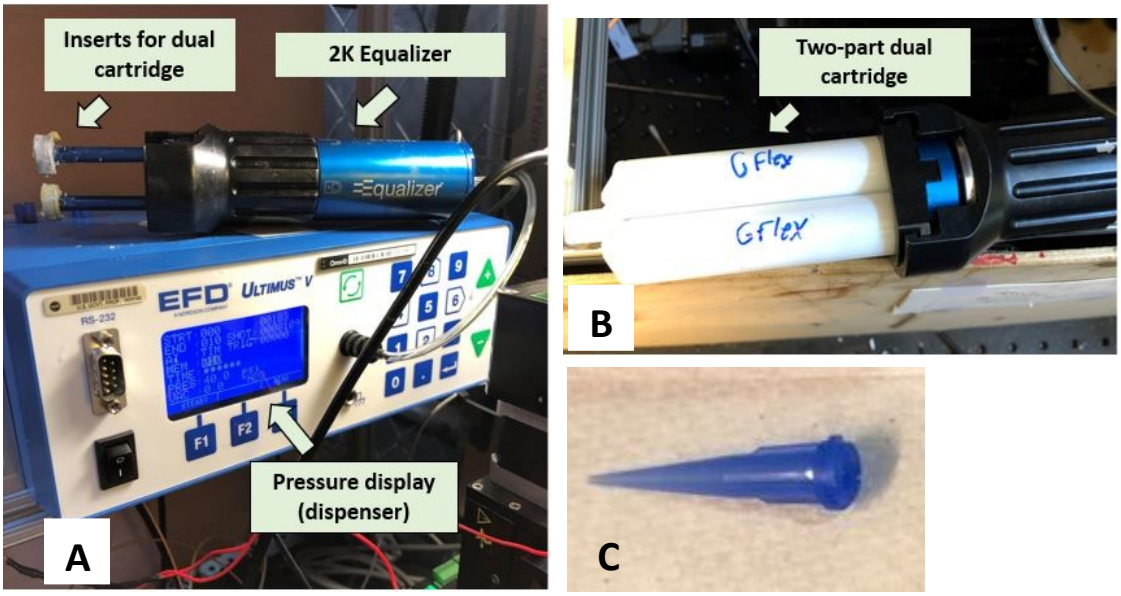

Figure 11. (a) Fluid dispenser and equalizer device (b) Dual chamber cartridge attached to equalizer (c) dispensing tip (d) dispensing medium assembly

Two motion control devices, a motor driver (X-MCB2, Zaber Technology, CA) for translatory motion (X and Y axes) and a third motor for administering motion along Z-direction principally achieves the guided motion. Furthermore, the dispensing assembly housing the equalizer and the cartridge is maintained at a fixed temperature (30°C) by a moderating chiller/heater (Series 6000, PolyScience, IL) so that the setup is not affected by the high heat of the extrusion. The square-shaped extrusion plate of 120 mm length subjected to high temperatures for AM is composed of a 6061 Aluminum sheet and is placed in the center of the setup. It is attached to the motion control stage and surrounded by the dispensing equipment on either side.

3.2. 3D printing (AM) Implementation

We implemented the nozzle-based AM mechanism with the interlinking of software elements generated by a computer to the hardware of the experimental arrangement described in the previous section. Similar to conventional AM, we exported the CAD model of the object as an STL format into slicer software. For this work, we used ‘Slic3r’, open-source software for importing the geometry [28]. In this application, we prescribed key printing process parameters, including the layer height, layer thickness, infill density of the extrusion material, speed of printing, default extrusion width, and perimeter. After the appropriate specification of variables is completed, we transformed the STL format into a G-code comprising the essential toolpath for AM. Here onwards, the task shifts over to the host computer that drives the hardware of our custom 3D printer. The exported G-code is transformed into a set of stream commands communicated by the computer to the experimental setup. These stream commands drive the motion of the heating plate along three axes via the displacement of the stages. A G-code translator

provided by ‘Zaber Console,’ achieves the generation of stream commands. These commands are a sequential motion of the stage with the path taking the form of geometric entities, such as circles, line segments, square, spiral, etc. It consists of numbers that correspond to the coordinates of displacement along three axes, respectively. Since the setup involves a set of motors, each for X-Y translation and motion along the Z-axis, two the translator generates two separate sets of stream commands. These directions are accumulated by a LabVIEW program (Ver 2016, National Instruments), which methodically drives the alternating motion along all three axes. The commands dictate the movement of the stage. In turn, the extrusion plate acts in conjunction with the application of pressure from the dispensing system to initiate and implement the process of nozzle-based additive manufacturing.

3.3. Iterative Efforts to Improve Printing Quality

Prior to implementing the proposed manufacturing of composite sandwich materials, we conducted a series of 3D printing tests with the experimental arrangement using several materials. The purpose of these tests was to evaluate the feasibility of the 3D printing setup (hardware and software system) and to ensure that the structural parts produced have good quality. These trials’ results were initially unsatisfactory with important issues such as bead deposition and poor part quality. By careful evaluation of the outcomes, we later developed an iterative approach for AM. This involved varying process parameters in the slicer software and alternating process conditions in the hardware and material dispensing systems. We were able to improve the quality of printed parts significantly. We deduced ideal process parameters for AM, namely layer height, nozzle

size, and elevation above the extrusion surface. The following sections summarize the progression of extrusion tests using numerous fibers and polymer system:

3.3.1. Carbon Nanotubes with G/flex Epoxy

As part of initial tests, we prepared a 20 g sample of G/flex epoxy mixed with 0.1 wt% carbon nanotubes and implemented the manufacturing tests. We set the flow rate (pressure) of extrusion at 30 psi due to the materials' viscous nature of and the nozzle tip used was 0.41 mm in outer diameter. We observed uneven mixing of the fibers and matrix upon extrusion, which led to insufficient curing of the material (as seen in Figure 12).

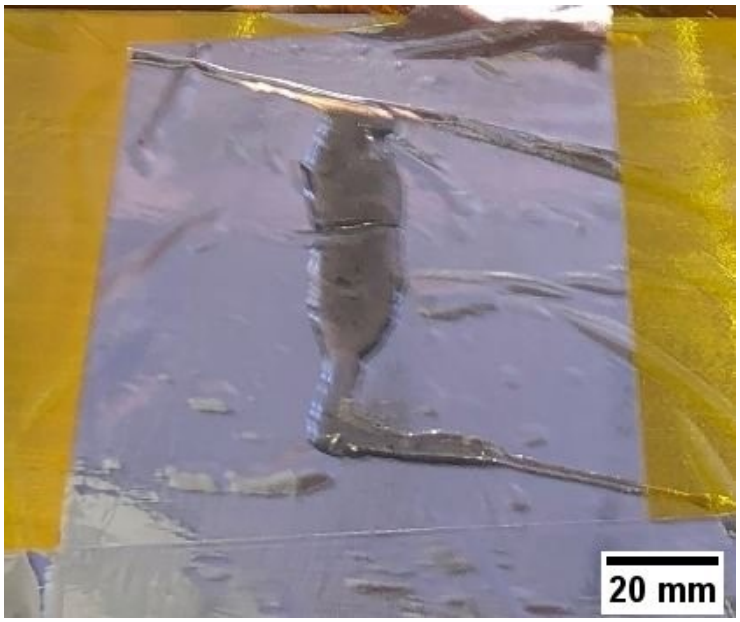

Figure 12. Partial extrusion of dog-bone model (CNT-G/flex mixture)

Additionally, there were visible fumes generated upon extrusion, and the bead deposition was not accurate, thus resulting in a part with irregular shape and poor quality.

3.3.2. Carbon Fibers with G/flex Epoxy

We performed a similar test to carbon nanotubes with milled carbon fibers as the reinforcing material (0.1 wt%) and mixed with G/flex polymer in 20 g of the mixture. As

shown in Figure 13, the result was identical to the carbon nanotube counterparts with inadequate curing and mixing of the materials on the printing bed. The nozzle size remained the same for this test.

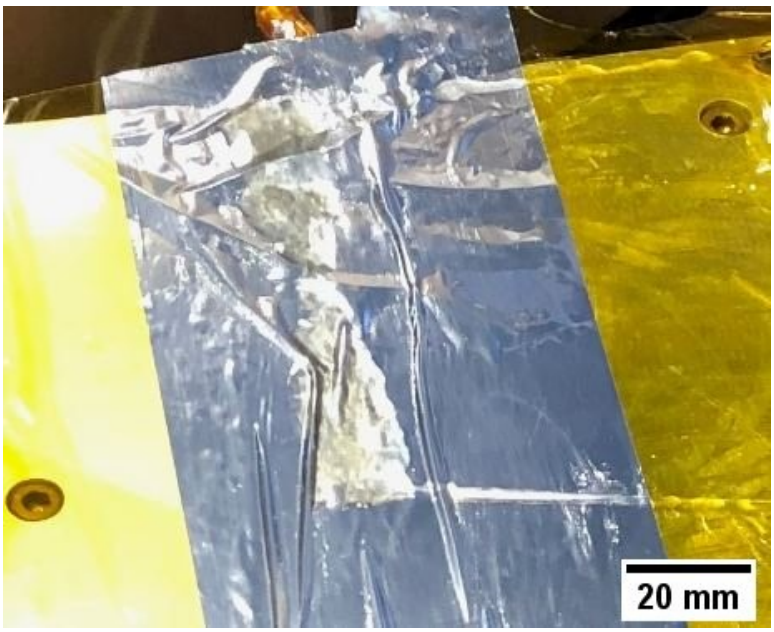

Figure 13. Extrusion of dog-bone model with insufficient curing (carbon fiber and G/Flex mixture)

3.3.3. Pure G/flex Samples

To optimize print quality, we aimed to increase the number of tests for improving the printing setup. Thus, to avoid material wastage, we conducted experiments to print dog-bone samples using pure G/flex epoxy.

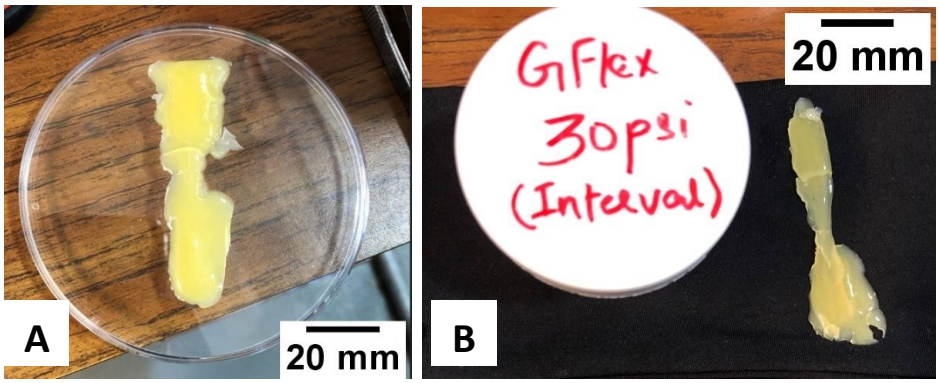

Figure 14. Irregular dog-bone shaped samples using pure G/flex at pressures (a) 26 psi and (b) 30 psi

We observed adequate mixing of the resin and hardener materials upon deposition, however, there was noticeable smearing of the material as the printing progressed to successive layers. This was primarily due to insufficient curing of the composite materials from the nozzle, which needed to be improved by evaluating the AM process's operating temperature. For pure G/flex, we performed trial runs at pressures of 25-30 psi, two of the printed parts are presented in Figure 14 (a) and (b).

3.3.4. Pure Ecoflex Samples

Following unsuccessful attempts to ameliorate the standard and quality of 3D-printed parts, we adopted an iterative approach and listed permutations of numerous manufacturing variables for performing extrusion trials. The objective of this iterative testing was to find the correct set of conditions for AM, which would collectively yield smooth extrusion from the dispensing medium and overcome the issues encountered in the previous attempts. For this purpose, we adopted Ecoflex 00-30 silicone as the extruding material. This selection was based on the fact that the material cures rapidly and is available abundantly, enabling rapid testing and evaluation.

The key parameters that we iterated were namely the flow rate (pressure), the height of nozzle tip above the bed, layer height of printing, first layer height, speed of travel, nozzle size, and temperature of AM. Table 4 lists numerous values that we tried for these variables and the mode of adjustment.

Table 4. Key extrusion parameters used in iterative testing

Parameter	Source of Adjustment	Typical Values
Extrusion flow rate	Fluid dispenser machine	15-20 psi
Distance between nozzle and heating plate (Bed-levelling)	Zaber Console hardware Application (Home Offset in Z-direction)	3-10 mm
First layer height	Slic3r print settings	0.4 – 0.5 mm
Layer height	Slic3r print settings	0.4 – 0.5 mm
Speed of travel	Slic3r print settings	30 mm/s and 60 mm/s
Default extrusion width	Slic3r print settings	0.6 or 0.8 mm
Nozzle tip size diameter	Slic3r print settings	1.1 mm or 0.4 mm
Temperature of heating plate	Thermal control unit	120 – 150 °C

As shown in Figure 15 (a) and (b), we produced several samples by 3D printing. The result was a gradual improvement in the quality of printed parts. We achieved this

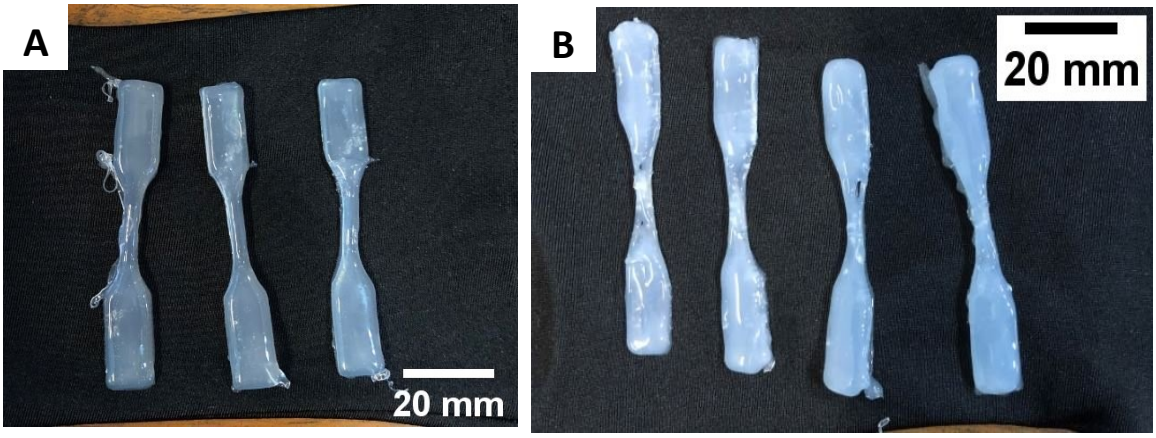

Figure 15. (a) Dog-bone tensile model printed using pure Ecoflex at pressure 19 psi (b) Parts extruded adjusting printing height at various offsets

explicitly by deducing values based on rigorous iteration and deducing the most favorable settings for 3D printing (Figure 16 shows improved results).

Figure 16. Pure Ecoflex dog-bone-shaped samples (iterative testing by varying layer height, offset height, extrusion pressure)

Table 5. Optimum extrusion settings for 3D-printed parts

Parameter	Optimum value for best quality
Extrusion flow rate	15-20 psi
Distance between nozzle and heating plate (Bed-levelling)	3 mm
First layer height	0.45 mm
Layer height	0.4 mm
Speed of travel	30 mm/s
Default extrusion width	0.6 mm
Nozzle tip size diameter	0.4 mm
Temperature of heating plate	150 °C

Table 5 depicts the final set of values that we deemed optimum for producing high-quality dog-bone samples. Using these settings, we performed additional AM of dog-bone samples to ensure repeatability of the refined quality and reinforce the parameters' selection. (refined parts are depicted in Figure 17 (a) and (b)).

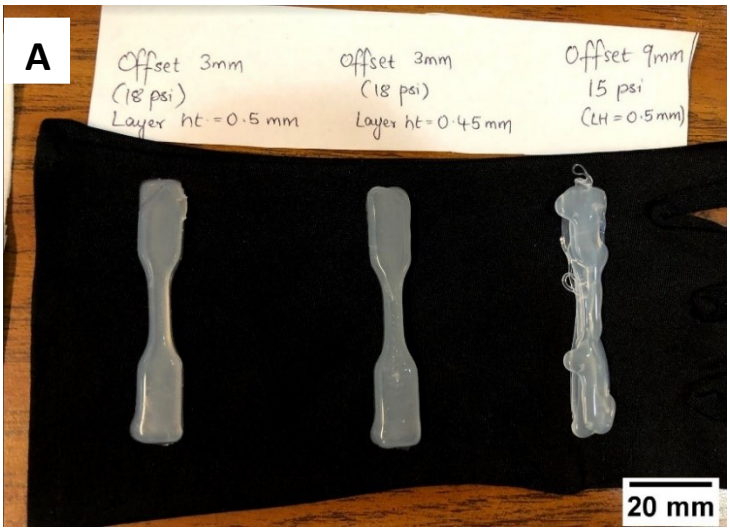

Figure 17. 3D printed Ecoflex samples to ensure repeatability (a) Dog-bone extruded at 3 mm and 9 mm offsets (b) improved quality tensile samples printed using smaller nozzle tips

3.4. Program Formulation for Nozzle-Based AM (G-Code and Stream Commands)

As described earlier, the motion of the heating plate facilitates the extrusion of thermoset composite materials to execute the potting of sandwich specimens. The translational and vertical motion of the XYZ stage attached to the extrusion plate drives the printing bed movement. The three-axis motion of the gantry stage is, in turn, governed by the stream commands generated from the G-code developed for 3D printing. Thus, the entire process of extrusion comprises a sequential manufacturing scheme spanning from the creation of the first G-code program to the final extrusion phase. Conceptually in a manufacturing discipline, a ‘G-code’ refers to a set of instructions (a programming language) that guides the motion of the tools used in fabrication. This programming language is mainly used in Computer Numerical Control (CNC) to direct the machine tools

to move in a specific direction and a particular path. This enables the machining operation to take place autonomously. Similarly, in additive manufacturing, a G-code program instructs the 3D printer to generate movement at a specific time, direction, and a specified path. In addition to these motion commands, G-code commands can perform a host of other AM functions. This includes setting the rate of extrusion, specifying the bed's temperature, and adjusting the elevation of extrusion [29]. For AM, an STL file of the desired geometry of the three-dimensional model generates the set of commands that constitute a G-code. Typically, the STL format of the CAD model is imported into a slicer software, and the resulting geometry is exported into a G-code. Furthermore, before the G-code generation, the slicer provides plenteous tools to alter the process parameters of 3D printing, such as the layer height, extrusion width, and speed of 3D printing.

In this work, for the potting of sandwich specimens, we produced the enclosure for potting the sandwich mold by a commercial 3D printer utilizing the above sequential manufacturing process. After casting Ecoflex into this enclosure to obtain the sandwich mold, the next step was to formulate a program of instructions for extruding thermoset materials into the mold cavity. As the cavity is in the shape of the rectangular or dog-bone beam, we generated the G-code for potting by importing the STL format of the beam in 'slic3r' software [28]. We specified essential process parameters such as initial and subsequent layer height, feed rate, extrusion width, and infill percentage of 3D printing before generating the G-code. To understand the general interpretation of a standard G-code program, Figure 18 shows a brief part of the commands incorporated in the G-code for extruding a dog-bone geometry.

```
M107
M104 S200 ; set temperature
G28
; Filament gcode

M109 S200 ; set temperature and wait for it to be reached
G21 ; set units to millimeters
G90 ; use absolute coordinates
M82 ; use absolute distances for extrusion
G1 Z0.400 F7200.000
G1 X14.833 Y93.867
G1 F1800
G1 X16.993 Y93.051
G1 X18.250 Y92.932
G1 X81.750 Y92.932
G1 X84.025 Y93.329
G1 X86.030 Y94.473
G1 X87.530 Y96.229
G1 X88.345 Y98.389
G1 X88.464 Y99.646
G1 X88.464 Y109.171
G1 X88.067 Y111.446
G1 X86.923 Y113.452
G1 X85.167 Y114.951
G1 X83.007 Y115.767
G1 X81.750 Y115.886
G1 X18.250 Y115.886
```

Figure 18. A brief part of the G-code program for a dog-bone model displaying various machine and position commands

As seen in the figure, the alphabets in the code correspond to various commands of the 3D printing (AM) operation [29]. For instance, the second line in the code ‘M104 S200’ directs the heating of the extrusion plate to a temperature of 200 °C. Here, ‘M’ codes drive the critical operations of the 3D printer. On the other hand, G-codes necessarily specify the motion of the heating plate of the 3D printer. Re-evaluating the figure, the command (G1 X16.993 Y93.051) directs the 3D printing machine plate to move along this position. Here X and Y values correspond the co-ordinates of the motion. Similarly, the command ‘G1 Z0.400 F7200.000’ regulates the plate’s movement vertically at a distance of 0.4 mm and at a feed rate of 7200 (F code corresponds to feed rate).

A significant challenge for this task is to ensure that the nozzle does not strike into the cavity walls as it would lead to poor quality of the sample and possible damage to the

equipment. For this purpose, the G-code program must be amended manually by incorporating particular motion commands. Correctly, at the first and final line of the G-code script for potting, we inserted a command ‘G1 Z20’ before the first and last XY motion. This modification assures the proper path of the nozzle tip without contacting the mold restricting its travel close to the walls.

We then converted the obtained G-code with the necessary modifications into a set of stream commands by a G-code translator in the hardware application ‘Zaber Console.’ As mentioned in Chapter 4, this hardware application serves as the medium of communication between the computer-generated LabVIEW program and the motion of the extrusion plate of the 3D printer. The stream commands comprise the XYZ stage’s critical motion which prompts the translational and vertical movement of the extrusion plate [30]. Figure 19 below shows a sample stream command for the extrusion of a dog-bone model.

```
/1 0 stream 1 set centripaccel 30000
/1 0 stream 1 set maxspeed 153600
/1 0 stream 1 line abs 0 0
/1 0 stream 1 set maxspeed 396312
# G1 Z806
/1 0 stream 1 line abs 29900 79537
/1 0 stream 1 set maxspeed 99078
/1 0 stream 1 line abs 34254 77893
/1 0 stream 1 line abs 36787 77653
/1 0 stream 1 line abs 164787 77653
/1 0 stream 1 line abs 169373 78453
/1 0 stream 1 line abs 173415 80759
/1 0 stream 1 line abs 176438 84299
/1 0 stream 1 line abs 178081 88653
/1 0 stream 1 line abs 178321 91186
/1 0 stream 1 line abs 178321 110386
/1 0 stream 1 line abs 177521 114972
/1 0 stream 1 line abs 175215 119016
/1 0 stream 1 line abs 171675 122037
/1 0 stream 1 line abs 167321 123682
/1 0 stream 1 line abs 164787 123922
/1 0 stream 1 line abs 36787 123922
/1 0 stream 1 line abs 32202 123122
/1 0 stream 1 line abs 28160 120816
/1 0 stream 1 line abs 25136 117276
/1 0 stream 1 line abs 23494 112922
/1 0 stream 1 line abs 23254 110386
/1 0 stream 1 line abs 23254 91186
```

Figure 19. A brief part of the stream commands Zaber Console obtained by translating the formulated G-code for dog-bone geometry

As seen from the figure, the commands formulated are easy to interpret. For instance, the first line in the control sets the centripetal acceleration of motion to 30000 units, while the second line sets the maximum speed of movement. Furthermore, the subsequent stream commands in the figure govern the heating plate's movement to various absolute positions [30]. The stream command '/1 0 stream 1 line abs 29900 79537' results in the heating plate's movement to an absolute position with an X coordinate value of 29900 and Y equal to 79537. The plate moves from one location to the other based on these commands. In this manner, the formulation of the stream commands from the G-code enables the additive manufacturing process (potting).

CHAPTER 4 – PROPOSED PLAN OF ACTION

4.1. Introduction – Transition of Research Activities

The main objective of this project was to demonstrate the unique capabilities of nozzle-based additive manufacturing and the structural novelty of sandwich composite construction to produce thermoset composite structures for the aerospace industry. To achieve this goal, our research project was a two-fold approach to programming and manufacturing composite specimens by AM, followed by mechanical characterization and numerical simulation. We successfully achieved the research activities (namely optimizing AM process conditions, developing G-code program and material selection) leading up to the potting of sandwich structures, as described in the preceding chapters. However, due to the unforeseen circumstances surrounding COVID-19, we could not perform the implementation of the potting process and mechanical characterization of 3D-printed parts by experimental tests.

Thus, we meticulously formulated a new strategy for this thesis to exhibit the additive manufacturing (AM) efficacy of thermoset composite materials. Our plan aimed to smoothly transition from the manufacturing realm of sandwich composite structures to adopting a numerical simulation approach for characterizing these laminated structures. Specifically, we proposed conducting a numerical simulation study of sandwich-structured specimens to evaluate their load-bearing capabilities. Next, in a diligent effort to develop a framework for numerical simulation, we attempted to perform design optimization of 3 novel structural components for applications in the aerospace industry. The objective of optimization was to analyze the structural parts composed of carbon fibers and thermoset

materials and generating the most effective design. We would govern the structural performance and efficiency of these parts by achieving the concurrent goal of lightweight design, low cost, and robust structural strength.

Thus, the next sections in this chapter provide a brief overview of the activities that were planned originally as part of this research work. The succeeding chapters of the thesis then present the utilization of numerical simulation to evaluate mechanical properties and to perform structural optimization of novel aerospace components that can be suitably fabricated by additive manufacturing.

4.2. Proposed Plan - Additive Manufacturing (Potting) of Sandwich Specimens

The generation of 3D printing G-code and stream commands coupled with the deduction of favorable processing conditions for production, we proposed the following scheme of action for manufacturing sandwich composite specimens. We would initiate the process would by preparing 20 grams of the composite sample (comprising 5 wt% carbon fiber with G/flex epoxy). We would weigh carbon fiber according to the desired percentage and place equal amounts in two separate containers. Each of these two containers would consist of one part of the G/flex thermoset epoxy (resin and hardener, respectively). The containers will be closed tightly after depositing the mixture. The next step would be to perform high-speed mixing of the containers comprising of the samples. We will achieve this primarily with the help of a SpeedMixer (DAC 150.1 FVZ-K, FlackTeck Inc., SC). The boxes would be placed in the mixer one at a time and allowed to mix by running the centrifuge machine at 3000 RPM for 1 minute. The main goal of combining the samples before extruding them is to remove any visible voids in the mixture and to ensure that the reinforcing fibers are efficiently disseminated in the sample. Following the completion of

the mixing process, we would transport the two sets of composite samples into separate chambers of the dual cartridge belonging to the dispensing system. The chambers of the dual cartridge would be enclosed with two pistons, and we would attach a special static mixer to the tip of the cartridge. The purpose of the static mixer is to mix the resin and hardener samples prior to deposition efficiently. The static mixer will be attached to a nozzle tip, which served as the primary dispensing medium for AM. We will finally attach the extrusion assembly to the equalizer forming the complete dispensing medium.

After setting the desired pressure of dispensing the material and placing the mold on the heating bed, we would execute the AM stream commands by running the LabVIEW program. This would prompt the translational movement of the heating plate while the material is extruding concurrently from the nozzle. In this manner, the layer-by-layer potting of the materials would take place into the mold, forming the sandwich structure's lower face skin.

We would allow the material to cure sufficiently into the mold. The next essential task is the bonding of the core to the extruded skin material. We would cut polyurethane foam sheet into the desired geometric dimensions (100 x 12 x 5mm) to form the rectangular-shaped specimen. Subsequently, the next task would be the assembly of this core material. For this activity, we planned using high-temperature adhesive material to bond the foam sheet to the lower face skin. This would result in efficient inter-locking of the core and the lower face sheet. Following this assembly, we would embed the top portion of the foam with the same adhesive material for the fusion of the upper face skin structure. After implementing the adhesive joint on the top portion and sufficient curing into the mold, we would execute the process of nozzle-based potting (mixing, programming, and

extrusion) again for carbon fiber – G/flex sample to form the upper face skin of the specimen. We would safely demold the entire assembly out of the enclosure after allowing to cure adequately. Thus, with the deposition of this material into the adhesive joint, we would successfully complete the formation of a sandwich-shaped flexural specimen.

We intended to adopt this sequential approach of AM based on nozzle extrusion for the similar fabrication of the tensile-shaped sandwich structure. The only difference is in the structure's geometry and, thus, the movement of the extrusion plate.

4.3. Proposed Plan – Mechanical Testing of Fabricated Sandwich Specimens

In an effort to evaluate the structural performance of the additively manufactured sandwich specimens by potting, the next step in this work was the mechanical testing (3-point bending and tensile test) of sandwich structures. The primary objective of these experiments was to demonstrate that sandwich structures fabricated from fiber-reinforced thermoset composites yields comparable structural properties with thermoplastic equivalents. By analyzing mechanical properties such as the deformation, bending stress, tensile stress, and shear stress acting on the structure, we aimed to evaluate the feasibility of the distinctive process of nozzle-based AM to produce high-strength structural components for the aerospace industry.

In this work, we intended to perform a 3-point bending test for the rectangular-shaped flexural sandwich specimen and a tensile test on the dog-bone model. The proposed framework of the 3-point bending test is as follows. Based on the mechanical properties desired, we selected ASTM C393 as the preferred standard to be adopted for the bending analysis. For this experiment, we would place the sandwich specimen on two supports at the bottom of a fixture. A concentrated load acts in the middle of the upper face of the

sample. The application of load deforms the structure and data for load-deflection, core shear properties and face bending stresses are obtained.

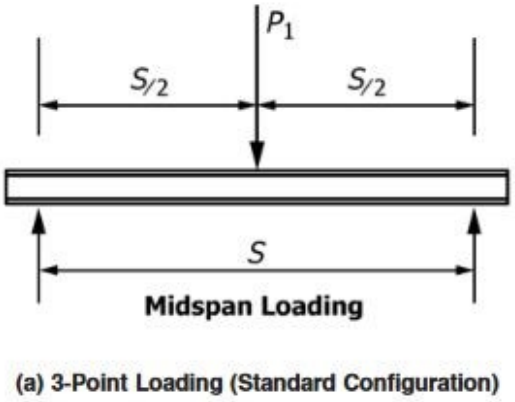

Figure 20. Schematic of 3-point bending test setup based on ASTM C393 [20]

Figure 20 shows the schematic of the 3-point bending test arrangement [20]. A brief overview of the planned bending test follows a systematic approach. We planned to perform the 3-point bending evaluation on an Instron 4415 machine with 500 N capacity in this work. We would subject the structure to a 100 N load, and we would terminate the test upon failure of the material. For the application of different loads, we planned to plot the force-displacement distribution on the sandwich structure. Furthermore, we would calculate the core shear ultimate stress and facing bending stress of the sandwich structure specimen.

We also proposed the evaluation of tensile properties of the dog-bone shaped sandwich specimens by conducting a tensile test according to the ASTM D638 standard. The research activity would primarily consist of applying a tensile force to the specimen attached firmly to a fixture in a universal testing machine. By applying a specified load on the structure and observing its failure, we aimed to evaluate the essential mechanical

properties of the specimen, particularly the ultimate tensile strength and the tensile modulus. These variables would provide us ample information about how the 3D-printed sandwich structure behaves under the application of stress.

CHAPTER 5 – NUMERICAL SIMULATION OF SANDWICH STRUCTURES (EXPERIMENTAL VALIDATION)

5.1. Introduction –Importance of Numerical Simulation

In conventional structural analysis, experimental testing plays an essential role in evaluating the mechanical properties of engineering components to ensure its structural integrity and performance. However, these preliminary tests involve applying analytical tools and the fabrication of a prototype to evaluate mechanical performance. This process is time-consuming and results in increased manufacturing costs. Moreover, the use of the analytical approach becomes tedious as more complex designs are proposed. The application of numerical simulation and Finite Element Analysis (FEA) has been rapidly gaining significance over the past few years. Numerical simulation provides the manifold benefit of applying mathematical tools to characterize a structure's mechanical performance (load-bearing capacity, fatigue, and bending characteristics) without the actual production of the part [31]. Moreover, FEA simulations enable the rigorous calculation of critical physical variables in a structure, such as stresses, strains, engineering constants, temperature profiles, etc. These parameters can be easily assessed for various areas in a structure [32]. The use of mathematical tools in the simulation provides a vital platform to predict the mechanical behavior of engineering structures. It prevents possible failure of the structure by making required modifications and mitigating design shortcomings.

5.2. Numerical Simulation of Sandwich Structures – Overview

There have been considerable research works in the realm of numerical simulation to evaluate the bending characteristics of sandwich composite structures. Anandan et al. performed a concurrent bending simulation and experimental verification of sandwich composites comprised of honeycomb core and carbon fiber-epoxy face sheets [33]. The authors successfully predicted the flexural properties and damage interaction of these laminated structures, which were in good agreement with the experimental findings. Chandra et al. presented multiple FEA simulations of glass fiber-epoxy and rigid foam core sandwich structure by utilizing ANSYS software [34]. The study evaluated shear failure forms for sandwich specimens by conducting lap shear tests and calculated flexural properties by varying density of the foam core materials. Hussain et al. conducted a unique fatigue evaluation of glass fiber-Aluminum honeycomb sandwich composites using FEA tools in ANSYS. They modeled a 3-point bending setup and performed a static and fracture analysis of the sandwich panels, yielding excellent agreement with experimental results [35]. Burlayenko et al. conducted an eccentric FEA study in ABAQUS to gauge the structural performance of a honeycomb core sandwich composites by adding foam material to the core structure [36]. The results demonstrated the relevant material significance of foam-induced structures.

Similarly, Czechowski et al. presented load-deflection data of sandwich structures utilizing a blend of face sheet and foam materials [37]. They carried out the simulation by contact modeling techniques in ANSYS. Arbaoui et al. adopted a sequential 4-point bending simulation in CASTEM 2008 to evaluate the engineering constants and load-bearing capacity of polypropylene and honeycomb core sandwich specimens [38]. There

were similar other works presented simulating the bending behavior of multi-material laminated structures.

In this work, we present a numerical simulation of a 3-point bending for a composite sandwich specimen obtained by the proposed method of nozzle-based potting described earlier. This numerical simulation aims to numerically replicate the bending test conditions in conformance with ASTM standards. The simulation would establish the importance of FEA in calculating fundamental physical variables of the 3D-printed sandwich specimens (deformation, stresses, and stiffness). The results of this work would provide an apt visualization of the bending tests, which were planned for the composite sandwich specimens utilizing polyurethane foam core and carbon fiber-epoxy face skin mixtures. A critical challenge of this work would be the accurate modeling of the layered sandwich geometry and the incorporation of thermoset material properties.

5.3. Preliminary FEA Study – Cantilever Beam Analysis

5.3.1. Motivation

In this thesis, we performed the numerical simulation of 3-point bending in the student version of ANSYS Workbench 2020 R1. Prior to implementing the bending test simulation of sandwich structures, we conducted the FEA of a simple cantilever beam problem and compared it with analytical solutions. The purpose of this study was to establish and justify the efficacy of results obtained within the constraints of the student version. With the results obtained for the beam's deformation and stress characteristics, this experiment aims to establish the efficiency of the student version and its limitations to deliver an excellent agreement with hand-calculated results.

5.3.2. Structural Analysis of a Cantilever Beam (Steel)

In the first experiment, we modeled a simple rectangular beam with steel as the material in ANSYS. The dimensions of the beam are 400 x 100 x 50 mm, and Table 6 shows its material properties.

Table 6. Properties of structural steel (ANSYS Material Library)

Material Property	Value
Density (kg/m^3)	7850
Young's Modulus (GPa)	209
Poisson Ratio	0.3

The beam is fixed at one end, and a concentrated force acts on the other free end. We analytically derived the deflection of the beam for different loads based on the formula provided below:

$$\delta_{max} = \frac{Pl^3}{3I}$$

where:

P = applied load

l = length of beam = 400 mm

I = moment of inertia of the beam = $bh^3/12$ = 1041666.67 mm^4

b = width of the beam (100 mm) and h = thickness of the beam (50 mm)

δ_{max} = maximum deflection of the beam

To validate these results, we performed the same analysis numerically in ANSYS. We modeled a cantilever beam, wherein a concentrated load acts on the structure, keeping the

other end fixed. We obtained the deflection plots for five load cases. Figure 21 (a) to (e) shows the results of the analysis.

A

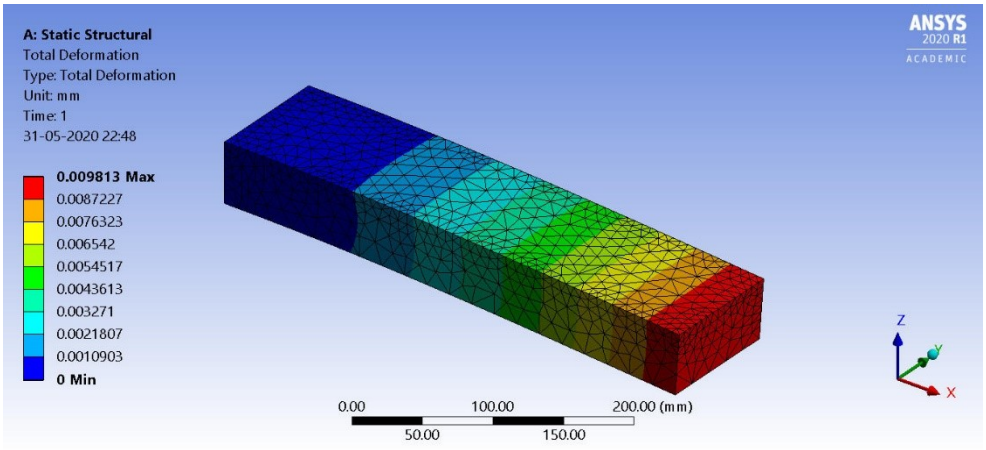

B

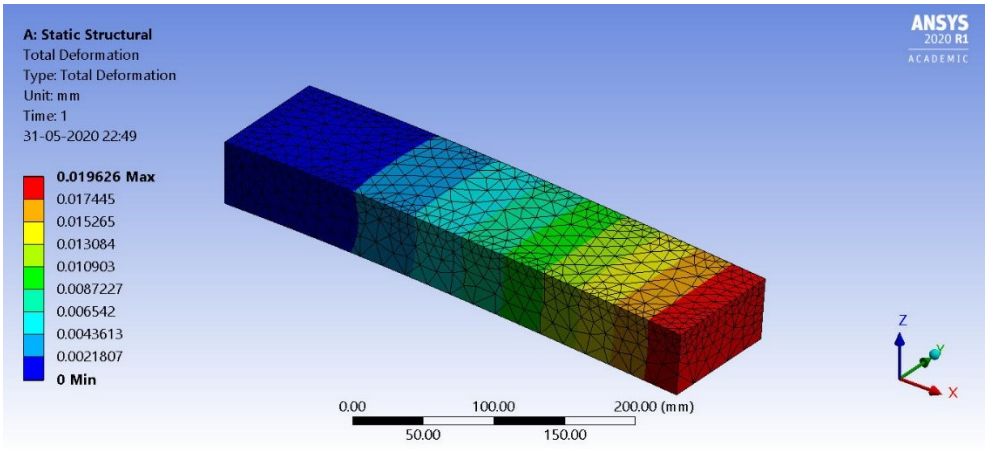

C

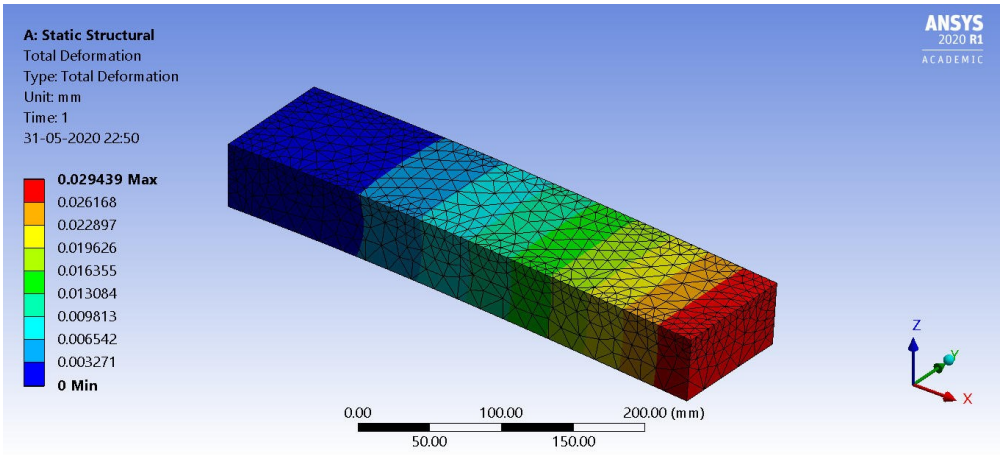

D

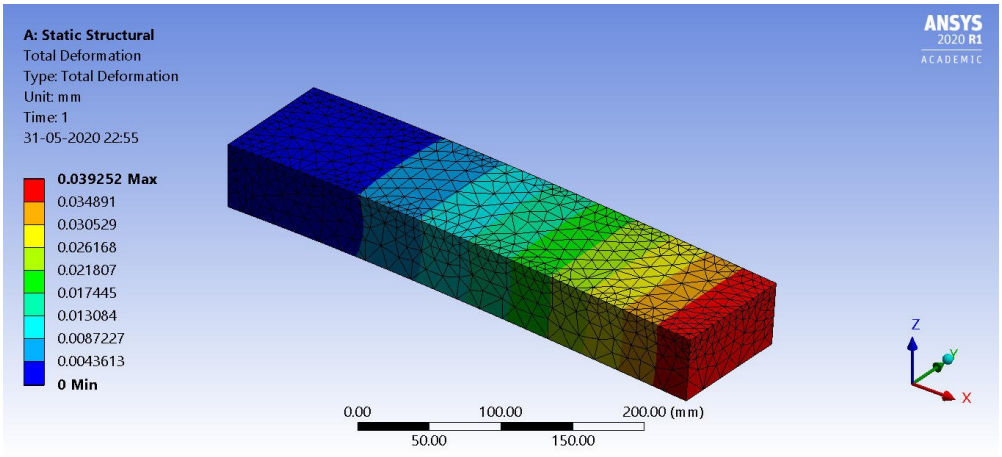

E

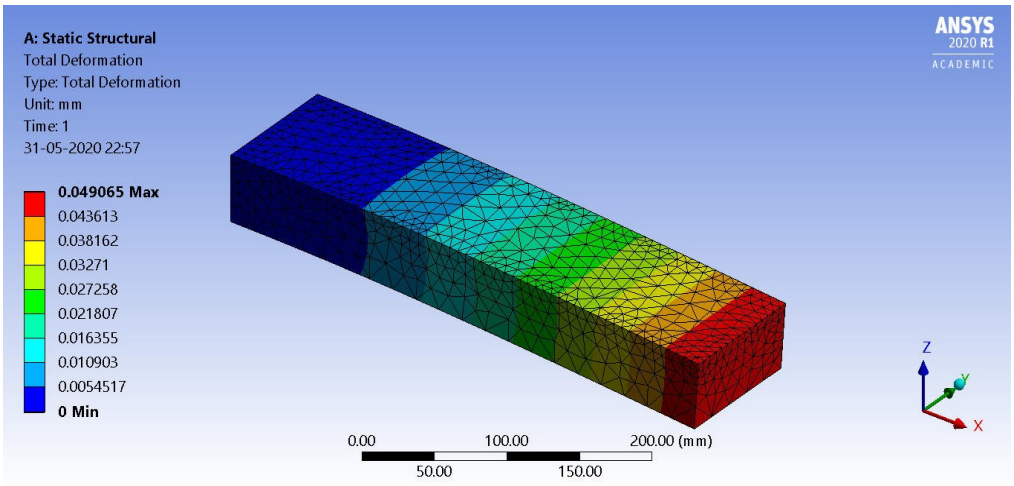

Figure 21. Results of total deformation obtained for load cases (a) 100 N (b) 200 N (c) 300 N (d) 400 N and (e) 500 N

Table 7. Comparison of total deformation (analytical vs simulation results)

Applied Load (N)	Analytical Deflection (mm)	Deflection – ANSYS (mm)	Error (%)
100	0.009799	0.009813	0.14 %
200	0.0195	0.019626	0.65 %
300	0.0293	0.029439	0.47 %
400	0.0391	0.039252	0.39 %
500	0.0489	0.049065	0.34 %

As seen in Table 7, we achieved agreement between the deflection obtained from simulation and the values attained by hand-calculations.

5.4. 3-Point Bending Simulation of Carbon Fiber-G/flex and Polyurethane Foam

5.4.1. Modeling

Figure 22 (a) and (b) depict the experimental setup of the 3-point bending test. It consists of a sandwich specimen supported by two equally spaced bars at the bottom. We subjected the beam to a concentrated force by a loading bar, that acts vertically on the beam's top face. The application of load results in the bending of the structure and permits the measurement of load-displacement data and shear properties of the beam.

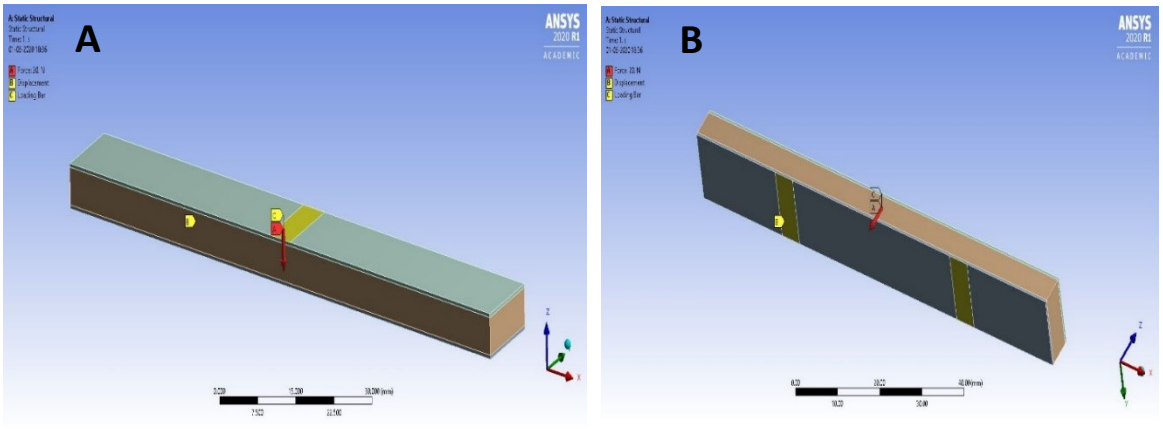

Figure 22. Setup of 3D model and boundary conditions (a) top face loading bar and (b) bottom face (supports)

Following this methodology, we simulated the sandwich beam in 3-point bending utilizing ANSYS Workbench. First, we produced a 3D model in ANSYS Design Modeler. It consisted of creating a beam and slicing it into three bodies by creating planes. These planes represent the corresponding thicknesses of the fiber face skins and the foam core material. A significant challenge while formulating boundary conditions for simulation is to prevent rigid body motion due to inadequate constraints. To model the support and loading bar acting on the structure, we split the beam into two small faces on the bottom and a partition face on the top for the application of load. As this specimen is for a non-standard configuration and of minimal dimensions, we relaxed the addition of pressure pads for simplicity.

5.4.2. Setup and Boundary Conditions

With the generation of geometry, we assigned composite materials to the sandwich specimen. This consists of allocating carbon fiber-G/flex (CF-GF) to the top and bottom

layers (skins) and polyurethane foam to the central body. Table 8 lists the relative properties of these engineering materials, which we constructed in ANSYS.

Table 8. Material properties of fillers, epoxy and foam core used in this study (obtained by hand-calculations for fillers and from Kim et al. [23] for foam)

Material	Young's Modulus (MPa)	Poisson's Ratio	Density (kg/m^3)
Carbon fiber – G/flex (CF-GF) epoxy	7242	0.3	1122
Polyurethane Foam	31.6	0.3	96.1

Next, we subjected the beam to appropriate boundary conditions. As shown in Figure 22, we constrained the two bottom face partitions in the vertical Z-direction to represent the supports. We applied five different sets of concentrated loads from 20 N to 100 N in the vertical direction (Z-axis) to simulate the application of force via the loading bar. We meshed the geometry with tetrahedron elements, as shown in Figure 23.

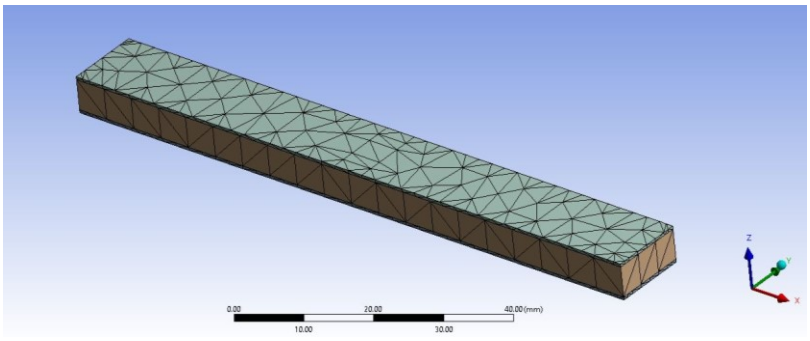

Figure 23. Mesh generation of the sandwich structure

5.4.3. Results

Figure 24 (a) to (e) depict the resulting deflections induced in the structure upon load application of 20, 40, 60, 80, and 100 N. Additionally, Figure 25 shows the sandwich structure specimen's load-deflection behavior which is plotted on a graph. With these load-deflection results, we attempted to provide a platform for numerically simulating the load-bearing capacity of sandwich structures. The idea was to model the conditions proposed in the experimental tests and evaluate the feasibility of numerical simulations. Key elements of this simulation were modeling the structure and the proper assignment of boundary conditions. This study also provides scope to explore more aspects of structural performance and evaluation of subsequent parameters.

A

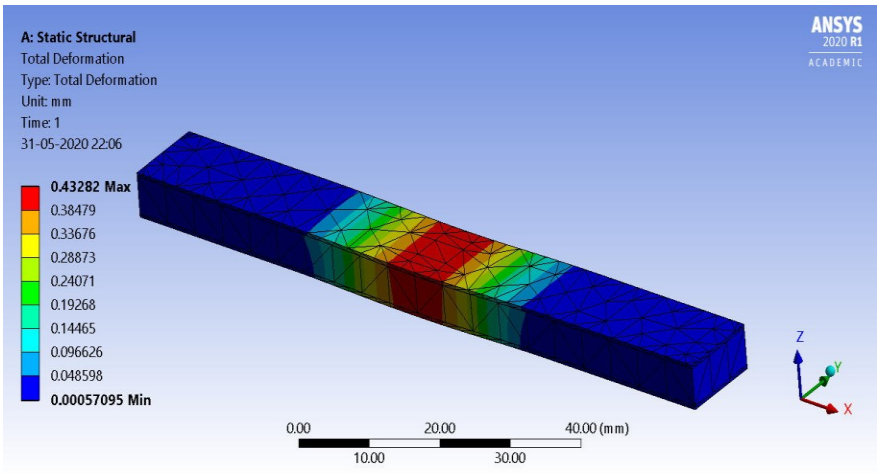

B

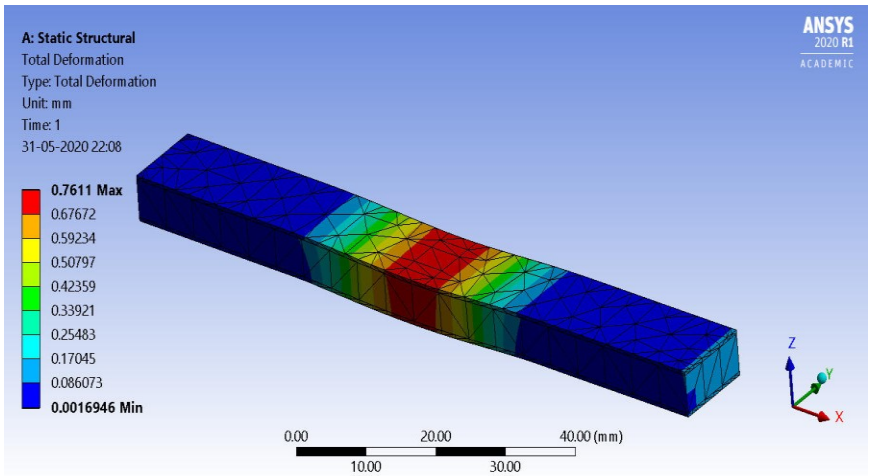

C

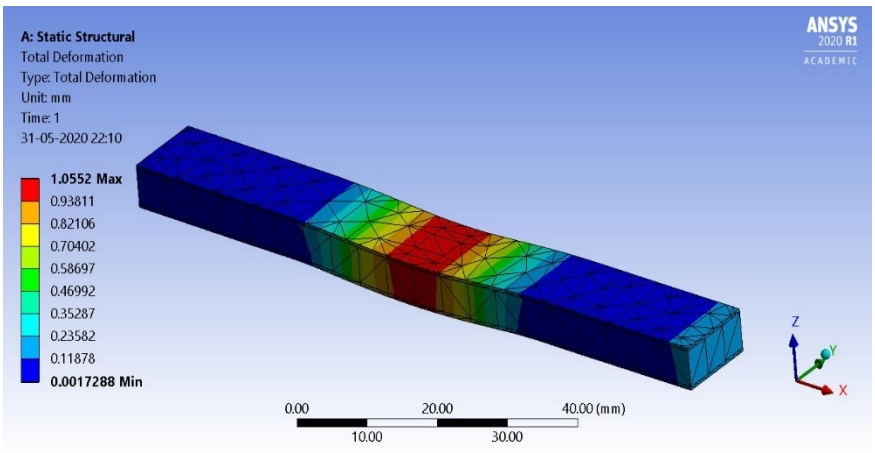

D

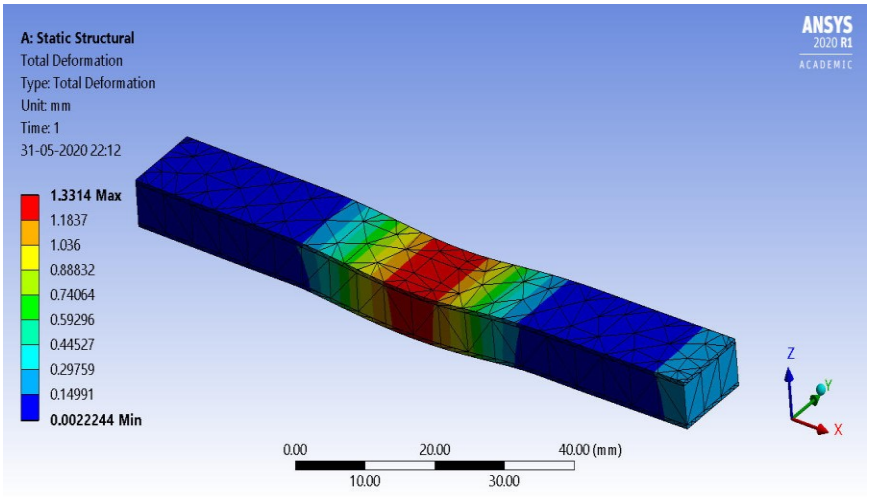

E

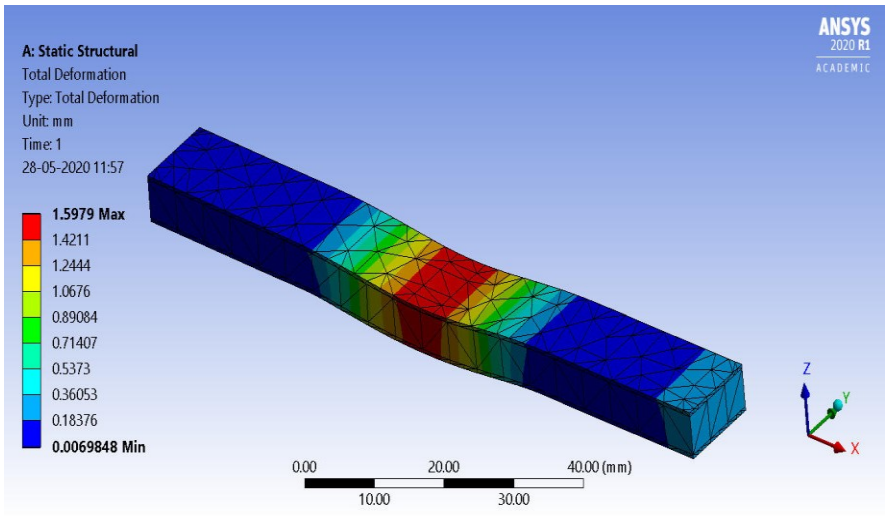

Figure 24. Results of total deformation obtained for load cases (a) 20 N (b) 40 N (c) 60 N (d) 80 N and (e) 100N

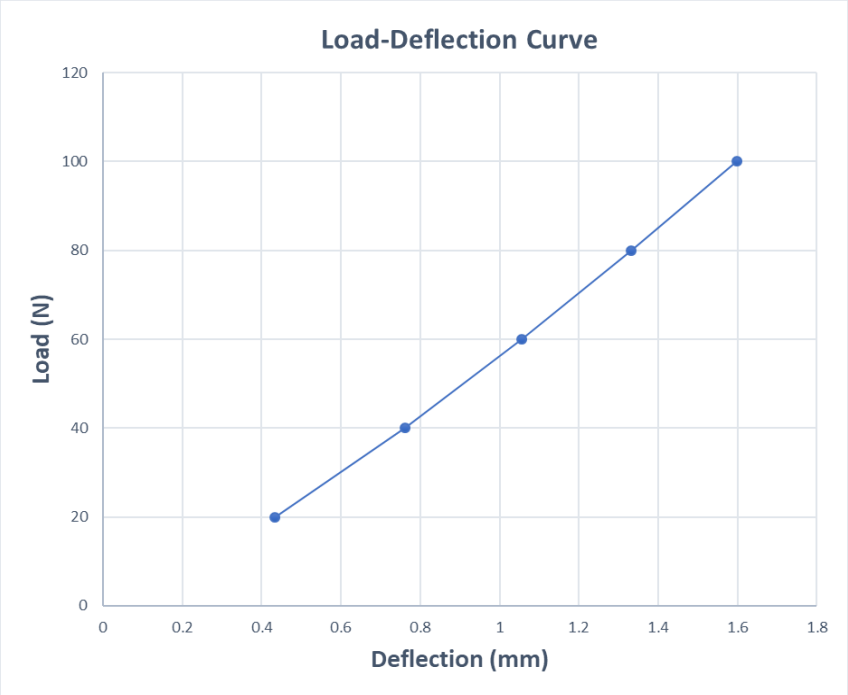

Figure 25. Plot of Load vs Deflection for 3-point bending test

CHAPTER 6 – STRUCTURAL OPTIMIZATION OF SANDWICH COMPOSITE STRUCTURES

6.1. Introduction

The composition of a sandwich structure must be a synchronous blend of characteristics, namely minimum weight, superior stiffness, excellent load-sustaining capacity, etc. These design goals must be achieved at the minimum cost possible while maintaining the structural integrity of the composites. Thus, one can aptly visualize the design of a sandwich structure as an optimization problem [39]. In engineering, structural optimization refers to finding the most efficient configuration of a structure that achieves intended design goals for the successful functioning of the component. In simpler terms, a design optimization problem of an engineering structure consists of the following elements:

Objective Function: a function which is intended to be minimized or maximized, based on the design goal

***Design Variables*:** a set of parameters that are varied to achieve the optimization of the objective function

Constraints: limits imposed on the optimization study (expressed as inequalities or equalities), which must be satisfied by the design variables.

Depending on the complexities of structure, numerous combinations are feasible for these constituents. When considering the optimal design of a composite sandwich structure, the primary goal is to minimize the structure's weight and reduce the fabrication cost. Thus, the weight and cost of the composition constitute essential objective functions

of the optimization. The design parameters are generally the dimensions of the sandwich structure, such as the respective thicknesses of the core and fiber-reinforced skin layers.

Alternatively, material properties (such as density, Young's modulus) is also of considerable importance when considering the efficient design of sandwich composites. One must successfully achieve the optimization process within the domain of certain critical engineering requirements. For instance, the sandwich structure's minimum weight and cost must be achieved for a configuration that has a pre-defined bending or torsional stiffness. Additionally, mathematical restraints exist linking the corresponding dimensions of the layered structure, which are essential to ensure the integrity of the structural parts. These limitations qualify as constraints of the optimization task.

There are numerous domains of optimization problems concerning the geometry of structure [40]. Design or sizing optimization refers to deducing the optimal dimensions of structural components based on design variables and constraints. Topology optimization is the novel technique of transforming a structure to a robust design by typically varying the material organization (removal or composition of the material) for weight and cost-saving. Shape optimization is another exiting branch which consists of finding the most suitable shape of a structure that satisfies a set of constraints while minimizing critical objective functions, such as deflection, loads, stress distributions, etc.

An eccentric classification of optimization problems depends on the objective functions employed. A single-objective optimization utilizes a single design goal (such as the weight of a structure), by its minimization. Multi-objective optimization problems involve more than one objective function. They are typically employed to establish a trade-

off between multiple design goals to achieve the most efficient configuration of the structure [41].

From the perspective of structural configuration, design and topology optimization methods are usually implemented by analytical tools for simple geometries. More recently, built-in algorithms in commercial FEA packages (ANSYS, COMSOL, ABAQUS, SolidWorks, etc.) perform optimization tasks for more complex engineering structures for which an analytical approach to formulate objective function becomes tedious. Moreover, mathematical algorithms and numerical analysis methods in software such as MATLAB and Python perform single-objective and multi-objective optimization problems involving linear and non-linear constraints.

6.2. Optimization of Composite Structures – Background

Copious research works with promising results have been documented for optimizing composite structures and sandwich construction designs. Alteyeb et al., in their research paper, presented the optimization of a cantilever I-beam for minimum mass in ANSYS [42]. By subjecting the beam to a static load at one end, he deduced the optimal flange width and the beam height for the minimum weight of the structure while remaining within the constraints of maximum allowable stress. Nandi et al. performed an efficient optimization study of an all-steel sandwich panel in ANSYS by specifying a set of criteria [43]. The elements involved minimum weight, a simply supported geometry, a deflection domain of 0.5 mm, and an allowable stress. Based on this analysis, the authors obtained the core and facings' relative thicknesses, achieving the minimization of the objective function. In his dissertation, Adeel presented a novel research work of a multi-objective weight and cost optimization of sandwich structures in the hybrid composition [44]. He

used carbon and glass fiber-epoxy hybrid mixture for the face skins while selecting foam for the core. He presented a comprehensive analysis of the optimum weight and cost of the sandwich composition. He obtained their resulting trade-off by utilizing the 'Active Set Algorithm' and 'Pareto filter' in MATLAB. The bending and torsional stiffness were the main constraints of this research work, while the ply configuration of the face sheets and core thickness constituted the design variables. Additionally, he documented a single-objective optimization minimizing the weight and cost separately with an interior-point algorithm.

Almeida et al. documented an intricate design optimization task of laminated composites by implementing the blend of the Genetic Algorithm (GA) and Finite Element Analysis (FEA). The authors performed a multi-objective optimization study minimizing the combination sets of weight, deflection, and cost of the composite structures for in-plane and transverse loading conditions [45]. They set the limiting parameters establishing the failure of the structure as the experimental constraints.

Abolfazl et al. adopted a chronological optimization work for a composite sandwich panel constructed by a corrugated core. They initially calculated the first objective function (deflection) using the Finite Element Method in ANSYS [46]. The authors later coupled the FEA code for this optimization with the NSGAII algorithm in MATLAB to simultaneously establish the trade-off between the obtained deflection and weight of the composite structure as a Pareto-front. As commonly employed, they set the thicknesses of the beam as the optimization variables.

6.3. Structural Optimization of Sandwich Composites – Thesis Overview

In this research, we performed a comparative analysis of five different structural optimization methods depending on the objective functions and the structure's geometrical complexity. The first three experiments in the thesis demonstrate the application of FEA and the optimization module in ANSYS to minimize the mass of three innovative design structures predominantly used in the aerospace industry. The next two optimization methods present single-objective optimization experiments utilizing algorithms in MATLAB on multi-material sandwich structures and their comparative performance with homogeneous material composition. Cost and weight constitute the single objective functions in these two studies, respectively. The primary goal of these extensive optimization analyses is to provide a platform for evaluating the design of sandwich structures for minimizing their weight, maximizing strength, both at a specified cost and material usage. Such a successful combination of design goals is a stringent requirement in the aerospace industry, where a fraction of design saving can result in a significant reduction of cost. At the same time, one must achieve this preservation in conjunction with maintaining the part's structural integrity.

As we have a unique fabrication process of nozzle-based additive manufacturing, the optimization efforts presented in this thesis aim to devise a numerical framework uniquely suitable for the three co-related disciplines of additive manufacturing, sandwich composites, and thermoset materials. The design geometries that we proposed can potentially best be produced by AM and can be fabricated efficiently using the potting process that we proposed in this work. Figure 26 presents a schematic of the optimization methods:

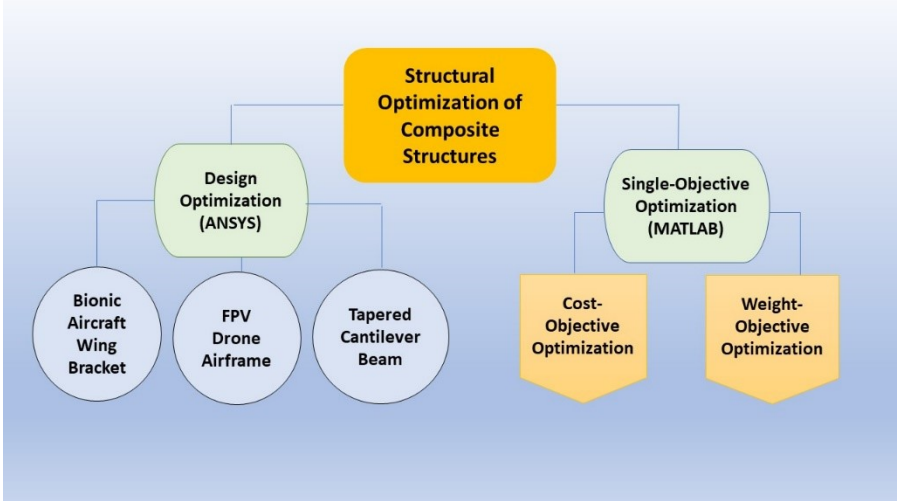

Figure 26. Overview of optimization studies performed

6.4. Design (Mass) Optimization of a 3D-printed Aircraft Wing Bracket

6.4.1. Overview

The first three evaluations in this thesis demonstrate the use of optimization modules in the commercial FEA package (ANSYS) to perform mass optimization of inventive engineering designs used in the aerospace industry. The objective of these designs is to model structures with dimensions that can be fabricated efficiently by additive manufacturing. The first optimization investigation in this thesis considers the unconventional design of an aircraft wing bracket produced by AM. As presented in Figure 27, this design is referred to as the 'bionic' concept and manufactured by GE Additive in collaboration with Concept Laser (German 3D printer company). They built this bionic wing bracket for the avant-grade generation of Airbus A350 XWB commercial aircraft [47]. As the name suggests, the geometry adopts design from nature and optimizes the production geometry in the commercial aircraft sector. The bionic wing bracket concept won the coveted German Federal President's prize in 2015.

Figure 27. Bionic wing bracket design of an Airbus A350 XWB aircraft fabricated by GE Additive. (Source: General Electric [47])

Considering this pioneering idea of a wing bracket produced by AM, this thesis aimed to explore how updating the model with a sandwich structure yields an optimal solution for the bracket's structural mass. Thus, we evaluated this design for the most optimum dimensions for superior strength by employing our thermoset materials and the proposed polyurethane foam core in this research. As described in the first chapter, we termed the mixture of carbon fiber-G/flex and polyurethane foam as a 'sandwich material' while we abbreviated pure carbon fiber-G/flex material as 'CF-GF'. We will use these terminologies frequently in the subsequent sections

6.4.2. Modeling

As shown in Figure 28, we designed a simplified version of the engine bracket in ANSYS Design Modeler. We assigned the sandwich material arrangement to the bracket base, while modeling the bionic curved part with carbon fiber and G/flex (CF-GF) materials.

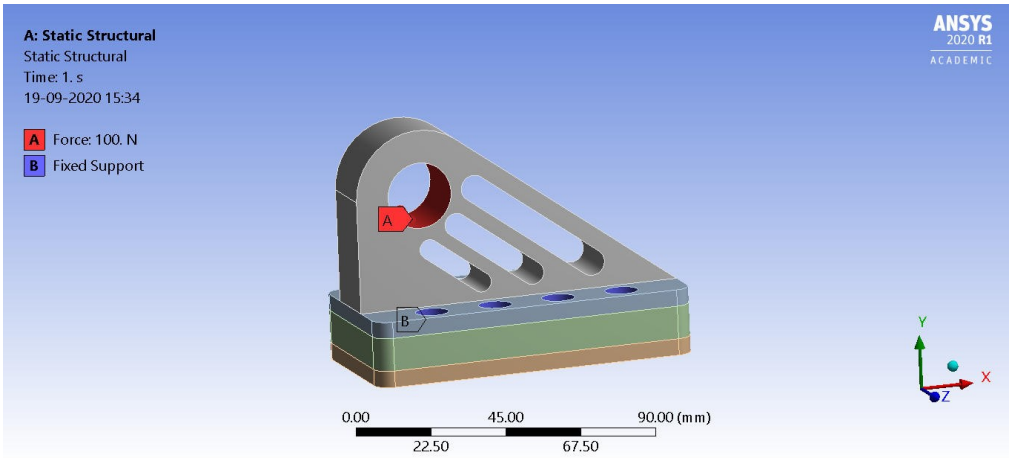

Figure 28. Simplified 3D model of the wing bracket in ANSYS (force applied and boundary condition) based on the GE bionic wing design [47].

To achieve a reduction in weight and optimize topology, we incorporated holes and fillets into the design, a concept widely adopted in the design of aircraft wing structures [40]. The overall thickness of the base structure is 20 mm. The core and the face skin of the base are 5 mm and 10 mm thick, respectively. We set the upper skin thickness (t) and core thickness (c) values as the design parameters of optimization. Additionally, we assigned the diameter (d) of the upper hole (20 mm) as a critical design parameter to evaluate its effect on the bracket's mass and corresponding stress and deflection distribution. For the case of a bracket consisting only of the fillers and the epoxy, the overall beam thickness and the hole diameter constitute the design variables.

6.4.3. Boundary Conditions and Setup

The structure is fixed in its base by applying constrained motion along each of the holes, while the hole in the vertical structure is subjected to a static load of 100 N. As shown in Figure 29, we meshed the entire model with a 'sweepable mesh arrangement,'

generating a tetrahedron distribution. This mesh arrangement is commonly known as ‘patch conforming mesh’ in ANSYS.

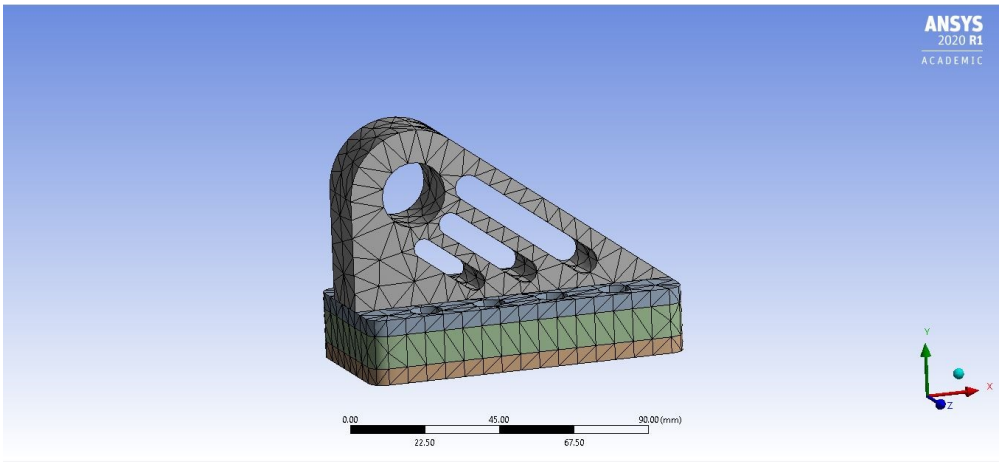

Figure 29. Mesh distribution of the sandwich-structured bracket

Essentially, a patch confirming method generates finer mesh at all specks of the structure and is ideal for simple geometric models [48]. Moreover, as a measure of refinement, we set the parameter ‘span angle center’ to the fine setting. It should be noted that the student version imposes certain limitations in terms of nodes and elements. Thus, we have adopted the most suitable mesh arrangement that yields accurate results for this version. We then solved the structure for total deformation and equivalent (Von-Mises) stress.

6.4.4. Structural Analysis Results – Setup of Optimization

A vital step before initiating the optimization evaluation is the definition of the elements of optimization. One must achieve this step by parametrizing the study variables while performing the basic static structural analysis in ANSYS. As described in the previous section, the input parameters were the thickness of the beam layers and the hole diameter. After performing the static structural analysis, we parameterized the geometry

mass in ANSYS Mechanical as an output parameter (known as an objective function). We additionally parameterized the maximum total deformation and maximum equivalent stress obtained, and these two elements constituted the constraints of the design problem. Following the structural simulation and definition of the constrained optimization problem, we implemented ANSYS 'Design of Experiments' algorithm from the 'Design Exploration Tab.' The concept of design exploration typically comprises of performing a parametric analysis based on a specified design domain. The module solves the 3D model developed in ANSYS Workbench according to the design input and output parameters specified in the study. It generates a robust overview of the effect of these parameters on the output variables of the problem. The optimization solution generates response surface plots, sensitivity analysis of the structural parameters, and the concurrent analysis of design points for a set of iterations [49]. This consolidated data generates a final optimized value of the objective function desired and is an efficient means to analyze the geometry. It constitutes a powerful model that enables engineers to make logical decisions based on FEA principles without manually fabricating and testing structural parts.

We assigned lower and upper limit values to the parameterized values of core and upper skin thicknesses for this study. Figure 30 shows the setup of the parameter window for optimization. We solved the model for various design points, and the results yield the minimum mass and corresponding dimensions of the beam to achieve the intended optimization goal.

A

Outline of Schematic A8: Parameters

	A	B	C	D
1	ID	Parameter Name	Value	Unit
2	Input Parameters			
3	Static Structural (A1)			
4	P1	hole.diameter	20	mm
5	P2	skin.thickness	5	mm
6	P3	core.thickness	10	mm
*	New input parameter	New name	New expression	
8	Output Parameters			
9	Static Structural (A1)			
10	P4	Geometry Mass	0.10282	kg
11	P5	Total Deformation Maximum	0.035555	mm
12	P6	Equivalent Stress Maximum	2.778	MPa
*	New output parameter		New expression	
14	Charts			

B

A	B
Property	Value
General	
Units	mm
Type	Design Variable
Classification	Continuous
Values	
Lower Bound	8
Upper Bound	12
Allowed Values	Any

Figure 30. A typical layout of the optimization window in ANSYS (a) Parameters Tab and (b) limits of design variables

6.5. Design (Mass) Optimization of a First-Person View (FPV) Drone Airframe

6.5.1. Overview

Composite materials have recently gained great significance in the production of small-scale parts for the drone industry. Their ability to withstand critical loads and being lightweight has rendered their popularity in the aerospace industry. The material superiority of composite structures has been merged with the rapid nature of additive manufacturing (AM) to produce structural parts such as airframe, wings, and support structures for unmanned aerial vehicles (UAVs). In this work, we attempted to amalgamate the convergent benefits of AM, sandwich design, and thermoset materials. The idea was to create a numerical platform to design a sandwich-structured airframe for drones employing First-Person View (FPV) technology. We conducted a mass optimization study for this novel design and compared the weight-saving results with pure fiber-reinforced construction. The model adopted in this study is based on carbon fiber-foam sandwich

structures, which is commonly known as ‘oreo-carbon’ in the drone industry [50]. Figure 31 (a) depicts the design of the drone airframe.

6.5.2. Modeling

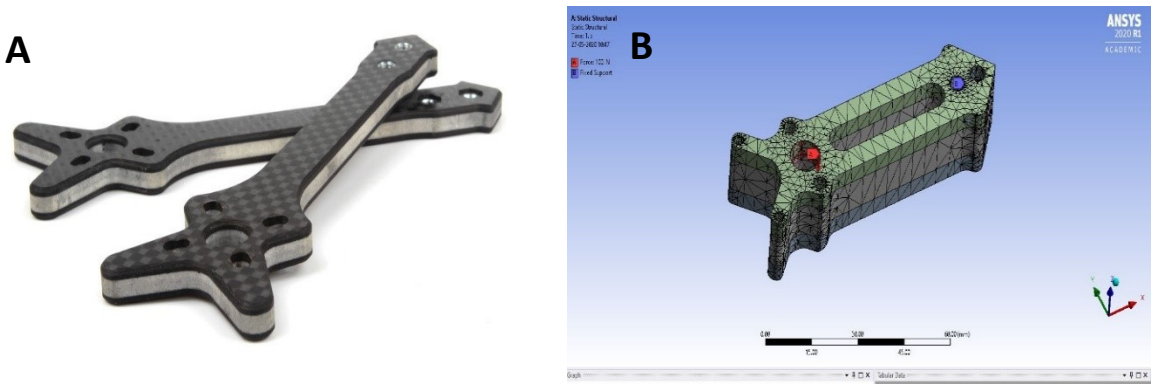

Figure 31 (a) An oreo-carbon foam sandwich structure (b) 3D model of the airframe in ANSYS (Source: GetFPV Learn [50])

Figure 31 (b) shows the designed geometry of the airframe in ANSYS Design Modeler. The overall thickness of the airframe is 20 mm. To obtain the sandwich structure, we segregated the component into the top and bottom domains of 5 mm each for fibers and a 10 mm central foam core component. For pure carbon fiber-G/flex (CF-GF) arrangement, we modeled a single entity of total thickness (20 mm) for this design.

6.5.3. Boundary Conditions and Setup

As shown in Figure 31 (b), we applied a static load of 100 N in the vertical direction to the top opening of the airframe. We restricted the motion of the circular openings at the tail of the airframe structure. We conducted a similar analysis of the bionic wing concept where we evaluated the structure for maximum deformation and equivalent stress to formulate the constraints of optimization. As described in the bionic wing model, we assigned a tetrahedron patch conforming mesh for the airframe structure.

6.5.4. Structural Analysis Results – Setup of Optimization

We obtained the total deformation and equivalent (Von-Mises) stress for sandwich material geometry and CF-GF construction. These comprise the constraints of the optimization problem. As the case with the bionic wing bracket design, the key element in this study is the assignment of design variables. As evident from the geometry, we have designed holes into the airframe construction. Incorporating holes is not an arbitrary decision. We employed holes to serve as an efficient means to reduce weight in the structure while maintaining its strength. This hollow-shaped design enables tremendous sustain of material cost in drone fabrication by removing material in non-critical areas of the structure. For this purpose, we assigned the circular hole's diameter (d) designed in the front part of the airframe as a design parameter along with the airframe's core (c) and lower skin thickness (t). This assignment lets us visualize the effect of varying the diameter of the opening on the optimum mass of the structure. Further, it facilitates an understanding of how stress, deflection and the remaining dimensions of the structure interact with the relative changes in the drone airframe's hollow design. Finally, we set the geometric mass of the model as the objective function of the problem. We performed the analysis similarly to the first study for the two cases of sandwich material and pure CF-GF compositions. The analysis implements the 'Design of Experiments' optimization tool in ANSYS.

6.6. Design Optimization of Tapered Cantilever Sandwich Beam

6.6.1. Overview

In the final optimization study, we performed mass optimization of a tapered cantilever beam employing the sandwich material configuration. The task primarily consists of fixing one end of the beam and applying a load at the other end. With the

deformation and stress distribution obtained, the aim was to evaluate the most suitable beam dimensions to achieve the minimum mass for a specified value of deformation and equivalent stress.

6.6.2. Modeling

Figure 32 shows the geometry of the tapered beam configuration in ANSYS Design Modeler. We sliced the model into three bodies to obtain the sandwich layout. As with the previous designs, we assigned carbon fiber-G/flex (CF-GF) to the upper and bottom portions and set polyurethane foam as the core material. For the case of the CF-GF beam, we adopted similar modeling without the need for slicing the beam geometry.

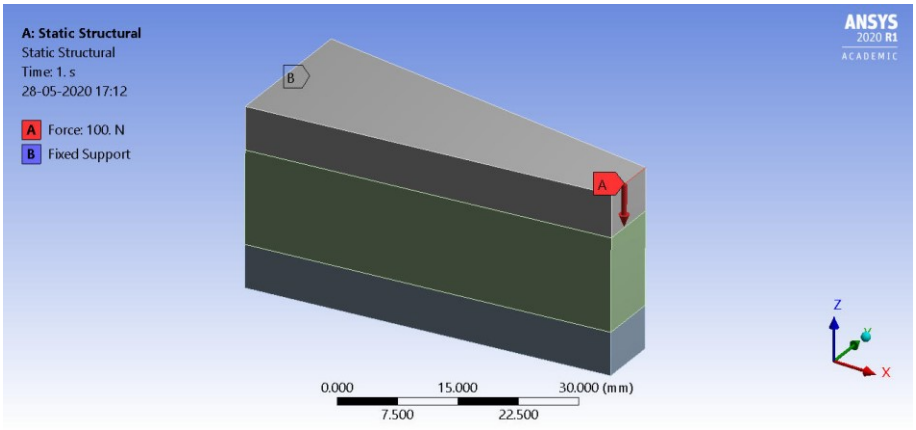

Figure 32. Modeling and specification of boundary conditions for a tapered sandwich beam in ANSYS

6.6.3. Boundary Conditions and Setup

As shown in Figure 32, we assigned fixed support to one end of the while a concentrated vertical load of 100 N acts on the free end. We solved the model in ANSYS

for total deformation and equivalent (Von-mises stress). We assigned tetrahedron distribution of patch conforming mesh to the structure of the beam.

6.6.4. Structural Analysis Results – Setup of Optimization

As the geometry, in this case, is a simple construction of tapered configuration, we assigned the core (c) and lower skin (t) thickness of the beam as the only design variables. We carried out the optimization without the incorporation of cut-outs in the structure. Upon solving the model, we attained the distribution of total deformation and equivalent stress by applying static load for the sandwich material construction and pure fiber-filled CF-GF configuration. Then, we set the maximum values of these entities as the output parameters (constraints) of optimization, while the geometry mass remains fixed as the objective function. We initiated the 'Response Surface' optimization and solved the model to obtain the most efficient mass.

6.7. Single-Objective 'Cost' Optimization of Sandwich and Pure Composite Beams

The next set of studies in this thesis focused on performing structural optimization using built-in algorithms in MATLAB to minimize a single objective function (design goal). For this work, we chose the cost and weight of engineering structures as the objective functions. In the first experiment, we performed a minimum-cost optimization for three rectangular beam configurations:

1. Sandwich material structure (Carbon fiber – G/flex skin and polyurethane foam core)
2. Solid carbon fiber – G/flex (CF-GF) beam
3. Solid aluminum alloy beam

Table 9 lists the essential physical characteristics and cost information of all the materials. employed in the optimization study.

Table 9. Physical properties and cost values of three material configurations. Calculations based on material data [25] and Adeel [44] for carbon fibers, Kim et al. [23] and material data [27] for foam and ANSYS Material library for aluminum alloy

Property	**Carbon fiber – G/flex (CF-GF)**	**Polyurethane Foam**	**Aluminum alloy**
Density (kg/m^3)	1122	96.1	2770
Cost per kilogram ($/kg)	183.84	44.2	2.18
Young's Modulus (MPa)	7242	31.6	7100

The objective of employing these materials was to analyze the effect of fiber-reinforced and sandwich materials on manufacturing costs. For this study, we selected a rectangular geometry. The formulation of cost objective function and constraints is more straightforward for rectangular beams as analytical expressions representing deflection, weight, and cost are readily available in the literature. The geometry of the sandwich material structure is a solid rectangular arrangement, as shown in Figure 33. However, we incorporated two circular openings on either end of the beam for a solid CF-GF and aluminum alloy beam. We introduced openings to increase the number of design variables in the optimization problem and as a weight-saving strategy described in the previous sections. Figure 34 shows the model of the beam.

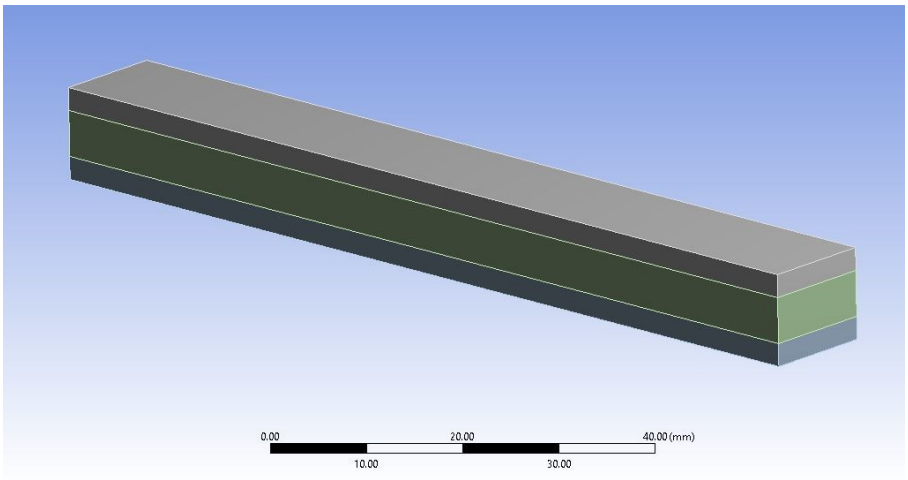

Figure 33. A representative model of a sandwich structure for optimization in MATLAB

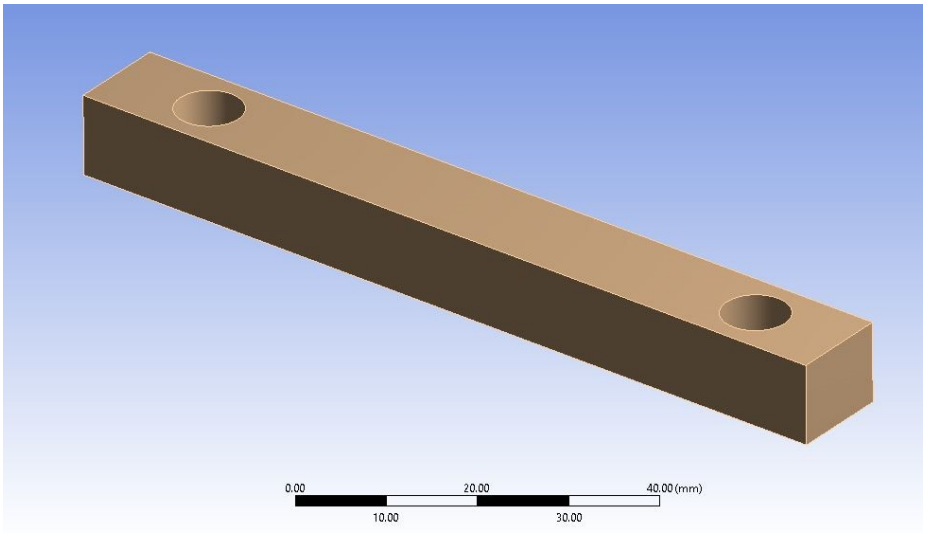

Figure 34. A representative model of carbon fiber-epoxy and Aluminum alloy beams for optimization in MATLAB (with circular openings at either

The following are the constituents of the optimization problem:

6.7.1. Objective Function:

Based on the objective function formulation presented in Adel's dissertation [44] and the cost function described by Hodicky et al. [51], a special equation represents the total cost of the sandwich structure ($):

$$C_{sandwich} = [2\ (t\ \rho_f\ C_f) * 2\ (lb+bt+lt)] + [(\rho_c\ C_c\ c) * 2\ (lb+bc+cl)]$$

Surface area of face skin

Surface area of core

where:

t = thickness of the carbon fiber – G/flex face skins

c = thickness of core

ρ_f = density of carbon fiber – G/flex face skins

ρ_c = density of polyurethane foam core

C_f = cost per unit weight of carbon fiber – G/flex face skins

C_c = cost per unit weight of polyurethane foam core

l and b = length and width of the sandwich beam, respectively

A careful observation of this equation is necessary to understand the formulation of the objective function. Mainly, the cost function is divided into terms, representing the cost of manufacturing the face skins and core of the sandwich beam. The first term in each of these two expressions corresponds to cost per area of the beam, while the second term corresponds to the surface area of the respective segments of the sandwich structure. In this equation, the thickness of the core and the face skin are the unknown values (design

variables) while we know all other parameters. After incorporating values of the beam geometry and material properties from Table 9, we get the following simplified equation:

$$C_{sandwich} = 412489.16\ t\ (0.0024 + 0.224\ t) + 4248.09\ c\ (0.024 + 0.224\ c)$$

Similar to the case of sandwich material structures, the cost-function for pure composite (carbon fiber-G/flex) and aluminum alloy beams generates a simple expression since no segregation of core or face skin exists. However, as the geometry for these beams incorporates holes, it is necessary to subtract the surface area of the hollow portions from the cost function. These can be evident in the following equations below:

Cost of carbon fiber-G/flex solid beam,

$$C_{CF\text{-}GF} = (t\ \rho_f\ C_f) * [2\ (lb+bt+lt) - 2\ (2\pi rt + 2\pi r^2)]$$

Surface area of face skin

Surface area of circular openings

Similarly, cost of aluminum alloy solid beam,

$$C_{Al\ alloy} = (t\ \rho_{Al}\ C_{Al}) * [2\ (lb+bt+lt) - 2\ (2\pi rt + 2\pi r^2)]$$

where

r = radius of the hole in the beam (design variable)

ρ_{Al} = density of aluminum alloy

C_{Al} = Cost per unit weight of aluminum alloy

Substituting values from Table 9, we get the resulting cost-functions depicted below:

$$C_{CF\text{-}GF} = (206244.58\ t) * [0.0024 + 0.224t - 12.56\ tr - 12.56r^2]$$

$$C_{Al\ alloy} = (6038.6\ t) * [0.0024 + 0.224t - 12.56\ tr - 12.56r^2]$$

6.7.2. Design Variables:

For a sandwich-structured beam, we assigned the core and face skin thicknesses as the two design parameters to minimize the cost. On the other hand, for solid CF-GF and aluminum alloy beams, a single entity (total beam thickness) exists in the absence of the core material. However, as these designs incorporate circular holes to save weight, we set the radius of this opening (r) as the design variable along with the beam's total thickness (t).

6.7.3. Constraints:

Considering the minimum cost design goal with the maximum strength, we set the bending stiffness (P/δ) as the nonlinear constraint in all three structural configurations. In solid mechanics, the bending stiffness of a structure is the ability to withstand or resist bending loads. Bending or flexural stiffness is a vital parameter in the design of aerospace structures. A high bending stiffness coupled with a reduced mass renders excellent structural rigidity; a trait highly desirable in commercial aircraft wing components. For a sandwich beam in a 3-point bending configuration, we can deduce the bending stiffness from the beam's compliance. According to Gibson and Ashby [39], the compliance of the beam for a sandwich structure is given by:

$$\frac{\delta}{\mathrm{P}} = \frac{2l^3}{48E_f btc^2} + \frac{l}{4bcG_c}$$

Where E_f = Young's modulus of face skin

G_c = Shear modulus of Polyurethane foam

l = support span

b = width of the beam

c = core thickness

t = face skin thickness

For a solid rectangular beam without sandwich structure in 3-point bending configuration, a simple equation below describes the bending stiffness:

$$\frac{P}{\delta} = \frac{48EI}{L^3}$$

Table 10. Bending stiffness constraint values for the three beams (obtained from literature – Gibson et al. [39], Rathnakar et al. [52], Soares et al. [53] and Ashby [54])

Material Configuration	Bending Stiffness constraint (N/m)
Sandwich – structured beam	10^5
Carbon fiber – epoxy solid beam	1.2 x 10^5
Aluminum alloy solid beam	7.2 x 10^5

From these equations, we obtained the constraint equation in terms of the free design variables for the three structural beams. We assigned a model value of bending stiffness to this constraint equation to attain the full non-linear equality constraint for the optimization process. We have obtained the model values of bending stiffness for sandwich

beams [39], carbon fiber-epoxy [52, 53], and aluminum alloys [54] after observing a range of values from relevant literature as shown in Table 10.

The main objective of selecting these model values for setting the bending stiffness is that it allows us to fix a design goal targeted for the aerospace industry. The materials employed in this optimization, namely carbon fibers, polyurethane foam, and Aluminum alloys, find extensive application in the manufacturing of aircraft structural components. Optimizing the 3D-printed beams for these reference values gives us an estimate of its cost and weight for a bending stiffness constraint that can be of potential application in aeronautical and space manufacturing.

Figures 35 (a), (b), and (c) depict the script functions for bending stiffness configuration for each of the three configurations. It can be observed in the figure that the variables ‘x1’ and ‘x2’ correspond to the design parameters, while the last term in the expression constitutes the model values of bending stiffness listed in Table 10.

A

constone.m

```
function [C, Ceq] = constone(x)
C = [];
Ceq = [((9.36e17*x(:,1).*x(:,2).^2)./(56100 + (8.69e10*x(:,1).*x(:,2))))-1e5];
end
```

B

consttwo.m

```
function [C, Ceq] = consttwo(x)
C = [];
Ceq = [(2.7808e15)*((0.001*x(:,1).^3)-(1.57*x(:,2).^4))-1.2e5];
end
```

C

constthree.m

```
function [C, Ceq] = constthree(x)
C = [];
Ceq = [(2.7264e16)*((0.001*x(:,1).^3)-(1.57*x(:,2).^4))-7.2e5];
end
```

Figure 35. MATLAB functions representing non-linear constraint (bending stiffness) for (a) sandwich-structured (b) CF-GF and (c) Aluminum alloy beam

Table 11 lists a summary of the constituents for the cost-objective optimization process for the three configurations.

Table 11. Summary of elements for cost-objective optimization of three beam configurations

Elements	**Sandwich Material**	**Carbon Fiber – G/flex (CF-GF)**	**Aluminum alloy**
Objective Function	Cost ($)	Cost ($)	Cost ($)
Design Variables	Skin thickness (t) core thickness (c)	Beam thickness (t) Radius of hole (r)	Beam thickness (t) Radius of hole (r)
Constraints	Bending Stiffness	Bending Stiffness	Bending Stiffness

6.7.4. Optimization Toolbox – MATLAB

With analytical expressions obtained, we created function scripts in MATLAB to perform for elements of the optimization process. We utilized the optimization to get the minimum function value (cost) of the designed composite beam and the optimum dimensions. The most important aspect of this problem is the selection of the algorithm. For this study, we adopted the 'fmincon' solver in MATLAB by applying the interior-point algorithm. Essentially, the 'fmincon' command in optimization solves constrained nonlinear optimization problems by deducing the minimum of an objective function [55]. A mathematical expression below describes the approach for solving by 'fmincon' solver:

$$\min f(x) \text{ such that } \begin{cases} c(x) \le 0 \\ ceq(x) = 0 \\ A \,.\, x \le b \\ Aeq \,.\, x = beq \\ lb \le x \le ub \end{cases}$$

where:

b and beq = vectors

A and Aeq = matrices

c and ceq = nonlinear constraint functions

$f(x)$ = objective functions

lb and ub = lower and upper bounds respectively

Among the various algorithms available for ‘fmincon’, we aptly selected the interior-point algorithm. The interior-point method calculates the minimum of a function subjected to a set of constraints [56]. From the description of the objective function (Cost) and the non-linear bending stiffness constraint, we chose the ‘fmincon’ solver with interior-point algorithm as the preferred approach to solve this optimization problem. We set the number of iterations at 1000. Figure 36 below shows the interface of the optimization toolbox, where the objective and constraint functions are called. We specified the bounds of the design variables and solved the problem to obtain the cost as a function value.

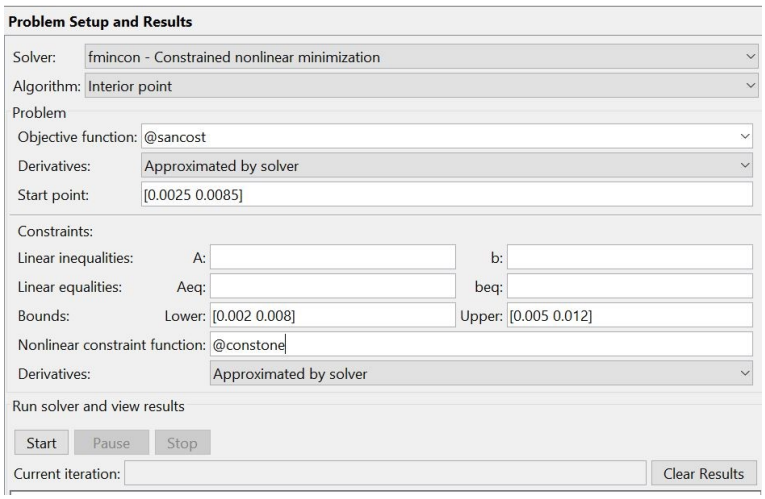

Figure 36. Interface of the optimization toolbox in MATLAB displaying input parameters of the optimization

6.8. Single-Objective 'Weight' Optimization of Sandwich and Pure Composite Beams

Designing a structural component with the minimum weight and greatest strength is of paramount importance in the aerospace and automotive industry. It renders significant savings in material cost of manufacturing and reduces material wastage. Thus, in the second study, we performed a single-objective weight optimization for a rectangular beam in the sandwich material construction, a solid carbon fiber-G/flex (CF-GF) and solid aluminum alloy beam. The process is similar to the first method of performing a cost-optimization study. Here, we replaced the objective function by the weight of the structure and obtained the results are identically. The following sections describe the elements of the optimization problem.

6.8.1. Objective Function:

According to Gibson and Ashby [39], the weight of a sandwich composite beam (N) is represented by the equation below:

$$W_{sandwich} = 2\,\rho_f\, g\, b\, l\, t + \rho_c\, g\, b\, l\, c$$

where:

ρ_f, ρ_c = densities of face skins and core respectively (described earlier)

g = acceleration due to gravity

Substitution of the corresponding values from Table 9 yields the resulting equation:

$$W_{sandwich} = 13.20\, t + 0.565\, c$$

where the unknown thicknesses ‘t’ and ‘c’ constitute the design variables of the study.

It is evident by analyzing the analytical formula for the weight function of a sandwich beam that it involves a volume term and density value. Thus, for a carbon fiber-G/flex (CF-GF) and aluminum alloy solid beam with circular holes, the weight function must be formulated by subtracting the volume of the circular openings from the weight function. The below equation expresses the weight function:

$$W_{CF\text{-}GF} = \rho_f\, g\, [(b\, l\, t) - 2\,\pi\, r^2\, t]$$

Volume of beam

Volume of circular openings

Similarly, for an aluminum alloy beam,

$$W_{Al\ alloy} = \rho_{Al}\, g\, [(b\, l\, t) - 2\,\pi\, r^2\, t]$$

After substituting known values from the table and keeping the thickness 't' and radius 'r' as the free design variables, these equations simplify as shown below:

$$W_{CF\text{-}GF} = 11005.54\ t\ (0.0012 - 6.28\ r^2)$$

$$W_{Al\ Alloy} = 27173.7\ t\ (0.0012 - 6.28\ r^2)$$

6.8.2. Design Variables:

The design variables remain the same as specified in cost-objective optimization. These include the core (c) and face skin thicknesses (t) for the sandwich material arrangement, and beam thickness along with the radius of the holes (r) for solid beams constructed by CF-GF and aluminum alloy.

6.8.3. Constraints:

We assigned the bending stiffness specified in cost-optimization as the singular non-linear constraint for weight-oriented optimization. Table 12 summarizes the key elements of the optimization setup.

Table 12. Summary of elements for weight-objective optimization of three beam configurations

Elements	Sandwich Beam	Solid Carbon Fiber – G/flex Beam	Solid Aluminum alloy Beam
Objective Function	Weight (N)	Weight (N)	Weight (N)
Design Variables	Skin thickness (t) core thickness (c)	Beam thickness (t) Radius of hole (r)	Beam thickness (t) Radius of hole (r)
Constraints	Bending Stiffness	Bending Stiffness	Bending Stiffness

6.8.4. Optimization Toolbox – MATLAB

Since analytical expressions for the weight and cost function are identical, we utilized the same optimization setup to obtain the minimum function value (weight). Here, we selected the ‘fmincon’ solver with the Interior-Point Algorithm again and specified the script functions for weight and bending stiffness constraints in the toolbox. We set the number of iterations at 1000 and defined the applicable limits of the design variables (beam thicknesses and holes). We solved the problem computationally to obtain the lowest weight and the corresponding value of thickness and hole geometries that satisfy the non-linear constraint.

CHAPTER 7 – RESULTS AND DISCUSSION

7.1. Introduction

The previous chapter demonstrates the critical methodology and setup of parameters for implementing the single-objective optimization process in MATLAB and design optimization in ANSYS. This section presents key results of the numerical experiments in terms of the objective functions (mass, weight, and cost) defined for three different material configurations: sandwich material structure, solid carbon fiber-G/flex (CF-GF), and aluminum alloy beam.

7.2. Design (Mass) Optimization of a 3D-printed Aircraft Wing Bracket

7.2.1. Sandwich Material Structure

Figure 37 (a) shows the total deformation obtained in the sandwich bracket structure (CF-GF face skin and polyurethane foam core) upon the application of load. Figure 37 (b) depicts the equivalent (Von Mises) stresses developed. With these parameters set as the constraints of the study, Figure 38 (a) shows the optimization process results. As seen from the chart, the process achieves an optimized mass of 0.096 kg (Design Point 8) from the original mass of 0.102 kg, rendering a weight-saving of about 6%. Figure 38 (b) shows the parallel variation of geometric mass for each iteration, depicting the lowest mass achieved.

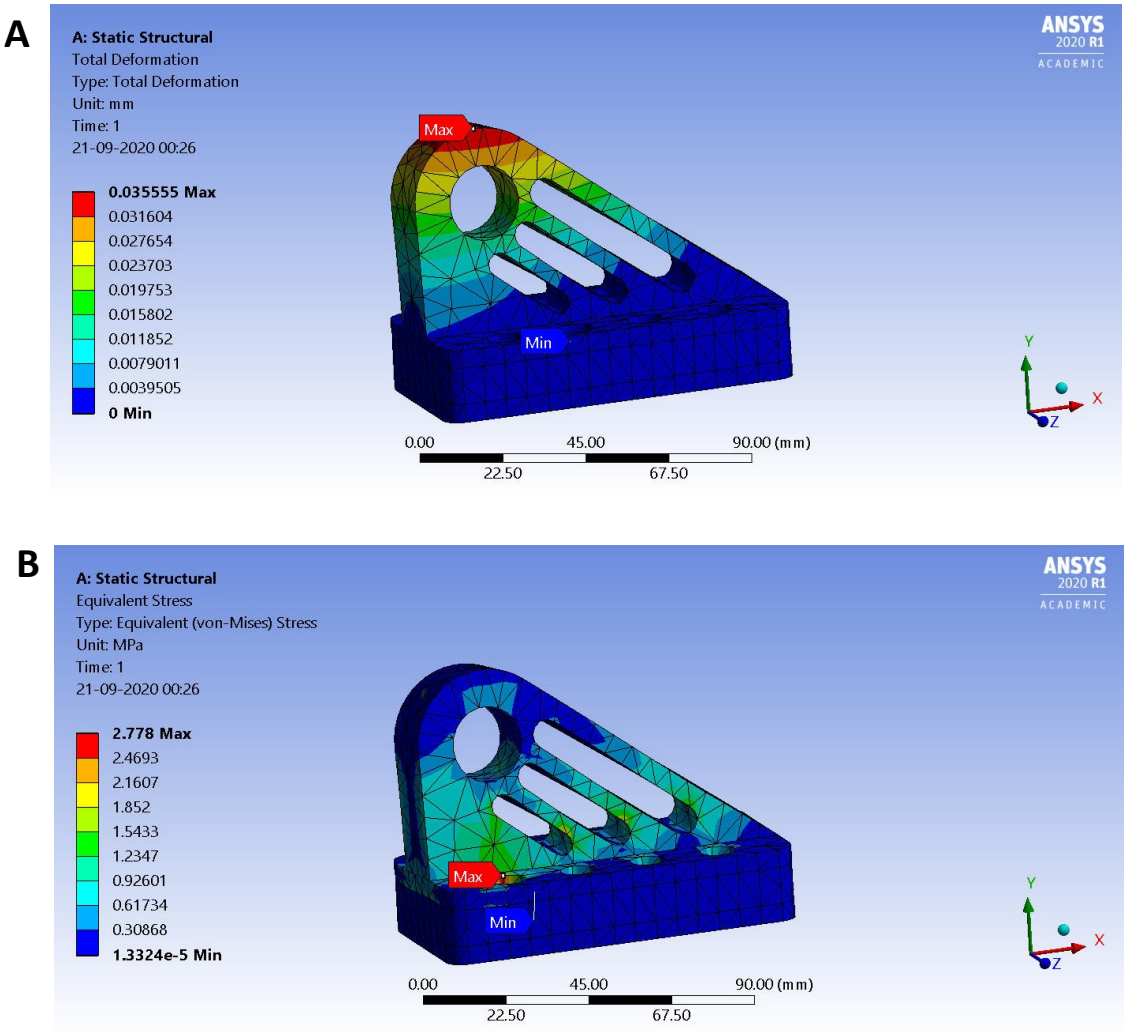

Figure 37. Distribution of (a) maximum total deformation and (b) maximum equivalent (von-Mises) stress

During the initial optimization experiment, we observed an anomaly. Contrary to the expectation that an increase in design parameter values (thickness of the beam) yields more mass of the structure, we obtained a mass reduction, which was inaccurate. Furthermore, the equivalent stress should be more extensive as dimensions are augmented, which we had not observed in the iterations. To discern the possible source of the error in mass calculations, we evaluated the 3D model and optimization setup again. We observed

that the problem lay in the assignment of design parameters for the optimization. Essentially, we had set up the distances of the plane along each sandwich layer to be the design variable. Thus, the optimization was varying the plane locations and not the extrusion thicknesses of core and skin, generating erroneous results. We fixed this error by proper assignments of core and upper skin 'extrusion thicknesses' as design variables and

A

Table of Schematic B2: Design of Experiments (Central Composite Design : Auto Defined)

	A	B	C	D	E	F	G
1	Name	P1 - hole.diameter (mm)	P2 - skin .thickness (mm)	P3 - core .thickness (mm)	P4 - Geometry Mass (kg)	P5 - Total Deformation Maximum (mm)	P6 - Equivalent Stress Maximum (MPa)
2	1 DP 0	20	5	10	0.10282	0.035555	2.778
3	2	18	5	10	0.10416	0.034416	2.7948
4	3	22	5	10	0.10134	0.037149	2.7015
5	4	20	4	10	0.097942	0.038137	3.3783
6	5	20	6	10	0.1077	0.033694	2.3361
7	6	20	5	8	0.10199	0.03557	2.7474
8	7	20	5	12	0.10366	0.035549	2.785
9	8	18.374	4.187	8.3739	0.099275	0.036742	3.2384
10	9	21.626	4.187	8.3739	0.096982	0.038678	3.2094
11	10	18.374	5.813	8.3739	0.10721	0.033192	2.4115
12	11	21.626	5.813	8.3739	0.10492	0.035247	2.3618
13	12	18.374	4.187	11.626	0.10063	0.036796	3.2539
14	13	21.626	4.187	11.626	0.098342	0.038786	3.2347
15	14	18.374	5.813	11.626	0.10857	0.033204	2.4259
16	15	21.626	5.813	11.626	0.10628	0.035315	2.3762

B

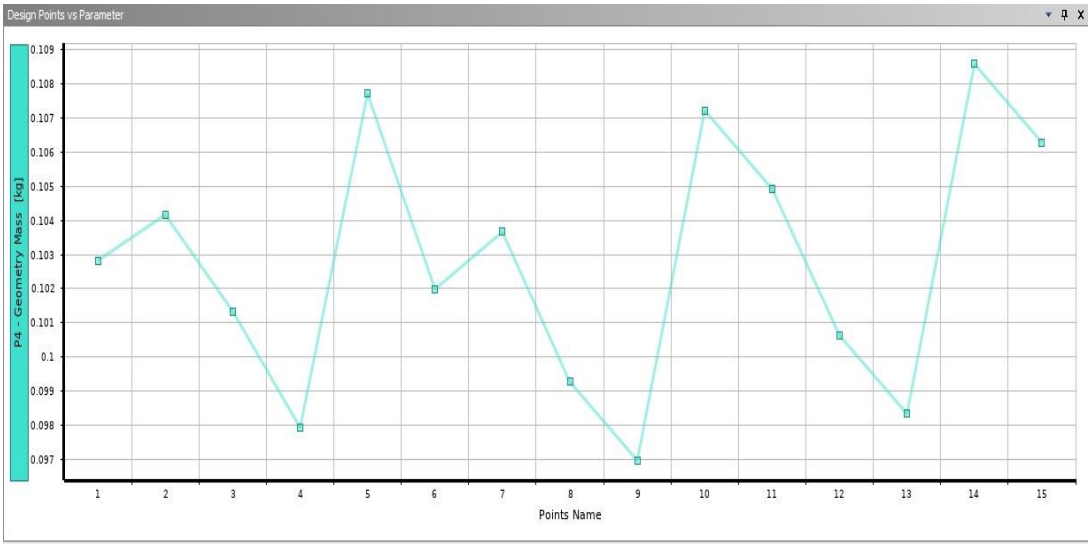

Figure 38. Optimization results for a sandwich-shaped configuration. (a) 'Design of Experiments' Tab with resulting output parameters for each design point and (b) Plot of design points vs geometric mass

performed the mass optimization again. As seen in Figure 38 (a) and (b), the mass calculations are now accurate without any irregularity.

Moreover, the optimization analysis performed in ANSYS generates a 'Goodness of Fit' (GOF) Curve. In statistics, 'goodness of fit' refers to the comparative variation between observed and predicted values. Figure 39 depicts the GOF curve for the output parameters for values obtained by the design points and predicted by the response surface optimization. In simpler terms, the proximity of the sampling points to the straight line indicates the level of accuracy of the optimization [57].

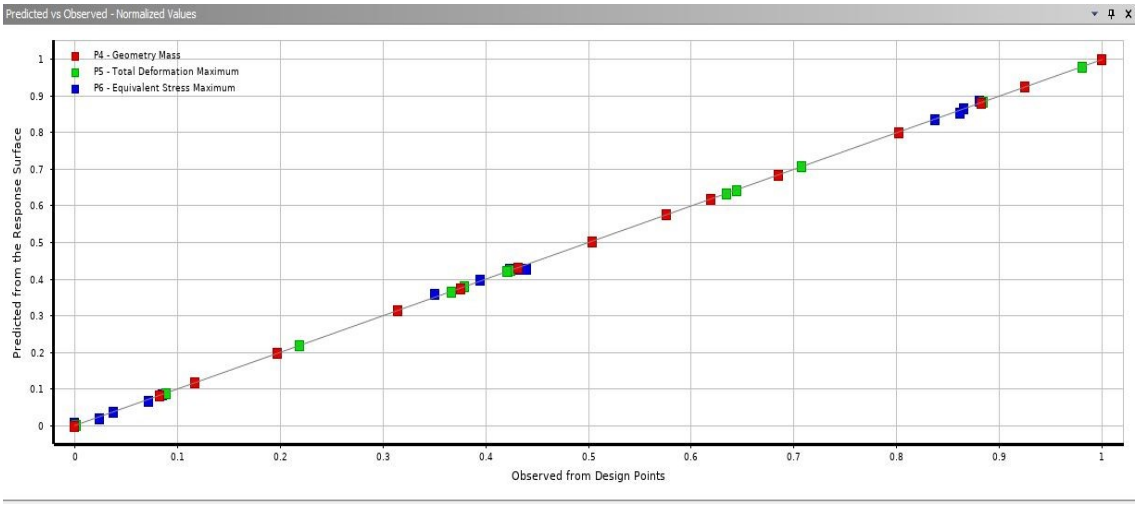

Figure 39. 'Goodness of Fit' (GOF) curve for sandwich-structured bracket

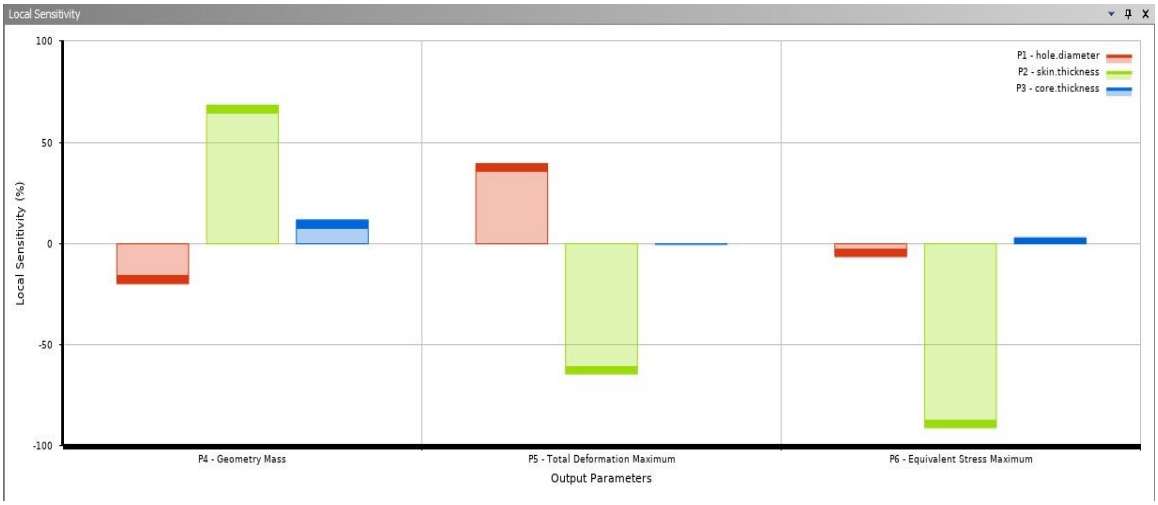

Figure 40. Local sensitivity data for sandwich-structured bracket

Figure 40 depicts the sensitivity plot of the output parameters. It is essentially a graphical representation of the effect of design variables on each variable. From the plot, we can deduce that the thickness of the sandwich bracket's upper face skin is the most sensitive to changes in the design variable. Figures 41 (a) and 41 (b) depict the 3D models of the sandwich-structured bracket before and after optimization, respectively.

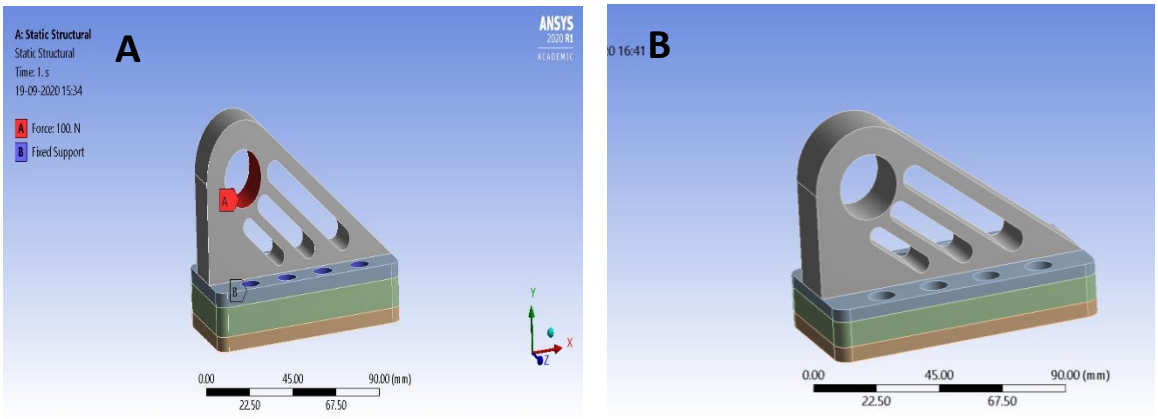

Figure 41. 3D model of the bionic sandwich bracket a) before optimization b) after optimization

7.2.2. Pure Carbon Fiber-G/flex (CF-GF) bracket

In a similar manner and to juxtapose the effects of a sandwich structure with a pure composite structure, we implemented the same optimization algorithm with a bracket design composed of only the fillers (carbon fiber and G/flex) abbreviated as CF-GF. We did not employ foam for this configuration and subjected the fiber-reinforced structure to a static load. Figures 42 (a) and (b) present the total deformation and equivalent stress obtained in the structure. Subsequently, the results of the optimization yield a mass reduction of 17.5% (from 147.5 grams to 121.5 grams) as depicted in Figures 43 (a) and (b).

A

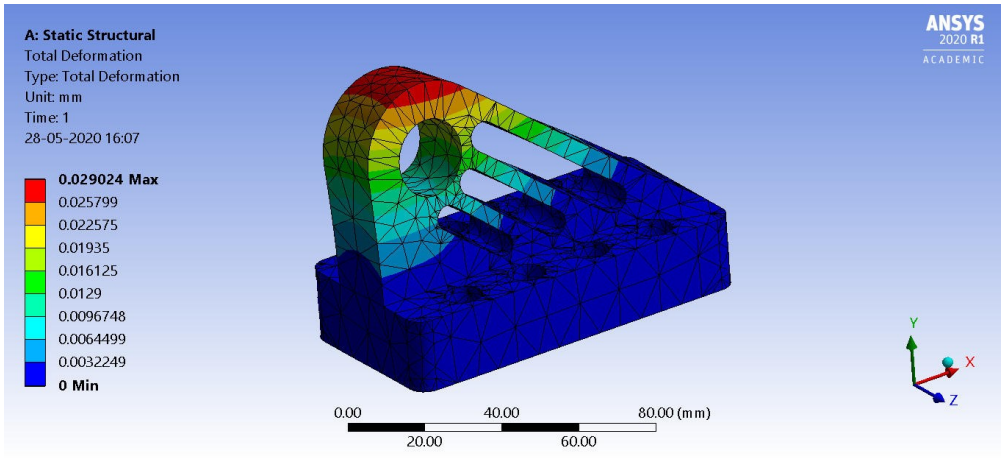

B

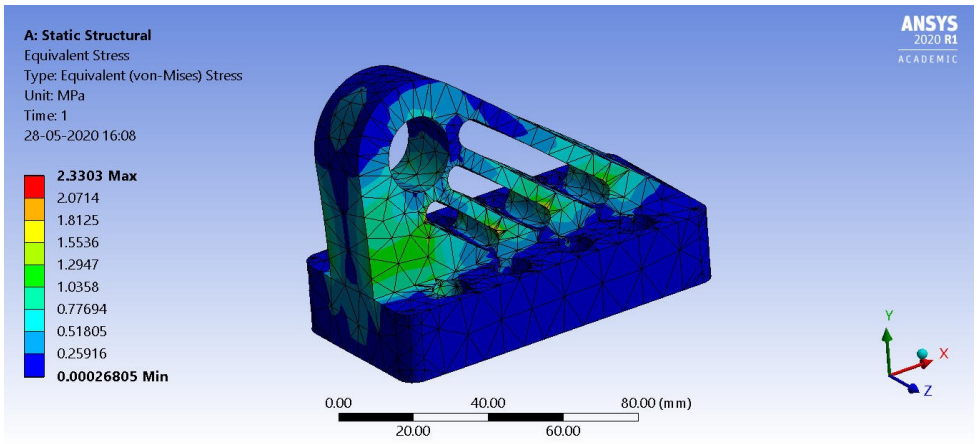

Figure 42. Carbon fiber – G/Flex bracket: Distribution of (a) maximum total deformation and (b) maximum equivalent (von-Mises) stress

A

Table of Schematic B2: Design of Experiments (Central Composite Design : Auto Defined)

	A	B	C	D	E	F
1	Name	P1 - hole.diameter (mm)	P2 - beam .thickness (mm)	P3 - Geometry Mass (kg)	P4 - Total Deformation Maximum (mm)	P5 - Equivalent Stress Maximum (MPa)
2	1 DP 0	20	20	0.14745	0.029024	2.3303
3	2	18	20	0.14878	0.027981	2.2895
4	3	22	20	0.14597	0.030725	2.2634
5	4	20	15	0.12304	0.029638	2.2332
6	5	20	25	0.17185	0.028884	2.2827
7	6	18	15	0.12438	0.02857	2.2225
8	7	22	15	0.12156	0.031221	2.1762
9	8	18	25	0.17319	0.027765	2.2597
10	9	22	25	0.17037	0.030525	2.2116

B

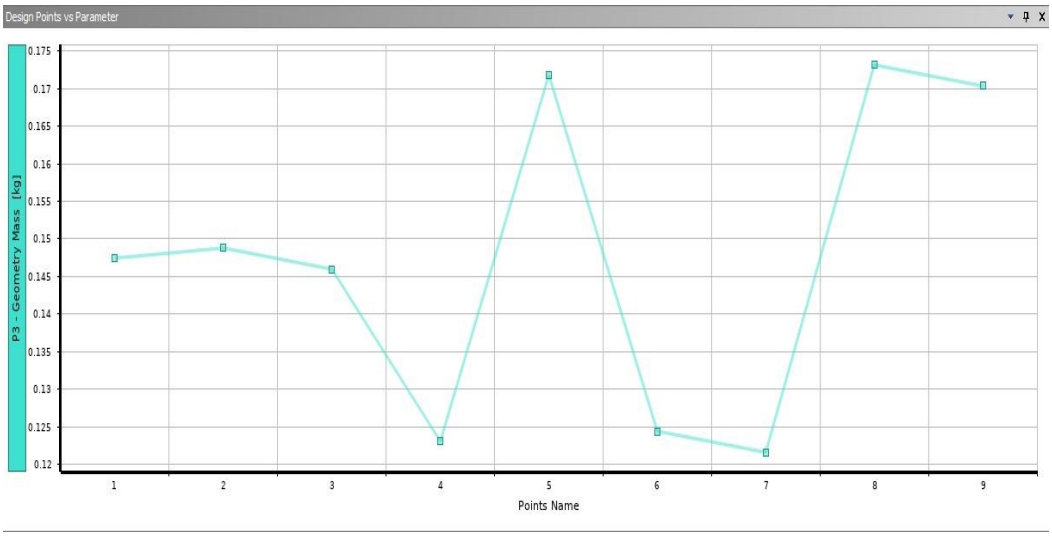

Figure 43. Optimization results for a carbon fiber – G/Flex configuration. (a) 'Design of Experiments' Tab with resulting output parameters for each design point and (b) Plot of design points vs geometric mass

Similar to the case of the sandwich structure, the 'goodness of fit' curve shows closeness between observed and predicted values (Figure 44). Further, the sensitivity data deduces the beam thickness to be more vulnerable to design changes than the diameter of the hole in the wing bracket structure (Figure 45).

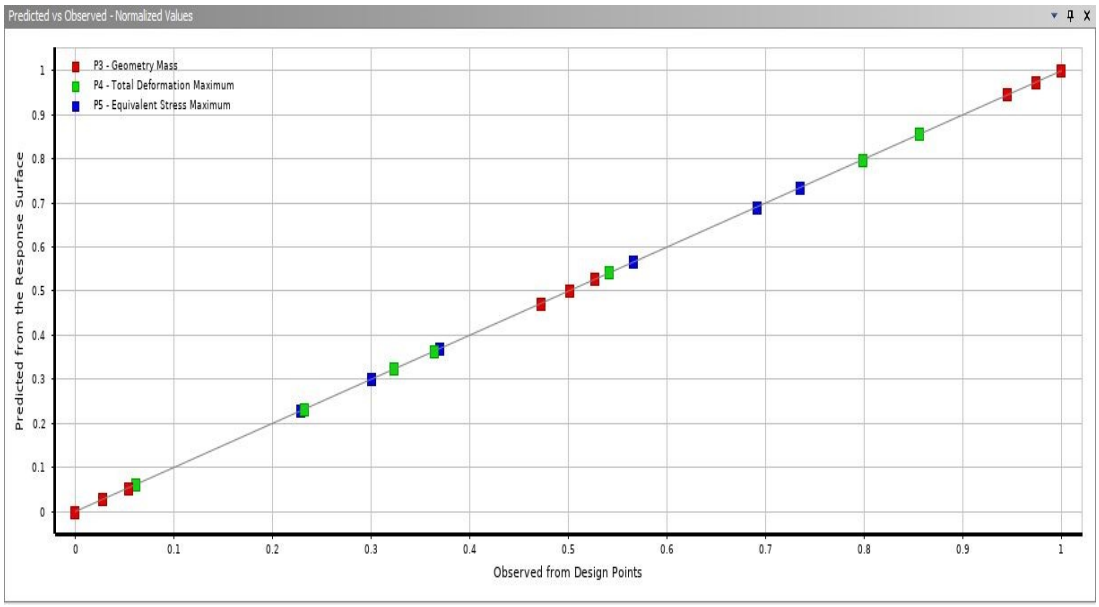

Figure 44. 'Goodness of Fit' (GOF) curve for carbon fiber – G/Flex bracket

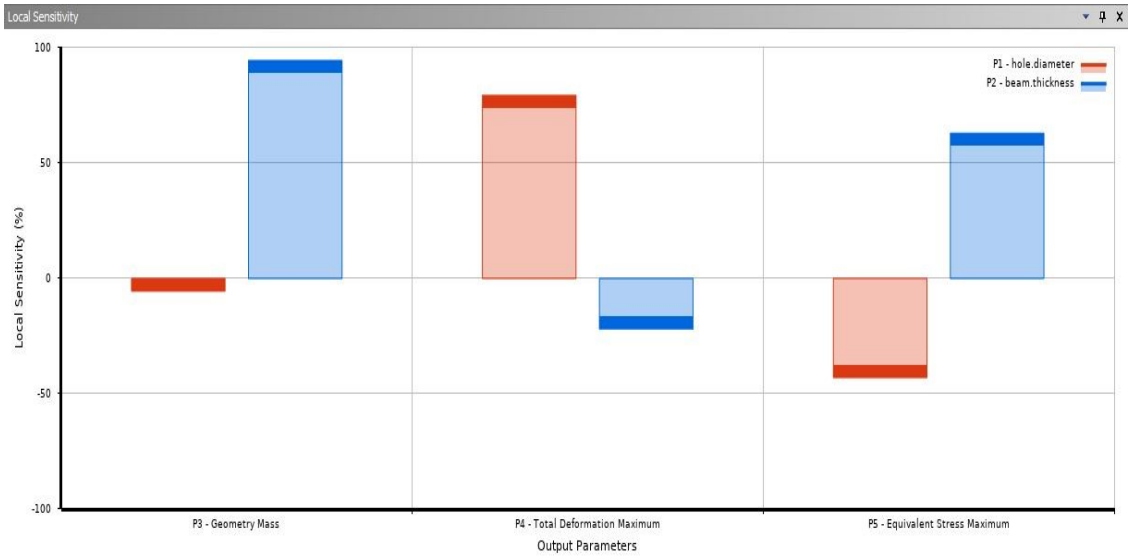

Figure 45. Local sensitivity data for carbon fiber – G/Flex bracket

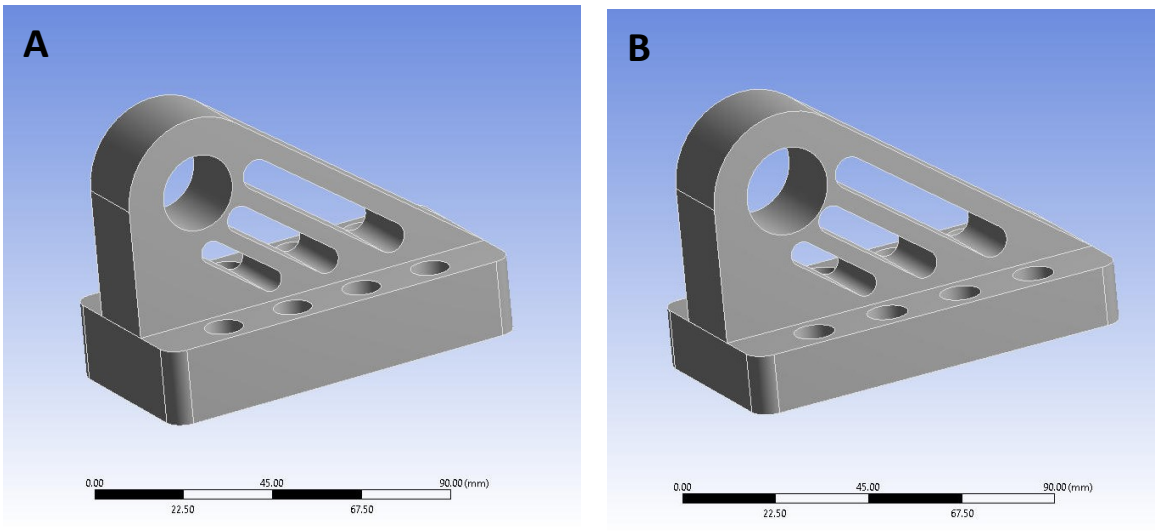

Figure 46. 3D model of the bionic CF-GF bracket a) before optimization b) after optimization

Figures 46 (a) and 46 (b) depict the 3D models of the carbon fiber-G/flex bracket before and after optimization, respectively.

7.2.3. Discussion

From this study, our aim to optimize structural designs employing thermoset materials for geometric mass yielded considerable preservation of mass, with a simple fiber-reinforced configuration performing better. Table 13 (a) presents a comparative review between optimized mass values (ANSYS) and those attained by hand-calculations. Table 13 (b) depicts the summary of optimized mass values for the bionic wing bracket for both material configurations.

Table 13 a. A comparative summary of original dimensions and mass of wing bracket with optimized dimensions and mass obtained from ANSYS and hand-calculations

Material	Original dimensions	Original mass (g)	Optimized dimensions	Optimized mass by ANSYS (g)	Optimized mass (analytical) (g)
Sandwich structure	d = 20 mm t = 5 mm c = 10 mm	102.82	d = 21.62 mm t = 4.18 mm c = 8.37 mm	96.98	96.98
Carbon fiber-G/flex	d = 20 mm t = 20 mm	147.45	d = 22 mm t = 15 mm	121.56	121.56

Table 13 b. Summary of optimized mass values (sandwich and carbon fiber composite brackets)

Material Configuration	Original mass (grams)	Optimized mass (grams)	Mass saving (%)
Sandwich Structure	102.82	96.98	5.8 %
Carbon Fiber – G/flex composite	147.45	121.56	17.5 %

7.3. Design (Mass) Optimization of a First-Person View (FPV) Drone Airframe

7.3.1. Sandwich Material Configuration

For this novel design of a sandwich material airframe for drone applications, Figure 47 (a) and (b) shows the total deflection and equivalent stress distributions by applying a load on the upper portion. With these parameters constituting the constraints, we executed the design optimization procedure within the design variables' bounds. As depicted in Figure 48 (a), the optimization performs a set of iterations in ANSYS within a design space.

The results show alleviation of mass from 14.95 grams to 12.19 grams for the sandwich construction (about 18% optimization in mass). An eccentric feature of this design is the presence of several holes and a central fillet which further aids in weight conservation, while maintaining the structural strength of the airframe model. Similar to a bionic bracket, the mass calculations initially showed erroneous trends due to improper assignment of design variables (locations of plane). We obtained accurate results by re-assigning the extrusion thicknesses of core (c) and skin (t) with the diameter (d) as the design parameters.

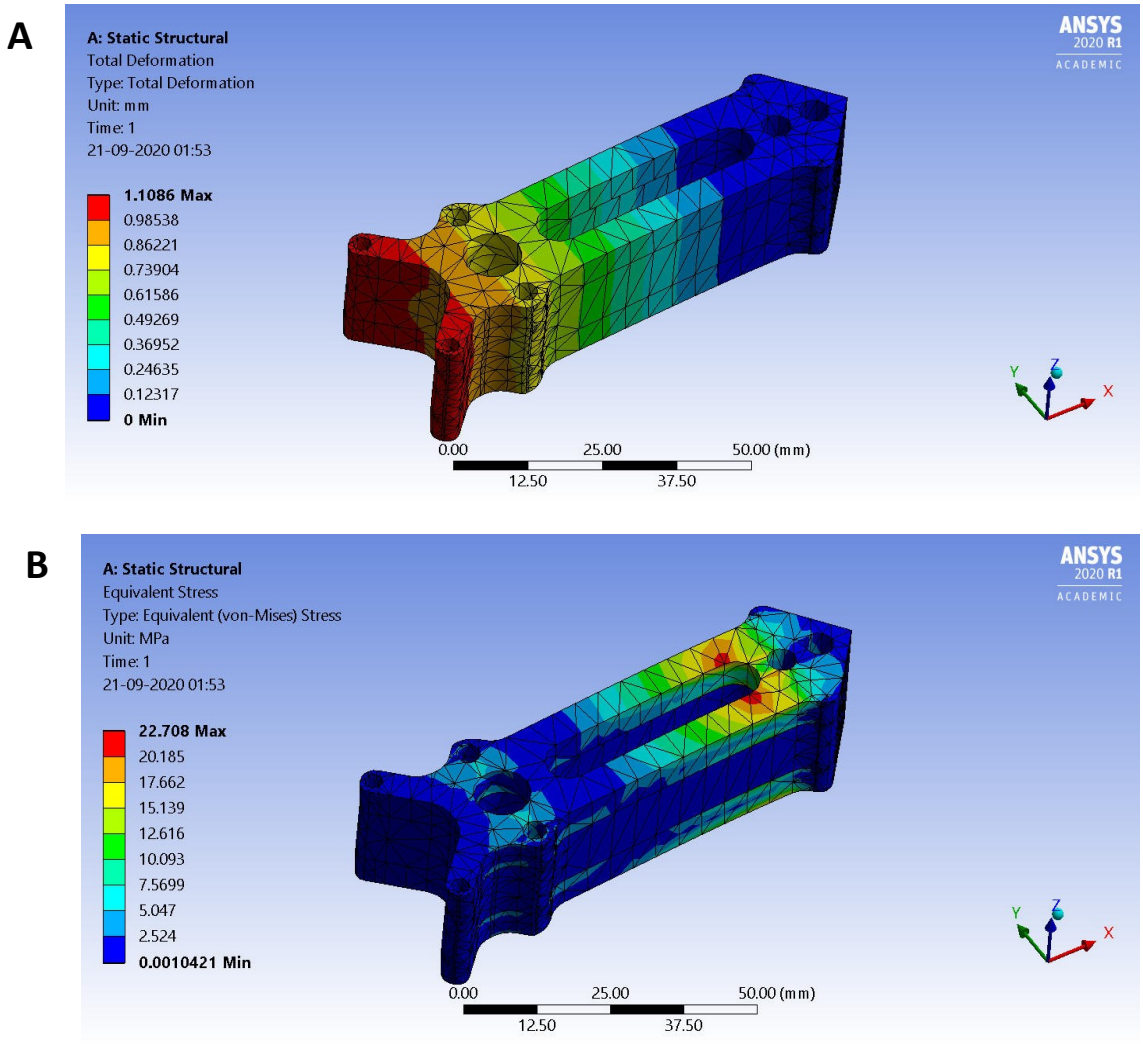

Figure 47. Sandwich-shaped drone airframe: Distribution of (a) maximum total deformation and (b) maximum equivalent (von-Mises) stress

Figure 48 (b) outlines the mass value achieved for each iteration performed in the analysis. The GOF curve (Figure 49) shows the predicted and obtained values close to the straight line while sensitivity analysis (Figure 50) reveals the lower skin thickness (t) to be the most effective factor for variation of output parameters.

A

Table of Outline A2: Design Points of Design of Experiments

	A	B	C	D	E	F	G
1	Name	P1 - hole.diameter (mm)	P2 - skin .thickness (mm)	P3 - core .thickness (mm)	P4 - Geometry Mass (kg)	P5 - Total Deformation Maximum (mm)	P6 - Equivalent Stress Maximum (MPa)
2	1	10	4.5	10	0.014264	1.1894	24.622
3	2	9	4.5	10	0.014438	1.173	24.85
4	3	11	4.5	10	0.014073	1.2077	25.132
5	4	10	3	10	0.012198	1.4528	30.005
6	5	10	6	10	0.01633	0.96726	20.917
7	6	10	4.5	8	0.014028	1.271	26.212
8	7	10	4.5	12	0.0145	1.1157	23.238
9	8	9.187	3.2804	8.3739	0.012516	1.4833	30.859
10	9	10.813	3.2804	8.3739	0.012258	1.5145	31.372
11	10	9.187	5.7196	8.3739	0.015909	1.0366	22.459
12	11	10.813	5.7196	8.3739	0.015581	1.0595	22.603
13	12	9.187	3.2804	11.626	0.012904	1.3023	27.432
14	13	10.813	3.2804	11.626	0.012638	1.3341	27.614
15	14	9.187	5.7196	11.626	0.016297	0.95292	21.206
16	15	10.813	5.7196	11.626	0.015961	0.97713	20.967

B

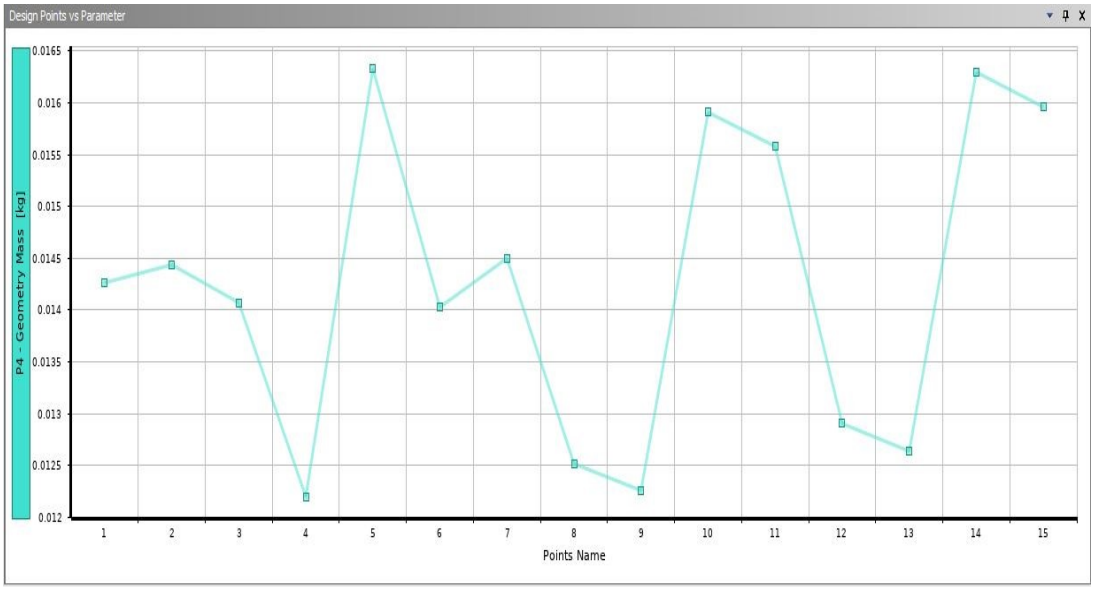

Figure 48. Optimization results for a sandwich-shaped FPV drone airframe. (a) 'Design of Experiments' Tab with resulting output parameters for each design point and (b) Plot of design points vs geometric mass

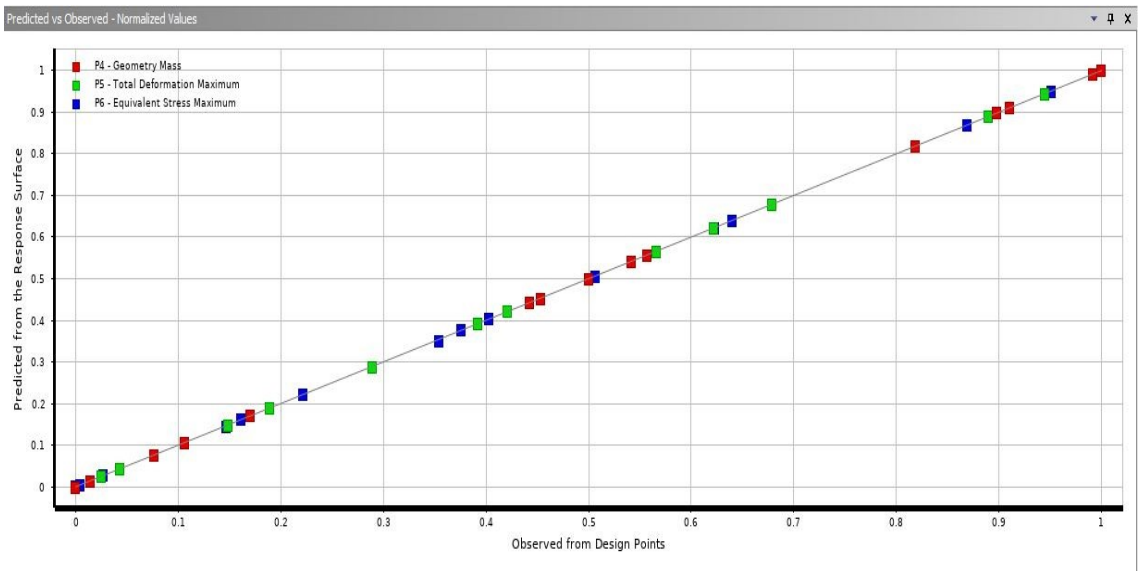

Figure 49. 'Goodness of Fit' curve for sandwich-structured drone airframe

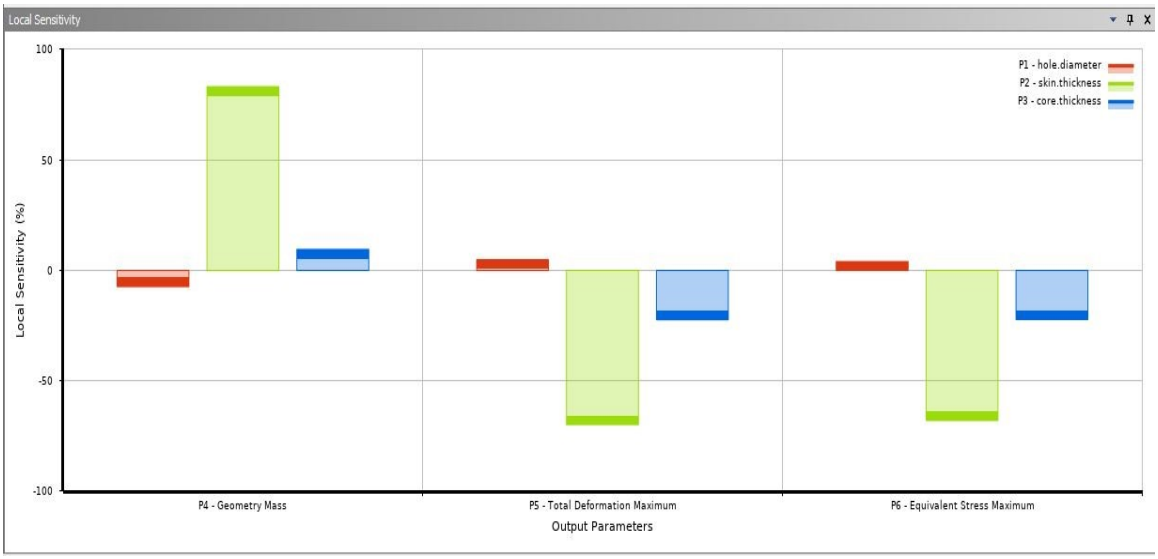

Figure 50. Local sensitivity data for sandwich-structured drone airframe

Figures 51 (a) and 51 (b) depict the 3D models of the sandwich-structured drone airframe before and after optimization, respectively.

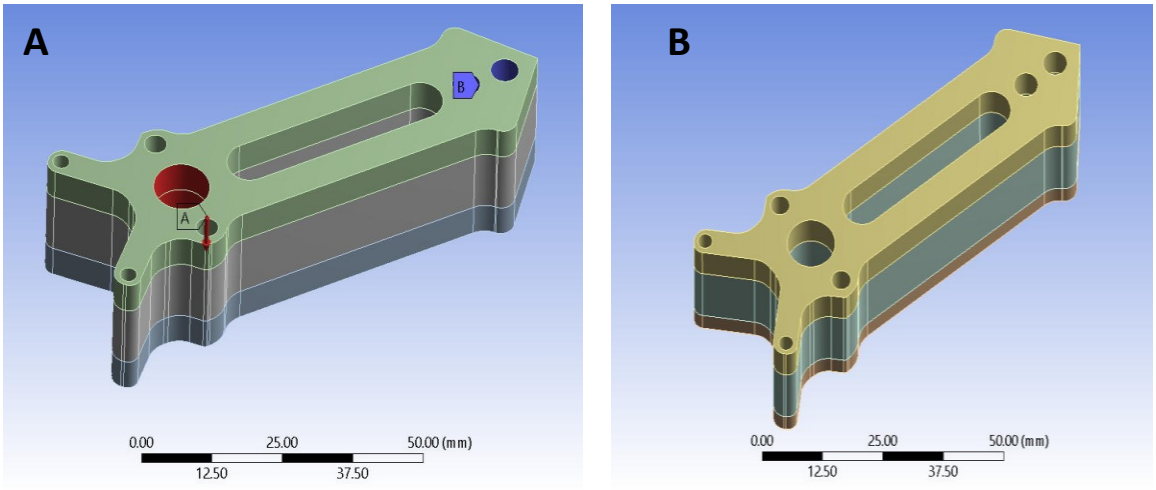

Figure 51. 3D model of the FPV drone sandwich airframe a) before optimization b) after optimization

7.3.2. Pure Carbon Fiber-G/flex (CF-GF) Airframe

Correspondingly, Figures 52 (a) and (b) depict the structural deformation and optimization results of an airframe without foam material in the center core. As the pure composite airframe deforms and develops stresses, the optimization generates nine design points iterating the design variables and rigorously calculating the deformation, mass, and stresses.

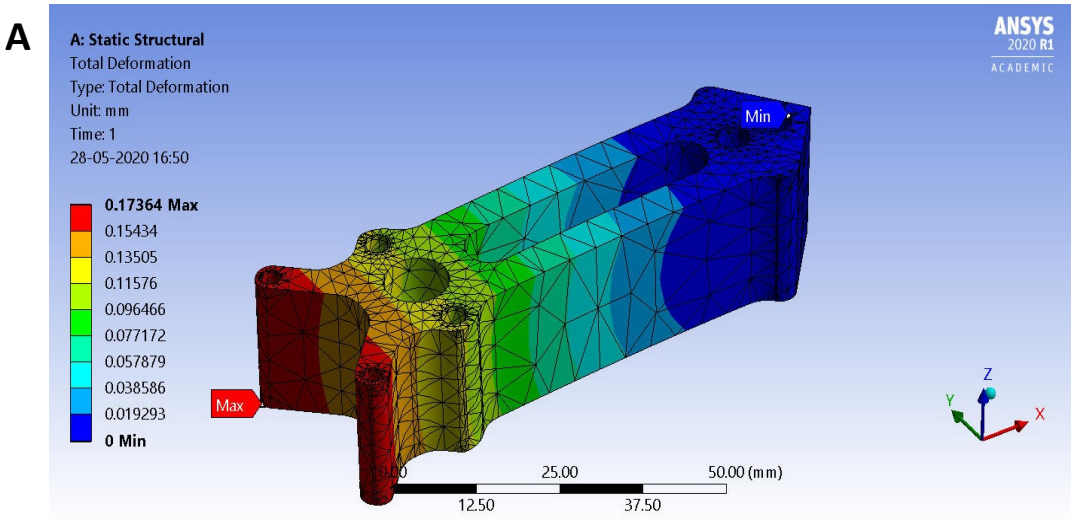

B

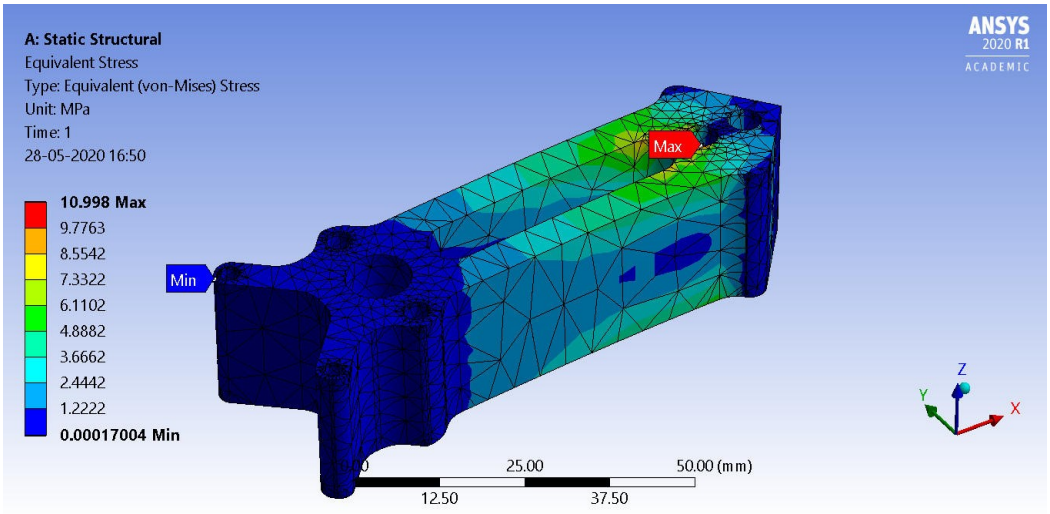

Figure 52. Carbon fiber – G/Flex drone airframe: Distribution of (a) maximum total deformation and (b) maximum equivalent (von-Mises) stress

A

Table of Schematic B2: Design of Experiments (Central Composite Design : Auto Defined)

	A	B	C	D	E	F
1	Name	P1 - hole.diameter (mm)	P2 - beam .thickness (mm)	P3 - Geometry Mass (kg)	P4 - Total Deformation Maximum (mm)	P5 - Equivalent Stress Maximum (MPa)
2	1 DP 0	10	20	0.027546	0.17364	10.998
3	2	8	20	0.02818	0.17326	11.111
4	3	12	20	0.02677	0.17439	11.145
5	4	10	15	0.020659	0.38713	17.922
6	5	10	25	0.034432	0.094271	7.4574
7	6	8	15	0.021135	0.38633	18.374
8	7	12	15	0.020078	0.38867	17.867
9	8	8	25	0.035225	0.094076	7.4651
10	9	12	25	0.033463	0.094727	7.4459

B

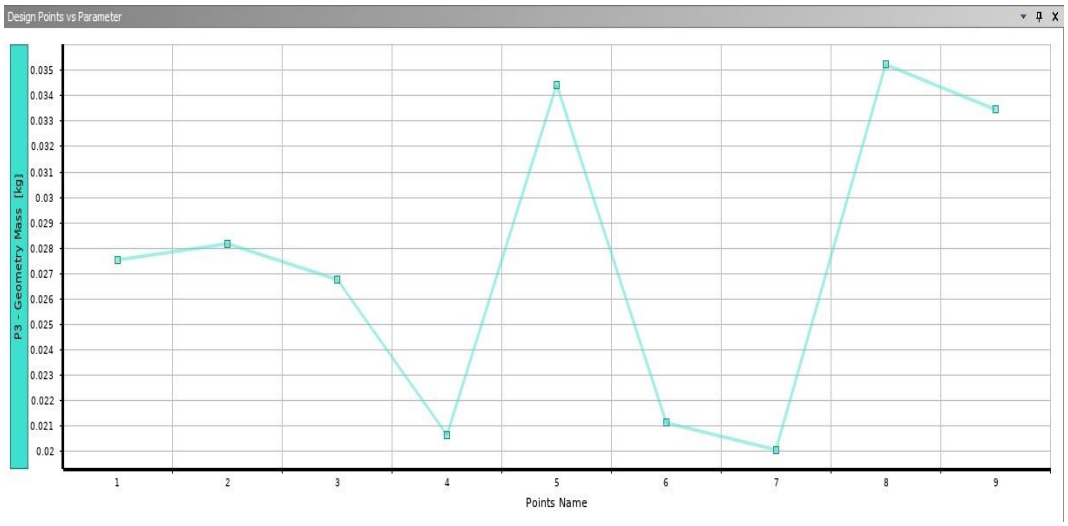

Figure 53. Optimization results for a carbon fiber – G/Flex drone airframe. (a) 'Design of Experiments' Tab with resulting output parameters for each design point and (b) Plot of design points vs geometric mass

As represented in Figure 53 (a), we achieved the minimum mass in the 8th iteration (20.078 grams), which renders a weight reduction of around 27% from the original mass of the structure. Figure 53 (b) depicts this variation. Likewise, Figures 54 and 55 show the GOF curve and sensitivity data, respectively, with the total beam thickness emerging as the dominant variable in optimization.

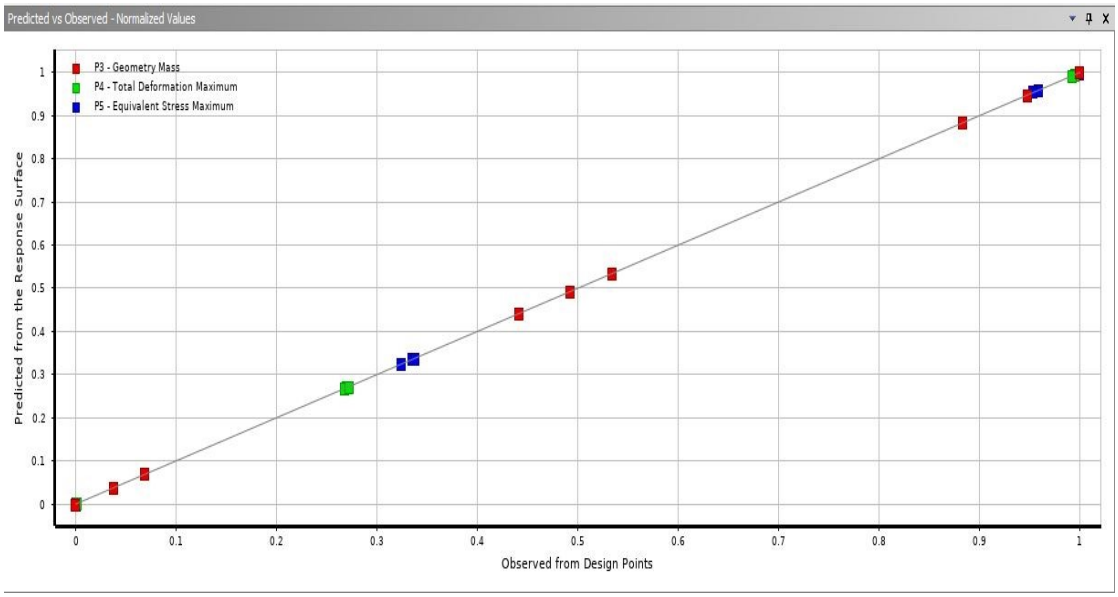

Figure 54. 'Goodness of Fit' curve for carbon fiber – G/Flex drone airframe

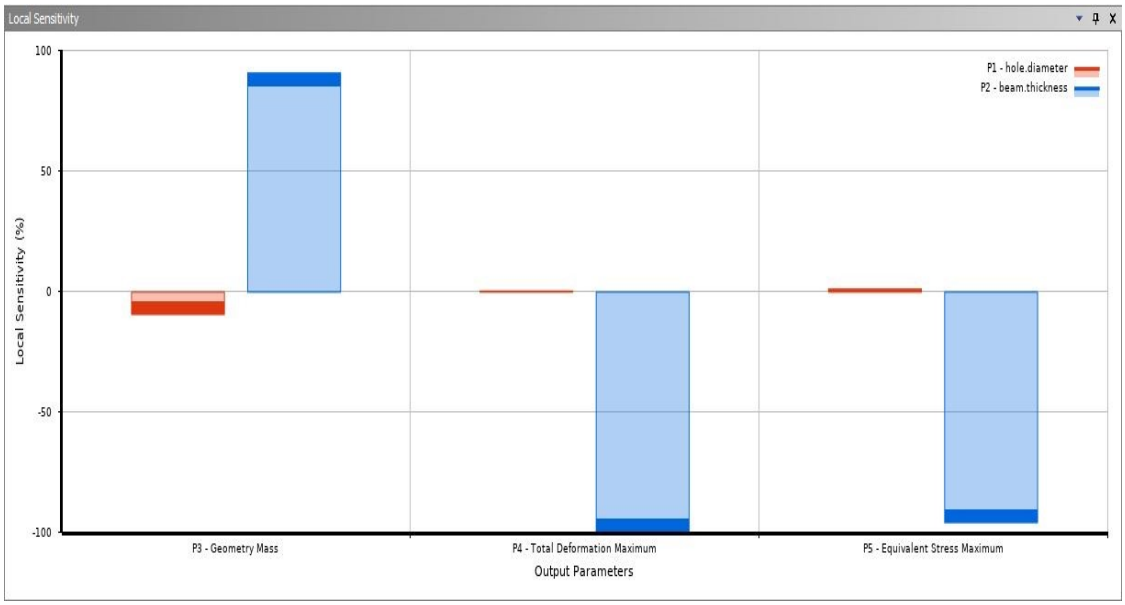

Figure 55. Local sensitivity for carbon fiber – G/Flex drone airframe

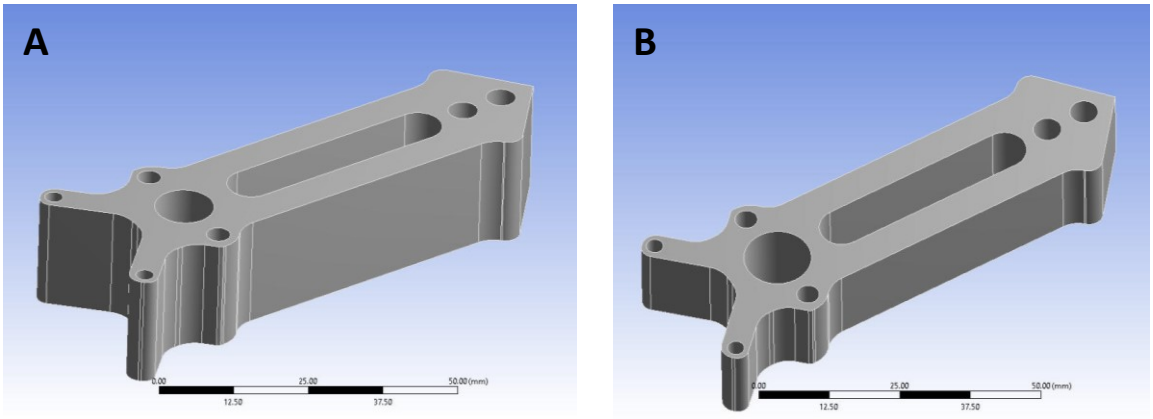

Figure 56. 3D model of the FPV drone CF-GF airframe a) before optimization b) after optimization

Figures 56 (a) and 56 (b) depict the 3D models of the carbon fiber-G/flex drone airframe before and after optimization, respectively.

7.3.3. Discussion

For the airframe design of a drone, both sandwich-structured and filler-based CF-GF designs exhibited mass preservation upon optimizing the 3D model, with carbon fiber-G/flex (CF-GF) composition providing superior performance in terms of lightweight design. Table 14 (a) presents a comparative review between optimized mass values (ANSYS) and those attained by hand-calculations. Table 14 (b) depicts the summary of optimized mass values for the FPV drone airframe for both material configuration.

Table 14 a. A comparative summary of original dimensions and mass of drone airframe with optimized dimensions and mass obtained from ANSYS and hand-calculations

Material	Original dimensions	Original mass (g)	Optimized dimensions	Optimized mass by ANSYS (g)	Optimized mass (analytical) (g)
Sandwich structure	d = 10 mm t = 5 mm c = 10 mm	14.95	d = 10 mm t = 3 mm c = 10 mm	12.19	12.19
Carbon fiber-G/flex	d = 10 mm t = 20 mm	27.54	d = 12 mm t = 15 mm	20.08	20.08

Table 14 b. Summary of optimized mass values (sandwich and carbon fiber composite drone airframe)

Material Configuration	Original mass (grams)	Optimized mass (grams)	Mass saving (%)
Sandwich Structure	14.95	12.19	18.4 %
Carbon fiber – G/flex composite	27.54	20.08	27.1 %

7.4. Design (Mass) Optimization of Tapered Cantilever Sandwich Beam

7.4.1. Sandwich Material Structure

Although the structure's geometry appears simple, the aerospace industry extensively employs tapered configurations as they provide 'weight-saving' design by trimming the structure from its rectangular domain. This design is standard in aircraft wing structures (ribs and spars) and helicopter blades.

For a tapered sandwich structure fixed at one end and a load of 100 N acting at the free end, Figure 57 (a) and (b) shows the resulting deflection and equivalent (Von-Mises) stresses. By performing an identical optimization as the previous two designs, the analysis results generate considerable weight-preservation for both the sandwich material structure and the filler-matrix (CF-GF) configuration.

A

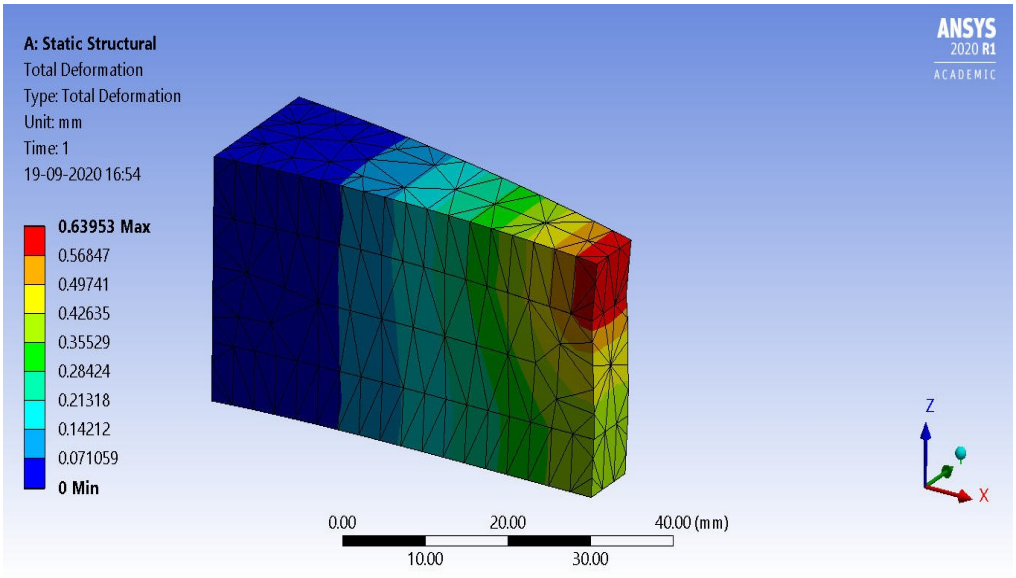

B

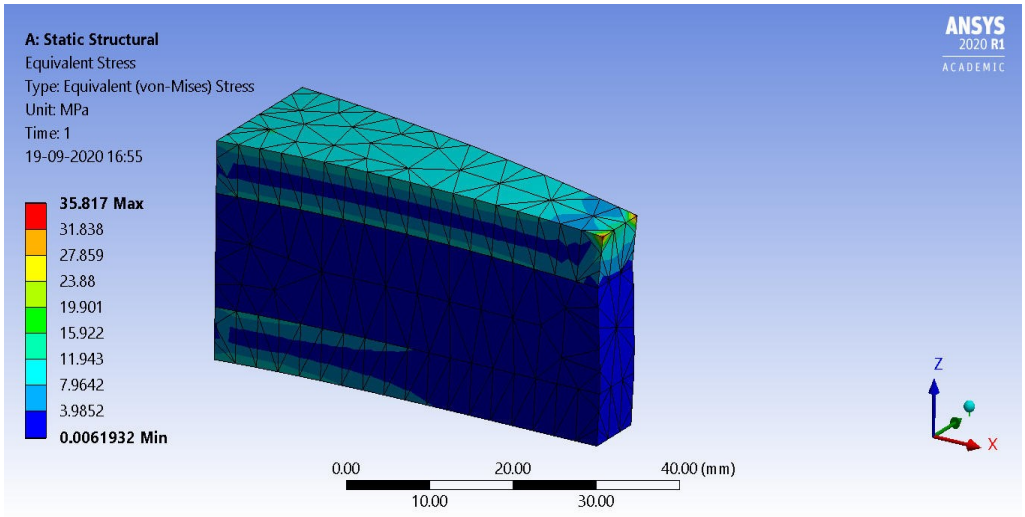

Figure 57. Tapered cantilever sandwich beam**:** Distribution of (a) maximum total deformation and (b) maximum equivalent (von-Mises) stress

The table presented in Figure 58 (a) shows the iterative design points and the minimum mass achieved while in Figure 58 (b) depicts the plot of the optimization results.

A

Table of Outline A2: Design Points of Design of Experiments

	A	B	C	D	E	F
1	Name	P1 - core.thickness (mm)	P2 - skin .thickness (mm)	P3 - Geometry Mass (kg)	P4 - Total Deformation Maximum (mm)	P5 - Equivalent Stress Maximum (MPa)
2	1 DP 0	13	6	0.010298	0.63953	35.817
3	2	10	6	0.010096	0.63953	35.71
4	3	16	6	0.0105	0.63846	35.791
5	4	13	4	0.0087277	0.76784	35.711
6	5	13	8	0.011869	0.533	35.647
7	6	10	4	0.0085259	0.79074	37.307
8	7	16	4	0.0089295	0.74784	35.647
9	8	10	8	0.011667	0.51613	35.818
10	9	16	8	0.012071	0.54667	35.791

B

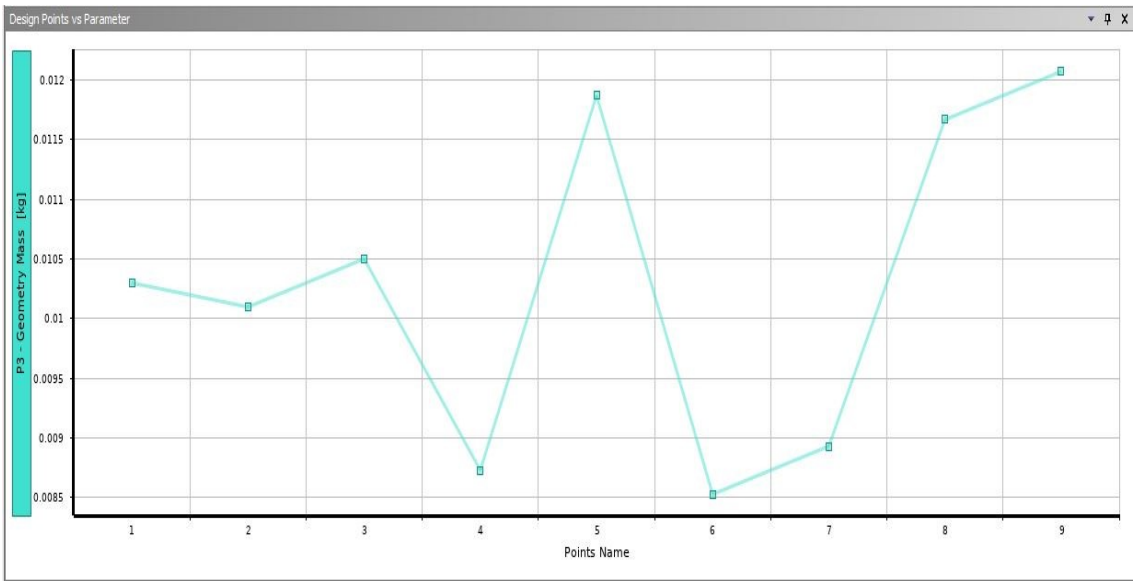

Figure 58. Optimization results for a sandwich-shaped tapered beam. (a) 'Design of Experiments' Tab with resulting output parameters for each design point and (b) Plot of design points vs geometric mass

In a similar trend to the wing bracket and drone airframe, the optimization results of mass for a tapered sandwich beam initially generated discrepancy. The overall mass of the model decreased in these results with an increase in core thickness, which was not possible. After fixing this error by assigning the extrusion thickness (c and t) as the design variable in place of the plane distances, we were able attain precise mass calculations after executing the optimization process.

Considering the simple geometry of the structure, we can assume that the design space for optimization is limited. For a polyurethane foam-filled sandwich beam, Figure 58 (b) shows a minimum mass of 8.52 grams, which corresponds to a reduction of 17.2% from the original geometric mass. The GOF curve shows considerable accuracy (Figure 59), while the sensitivity plot shows maximum effect between the mass of the beam and the thickness (c) of the foam core (Figure 60).

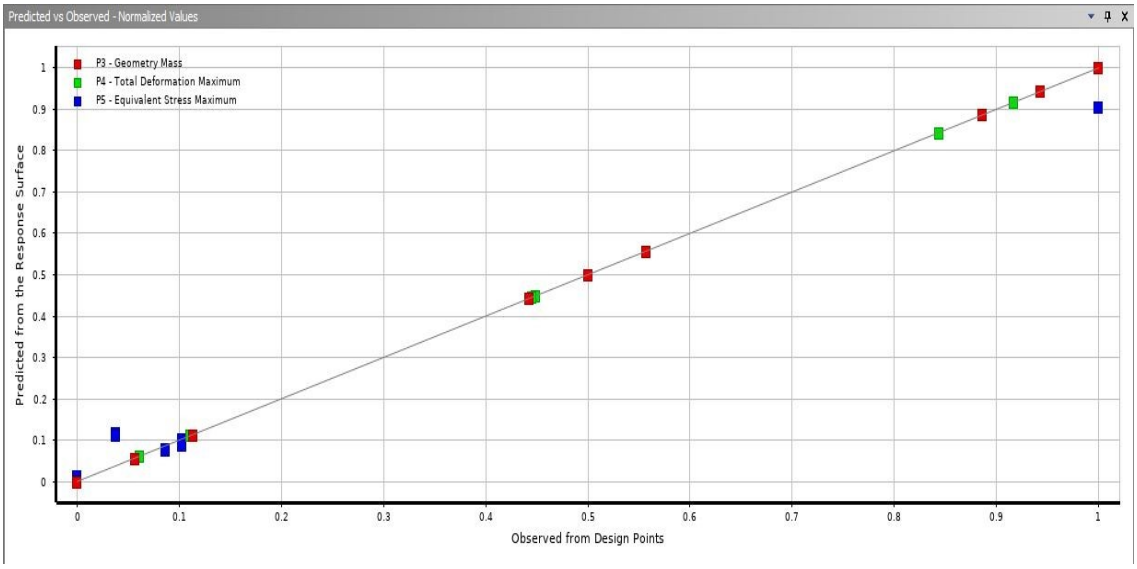

Figure 59. 'Goodness of Fit' curve for sandwich-structured tapered beam

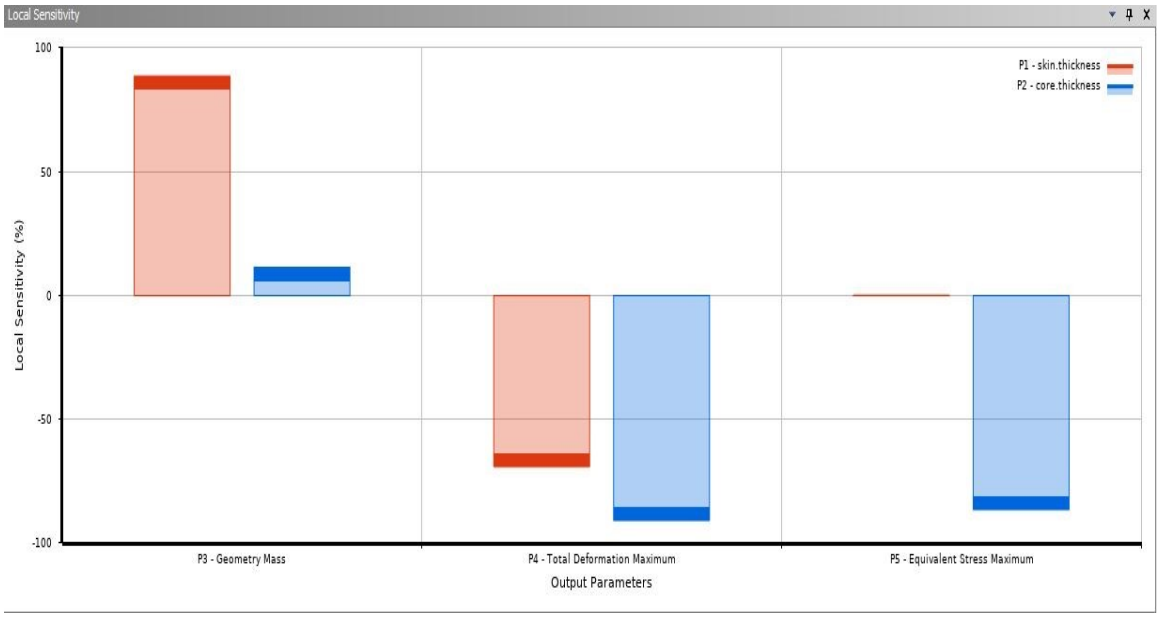

Figure 60. Local sensitivity for sandwich-structured tapered beam

Figures 61 (a) and 61 (b) depict the 3D models of the tapered sandwich beam before and after optimization, respectively.

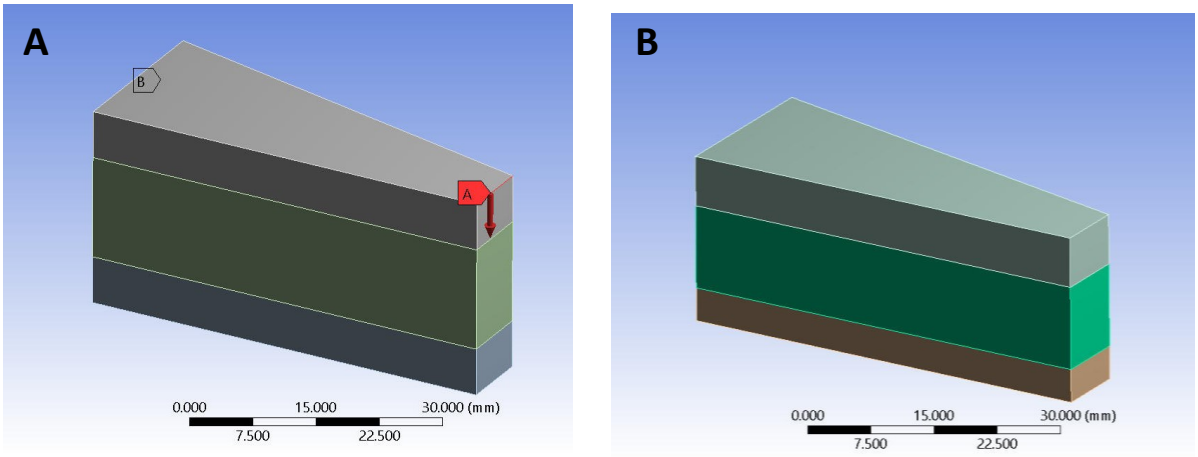

Figure 61. 3D model of the tapered sandwich beam a) before optimization b) after optimization

7.4.2. Pure Carbon Fiber-G/flex (CF-GF) Tapered Beam

Figures 62 (a) and (b) show the deformation and Von-misses stress distributions for a carbon fiber-G/flex matrix arrangement. The optimization results for this structure in Figures 63 (a) and (b) render a 36% minimization of mass (from 19.63 grams to 12.56 grams), offering tremendous potential for tapered-beam composite structures.

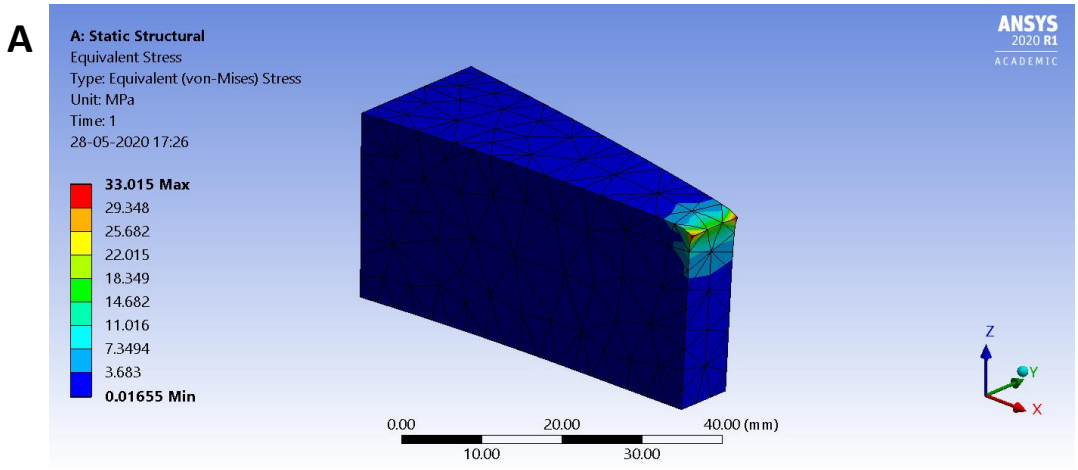

B

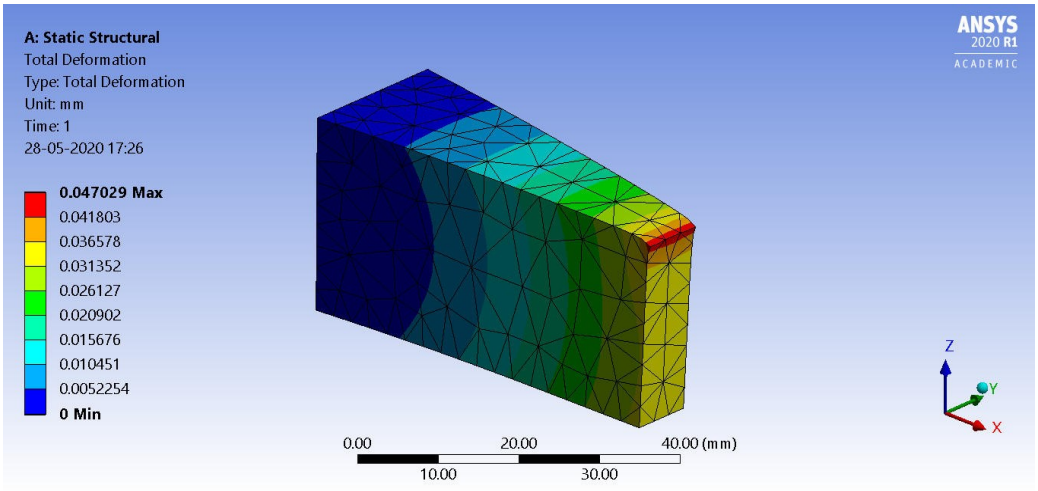

Figure 62. Tapered cantilever carbon fiber – G/Flex beam**:** Distribution of (a) maximum total deformation and (b) maximum equivalent (von-Mises) stress - constraints of optimization

A

Table of Schematic B2: Design of Experiments (Central Composite Design : Auto Defined)

	A	B	C	D	E
1	Name	P6 - beam.thickness (mm)	P3 - Geometry Mass (kg)	P4 - Total Deformation Maximum (mm)	P5 - Equivalent Stress Maximum (MPa)
2	1	24	0.018847	0.050362	33.159
3	2	16	0.012565	0.12377	33.308
4	3	32	0.02513	0.031673	30.991
5	4	20	0.015706	0.073207	32.622
6	5	28	0.021989	0.038731	31.482

B

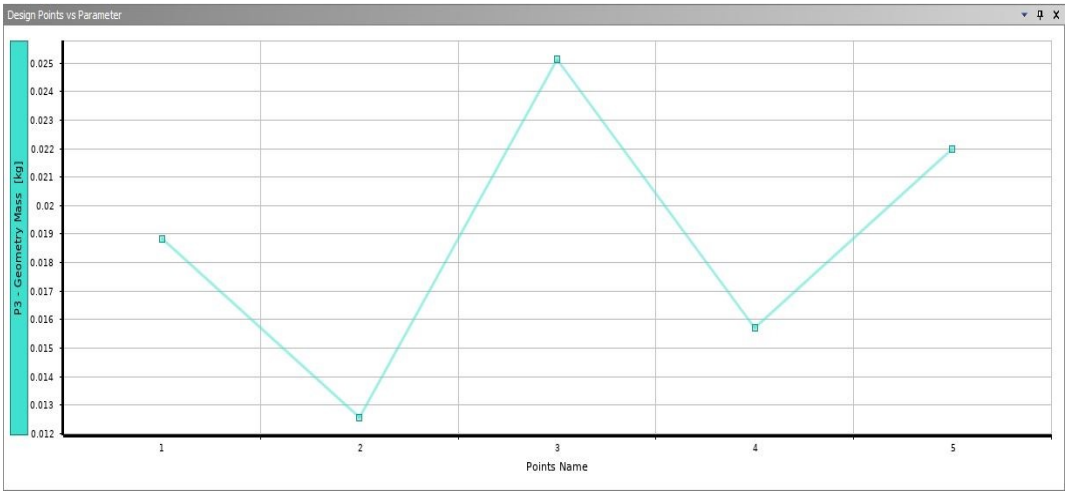

Figure 63. Optimization results for a carbon fiber – G/Flex tapered beam. (a) 'Design of Experiments' Tab with resulting output parameters for each design point and (b) Plot of design points vs geometric mass

Likewise, Figures 64 and 65 demonstrate the GOF curve and sensitivity plots for output parameters, respectively.

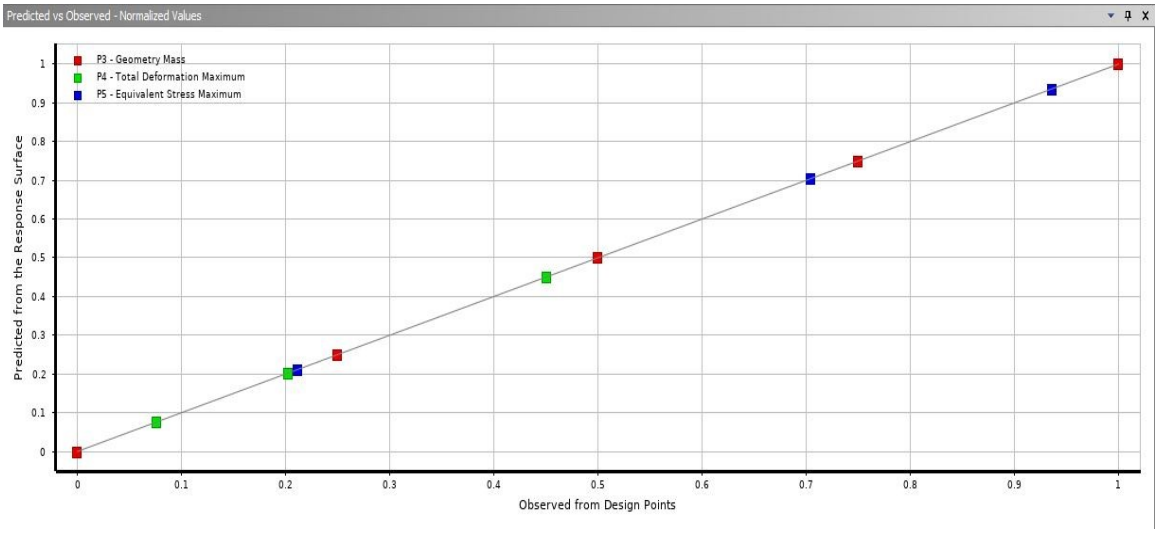

Figure 64. 'Goodness of Fit' curve for carbon fiber – G/Flex tapered beam

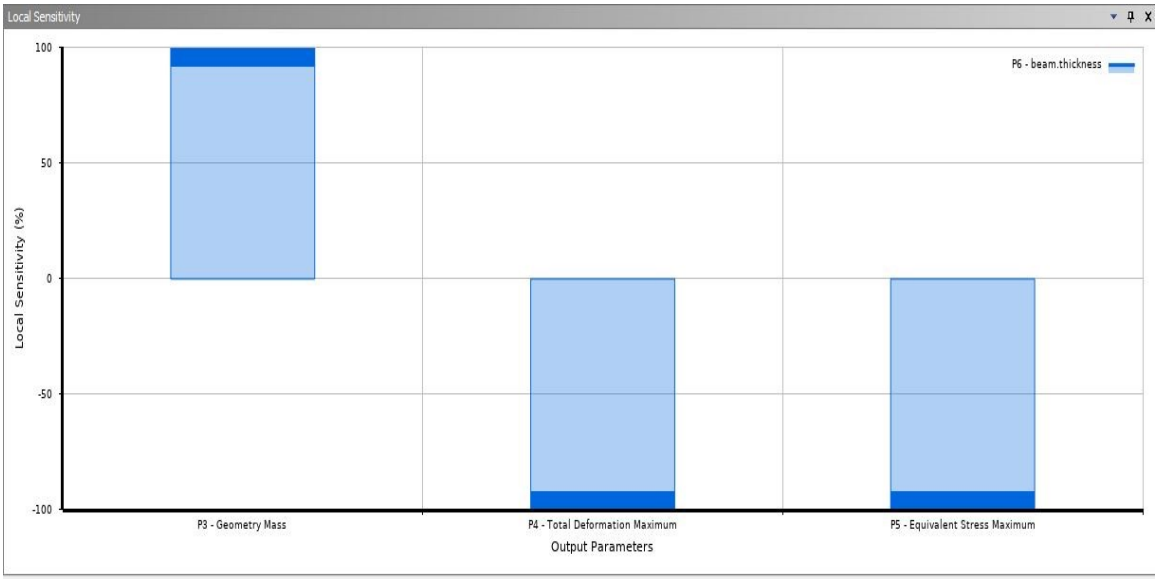

Figure 65. Local sensitivity for carbon fiber – G/Flex tapered beam

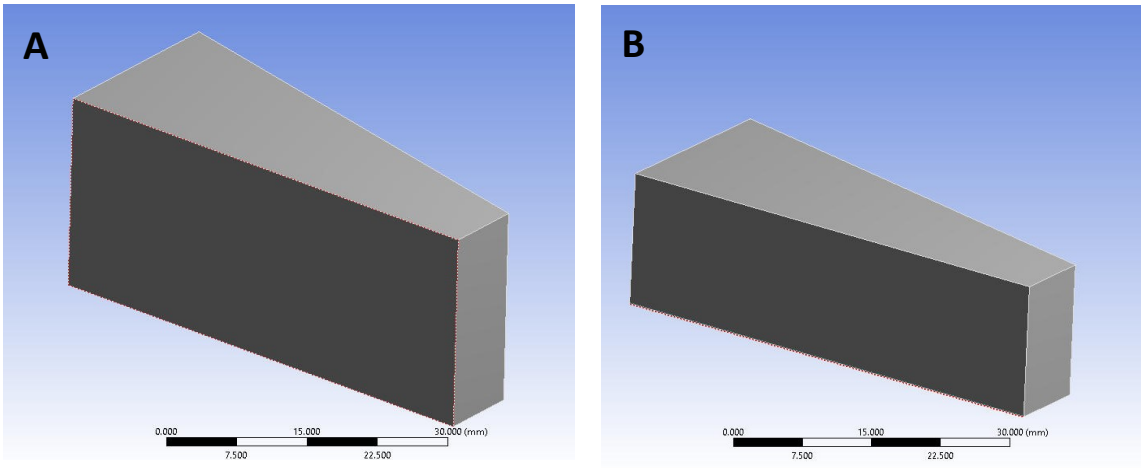

Figure 66. 3D model of the tapered CF-GF beam a) before optimization b) after optimization

Figures 66 (a) and 66 (b) depict the 3D models of the tapered carbon fiber-G/flex beam before and after optimization, respectively.

7.4.3. Discussion

Tapered beam designs offer tremendous potential to manufacture structural parts for high-stress applications where preservation of the mass is critical to reduce cost and maximize strength. Both the sandwich-structured beam and the simple CF-GF composite layout of the tapered geometry show promising results for optimization of mass while remaining within the constraints specified by the structural analysis. Table 15 (a) presents a comparative review between optimized mass values (ANSYS) and those attained by hand-calculations. Table 15 (b) depicts the summary of optimized mass values for the tapered cantilever beam for both material configurations.

Table 15 a. A comparative summary of original dimensions and mass of drone airframe with optimized dimensions and mass obtained from ANSYS and hand-calculations

Material	**Original dimensions**	**Original mass (g)**	**Optimized dimensions**	**Optimized mass by ANSYS (g)**	**Optimized mass (analytical) (g)**
Sandwich structure	t = 6 mm c = 13 mm	10.29	t = 4 mm c = 10 mm	8.52	8.52
Carbon fiber-G/flex	t = 25 mm	19.63	t = 16 mm	12.56	12.56

Table 15 b. Summary of optimized mass values (sandwich and carbon fiber composite tapered beam)

Material Configuration	**Original mass (grams)**	**Optimized mass (grams)**	**Mass saving (%)**
Sandwich Structure	10.29	8.52	17.2 %
Carbon Fiber – G/flex composite	19.63	12.56	36.00 %

7.5. Single-Objective Cost Optimization of Composite Flexural Beam

7.5.1. Sandwich Material Beam (Carbon Fiber-G/flex and Polyurethane Foam)

As Chapter 6 describes the detailed procedure of the optimization setup and the formulation of objective functions, this section presents the single-objective optimization

results. Figure 67 shows the minimum cost of the sandwich material structure for a set of iterations.

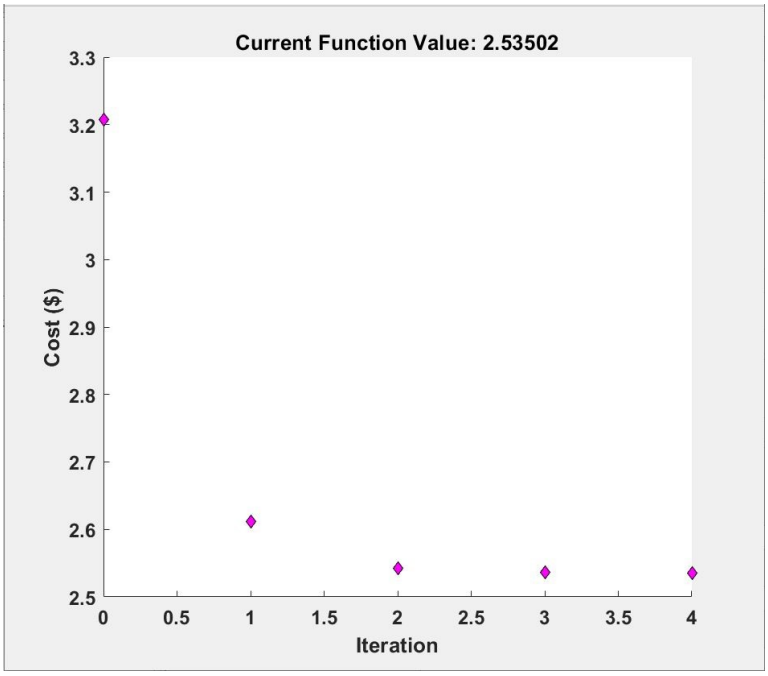

Figure 67. Plot displaying minimum cost function of a sandwich beam for a set of iterations

As seen in the figure, we attained an optimized cost of 2.53 $ for the sandwich beam. The solver terminates after a set of iterations based on if the minimum value is achieved. As depicted in the plot, this result is demonstrated in the 4^{th} iteration. Additionally, we obtained this cost function value for a core thickness (c) of 10 mm and skin thickness (t) of 2 mm.

These results provide an apt framework to devise a numerical approach for obtaining the most efficient design of a structure based on the materials employed and the constraints of bending stiffness applied. The cost-optimization results provide us the future

scope to perform a more robust analysis introducing additional constraints and incorporating complex geometries with a different objective function.

7.5.2. Pure Carbon Fiber-G/flex (CF-GF) Solid Beam

In an identical investigation as the sandwich structure, we conducted an optimization study for a solid carbon fiber and G/flex beam without incorporating polyurethane foam as the core. The CF-GF beam has two circular openings, as described earlier. Figure 68 shows the optimized cost (13.93 $) for the composite CF-GF beam configuration. We achieved this value for a 15 mm thick beam incorporating two holes of 5 mm radius.

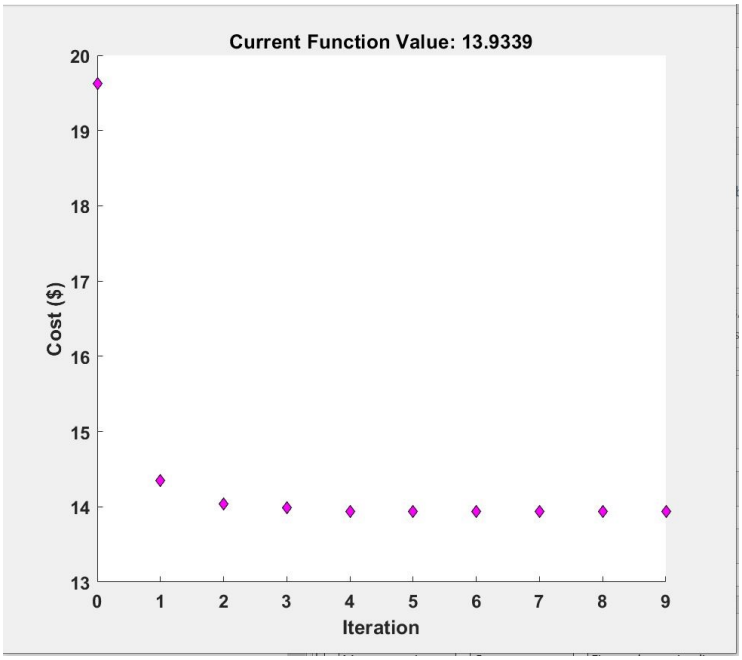

Figure 68. Plot displaying minimum cost function of a carbon fiber-G/Flex solid beam for a set of iterations

7.5.3. Aluminum alloy Solid Beam

To demonstrate aluminum alloys' application, particularly in space applications, we executed a minimum cost-objective analysis of a flexural beam with aluminum alloy as the material of construction.

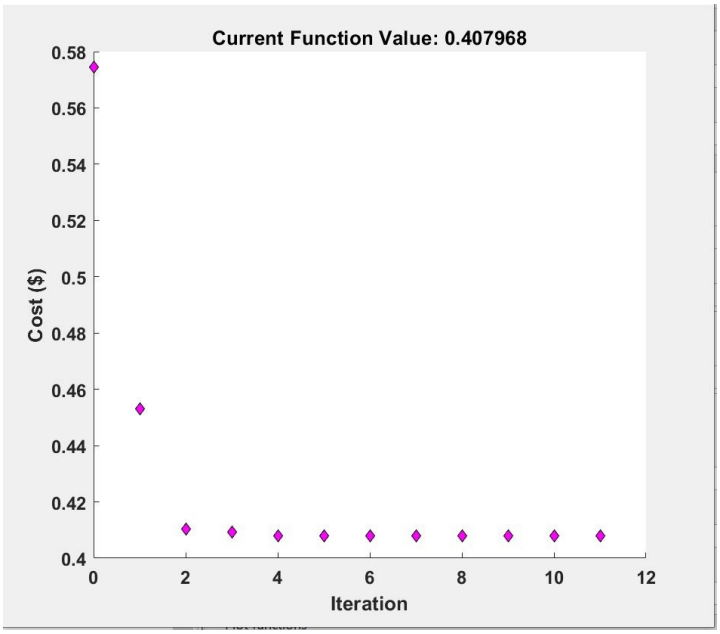

Figure 69. Plot displaying minimum cost function of an Aluminum alloy solid beam for a set of iterations

Figure 69 exhibits the low-cost value attained for this beam (0.407 $) for a 15 mm thick beam with a 5 mm radius of the openings.

7.5.4. Discussion

A general inference that can be made by analyzing these plots is that all three configurations provide an efficient estimate of production cost based on design complexities. Notably, due to their superior density and individual costs, pure carbon fiber-

filled matrix (CF-GF) compositions generate elevated manufacturing costs. The results of the cost-objective optimization is summarized below in Table 16

Table 16. Summary of cost function values and beam dimensions obtained after executing the optimization

Beam Configuration	Cost Function Value ($)	Design variables final value (mm)
Sandwich Structure	2.535	t = 2 mm ; c = 10 mm
Carbon Fiber – G/flex beam	13.933	t = 15 mm ; r = 5mm
Aluminum alloy beam	0.407	t = 15 mm ; r = 5mm

7.6. Single-Objective Weight Optimization of Composite Flexural Beam

7.6.1. Sandwich Beam (Carbon Fiber-G/flex and Polyurethane Foam)

Weight and cost are the two most critical modeling parameters when fabricating structural parameters for essential applications of stress such as the aerospace and marine industry. With an initial estimate of the optimization study for structural cost, we carried out an individual optimization analysis by replacing the cost objective function with a weight objective function. Section 6.5 described the formulation of this function and we present results of the sandwich structure configuration below.

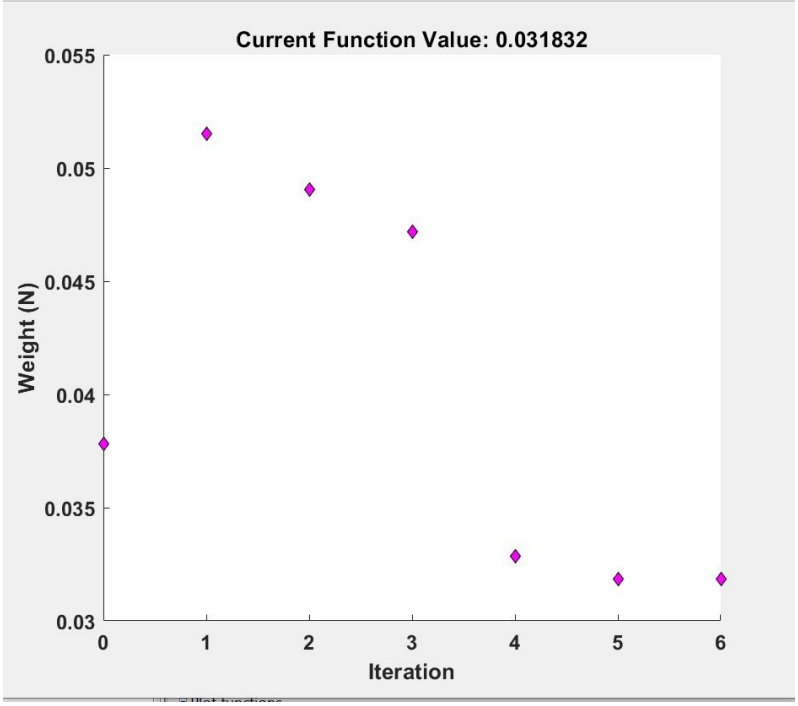

Figure 70. Plot displaying minimum weight function of a sandwich beam for a set of iterations

Figure 70 describes the minimum weight achieved for a sandwich material beam. By concurrent observation with the objective function, we can see that the algorithm generates an optimized weight value of 0.031 N in MATLAB. Like the cost estimate, we achieved this function value for the optimal core and skin thicknesses of 2 mm and 10 mm, respectively. From the plot, we can observe that the optimization solver starts with a much higher weight and works iteratively to deduce diminished value that satisfies the bending stiffness constraint successfully.

7.6.2. Pure Carbon Fiber-G/flex (CF-GF) Solid Beam

We executed the minimum weight design optimization experiment for the pure carbon Fiber-G/flex flexural beam similarly to the cost-objective method. Figure 71 depicts the distribution of the weight for each iteration. We obtained a numerical weight entity of

0.172 N for the CF-GF beam, which must ideally be 15 mm thick and employ a hollow opening of a 5 mm radius.

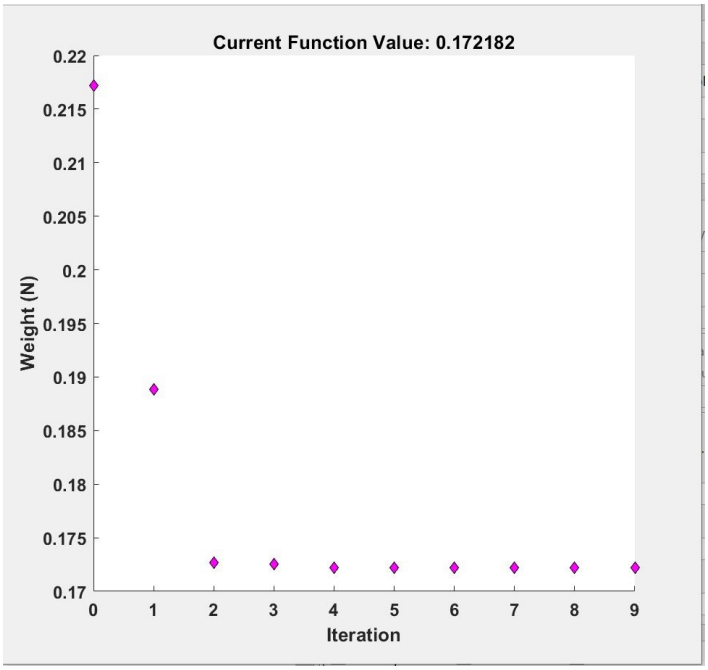

Figure 71. Plot displaying minimum weight function of a carbon fiber – G/Flex solid beam for a set of iterations

7.6.3. Aluminum Alloy Solid Beam

The evaluation for a solid aluminum alloy beam yields a minimum weight of 0.425 N for identical beam geometry (shown in Figure 72) as the carbon fiber-G/flex material structure (15 mm thick with 5 mm radius holes).

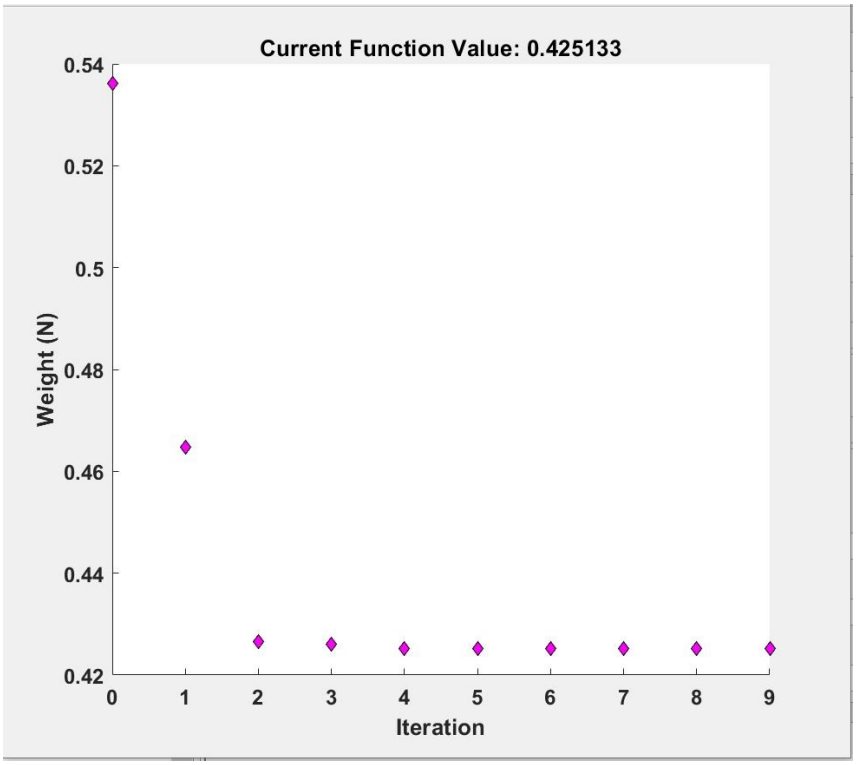

Figure 72. Plot displaying minimum weight function of an Aluminum alloy solid beam for a set of iterations

7.6.4. Discussion

Table 17 summarizes the weight-optimization analysis performed using the interior-point algorithm. By observing the minimum weight distribution for each of three material configurations, we can infer that aluminum alloy materials have augmented weight for a specified bending stiffness imposition. Future work in this study entails the exploration of additional constraints and design variables to achieve the desired objective function, commonly referred to as the design goal.

Table 17. Summary of weight function values and beam dimensions obtained after executing the optimization

Beam Configuration	**Weight Function Value (N)**	**Design variables final value (mm)**
Sandwich Structure	0.031	t = 2 mm ; c = 10 mm
Carbon Fiber – G/flex beam	0.172	t = 15 mm ; r = 5mm
Aluminum alloy beam	0.425	t = 15 mm ; r = 5mm

CHAPTER 8 – CONCLUSIONS

In this work, we demonstrated an unconventional nozzle-based additive manufacturing technique to perform 3D printing (potting) of composite sandwich specimens. We adopted milled carbon fibers, thermoset epoxy (G/flex), and polyurethane foam systems to produce sandwich composite specimens. First, we performed extensive iterative tests for AM of dog-bone geometries, intending to deduce the optimal processing conditions for nozzle-based AM. Next, we developed 3D models of two enclosures for potting dog-bone and rectangular-shaped specimens. We obtained the structure by utilizing a commercial 3D printer. Next, we poured Ecoflex 00-50 into this enclosure to acquire the mold for extruding the sandwich materials. With the final mold obtained, we devised a G-code program and subsequent stream commands with manual modifications. This program generated the toolpath for potting (extruding) the blend of carbon fiber and G/flex mixture and bonding it with foam material.

Due to the circumstances surrounding the pandemic (COVID-19), we could not implement the actual potting process. Thus, we presented a comprehensive proposition of the additive manufacturing process in this thesis. Furthermore, we described the proposed plan of the scheme for conducting 3-point bending and tensile tests over the fabricated sandwich specimens.

To methodically transition the thesis activities from manufacturing experiments to computational work, the next part of the thesis focused on numerical simulation, Finite Element Analysis, and objective-oriented optimization studies. These activities aimed to characterize the performance of 3D-printed structural components. First, we performed a

3-point bending simulation over a rectangular sandwich beam, intending to replicate the loading and support conditions specified in the ASTM C393 standard. We obtained the load-deflection data of the sandwich structures and established a preliminary framework for numerical simulation.

Next, we utilized the commercial FEA package in ANSYS (Student) to perform structural (mass) optimization of three different parts used predominantly in the aerospace industry. By adopting the built-in 'Response Surface Optimization' module in ANSYS, we conducted the design optimization of an aircraft wing bracket, an FPV drone airframe, and a tapered cantilever beam. The objective was to model these functional components and deduce the minimum geometric mass of each part that satisfies the appropriate bounds of part thickness, total deformation, maximum equivalent stresses, and cut-outs in geometries. Initially, we obtained imprecise results for a few iterations in the optimization involving mass calculations. However, after properly assigning design variables, we successfully obtained significant mass savings by running the optimization study for sandwich materials and carbon-fiber thermoset epoxy configurations.

Finally, we proposed a numerical approach to execute single-objective optimization of composite beams in MATLAB. Specifically, we carried optimization analysis to find out the minimum cost and weight of rectangular beams for three different material configurations. These arrangements were namely, carbon fiber-epoxy and foam-filled sandwich structures, carbon fiber-epoxy solid, and aluminum alloy solid materials. The weight of the beam and fabrication cost were the two essential design goals (objective functions) and we optimized these goals separately, constituting the single-objective study. We meticulously modeled mathematical equations representing non-linear constraints,

weight, and cost of the structure and relevant input parameters about beam geometry. Using the interior-point algorithm under ‘fmincon’ solver in MATLAB, we systematically implemented the optimization experiment. We achieved optimum values of weight and cost of fabrication. We specified the constraints of bending stiffness for materials following model values that are potentially used in the aerospace industry. This allowed us to set a target goal based on the results of the optimization. Aluminum alloy yielded significant less construction cost, while the use of sandwich materials generated considerably truncated weight.

Overall, this work established a unique platform to adopt the formulated G-code program and toolpath to fabricate high-strength sandwich composite specimens. Future work also includes performing experimental characterization of these parts. The mechanical properties obtained would then be compared with thermoplastic and conventionally manufactured components for comparable performance. Moreover, this thesis provides scope to explore further numerical simulation tools to validate experimental results. This task involves the evaluation of additional parameters and comparability with conventional engineering materials.

Finally, the optimization analysis conducted for novel aerospace structures provides the potential to explore complex geometries. Future experiments could centralize incorporating additional design variables, non-linear constraints, and advanced materials. Further, it offers an opportunity to implement the optimization of multiple objective functions at once (known as multi-objective optimization) to evaluate the trade-off between intended design goals.

REFERENCES

1. Diab, "Basics of Sandwich Technology." [Online]. Available: http://www.diabgroup.com/en-GB/Knowledge/Sandwich-technology/Basics-of-sandwich-technology [Accessed: 06-March-2020]

2. V. Birman and G.A. Kardomateas, "Review of current trends in research and applications of sandwich structures," *Composites Part B: Engineering*, 2018. **142**: p. 221-240.

3. P. Sivák, I. Delyová, and P. Diabelková, "Analysis of Sandwich Structures by the FEM," *American Journal of Mechanical Engineering*, 2017. **5**(6): p. 243-246.

4. W.D. Callister and D.G. Rethwisch, *Materials science and engineering : an introduction*, Vol.9. New York: Wiley, 2018.

5. R. Rikards, "Analysis of Laminated Structures: Course of Lectures," *Riga Technical University,* 1991, https://wpweb-prod.rtu.lv/ims/wp-content/uploads/sites/86/2017/07/R61.pdf

6. Aerospace Engineering Blog, "Fancy a Sandwich?", 2013 [Online]. Available: https://aerospaceengineeringblog.com/sandwich-panel/ [Accessed: 13-March-2020]

7. K.F. Karlsson and B. TomasÅström, "Manufacturing and applications of structural sandwich components," *Composites Part A: Applied Science and Manufacturing*, 1997. **28**(2): p. 97-111.

8. I. Gibson, D. Rosen, and B. Stucker, *Additive Manufacturing Technologies: 3D Printing, Rapid Prototyping, and Direct Digital Manufacturing*. New York, NY: Springer New York, 2015

9. K. Sugiyama, R. Matsuzaki, M. Ueda, A. Todoroki, and Y. Hirano, "3D printing of composite sandwich structures using continuous carbon fiber and fiber tension," *Composites Part A: Applied Science and Manufacturing*, 2018. **113**: p. 114-121.

10. S. Brischetto, C.G. Ferro, R. Torre, and P. Maggiore, "3D FDM production and mechanical behavior of polymeric sandwich specimens embedding classical and honeycomb cores," *Curved and Layered Structures*, 2018. **5**(1): p. 80-94.

11. L. Azzouz, Y. Chen, M. Zarrelli, J.M. Pearce, L. Mitchell, G.Ren, and M. Grasso, "Mechanical properties of 3-D printed truss-like lattice biopolymer non-stochastic structures for sandwich panels with natural fibre composite skins," *Composite Structures*, 2019. **213**: p. 220-230.

12. T. Li and L. Wang, "Bending behavior of sandwich composite structures with tunable 3D-printed core materials," *Composite Structures*, 2017. **175**: p. 46-57.

13. Z. Hou, X. Tian, J. Zhang, and D. Li, "3D printed continuous fibre reinforced composite corrugated structure," *Composite Structures*, 2018. **184**: p. 1005-1010.

14. V. Dikshit, Y.L. Yap, G.D. Goh, H. Yang, J.C. Lim, X. Qi, W.Y. Yeong, and J. Wei, "Investigation of out of plane compressive strength of 3D printed sandwich composites," *IOP Conference Series: Materials Science and Engineering*, 2016. **139**: p. 012017.

15. A. Galatas, H. Hassanain, Y. Zweiri, and L. Seneviratne, "Additive Manufactured Sandwich Composite/ABS Parts for Unmanned Aerial Vehicle Applications," *Polymers*, 2018. **10**(11).

16. Modor Plastics, "Thermoset vs Thermoplastics", [Online]. Available: https://www.modorplastics.com/plastics-learning-center/thermoset-vs-thermoplastics/ [Accessed: 03-April-2020]

17. J. Xie, "Nozzle-based Additive Manufacturing of Fiber-filled Thermosets: A Case Study on Soft and Hard Materials", A. Mazzeo, Editor. 2018, *ProQuest Dissertations Publishing.*

18. J. Xie, R. Randolph, G. Simmons, M. Vinciguerra, S. Suri, N. Bonini, A. Root, P. V. Hull, and A.D. Mazzeo, "Spreading of fast-curing, thermosetting silicones," *Applied Physics Letters*, 2019. **115**(25): p. 253701.

19. ASTM D638-14, Standard Test Method for Tensile Properties of Plastics, ASTM International, West Conshohocken, PA, 2014, www.astm.org

20. ASTM C393 / C393M-20, Standard Test Method for Core Shear Properties of Sandwich Constructions by Beam Flexure, ASTM International, West Conshohocken, PA, 2020, www.astm.org

21. Smooth-On Inc., "Ecoflex™ Series Technical Bulletin", https://www.smooth-on.com/tb/files/ECOFLEX_SERIES_TB.pdf

22. T.C. Triantafillou and L.J. Gibson, "Failure mode maps for foam core sandwich beams," *Materials Science and Engineering*, 1987. **95**: p. 37-53.

23. J. Kim and S.R. Swanson, "Design of sandwich structures for concentrated loading," *Composite Structures*, 2001. **52**(3): p. 365-373.

24. Y.-J. You, J.J-H. Kim, K.-T. Park, D.-W. Seo, and T.-H. Lee, "Modification of Rule of Mixtures for Tensile Strength Estimation of Circular GFRP Rebars," *Polymers*, 2017. **9**(12).

25. SGL Carbon, "SIGRAFIL ® milled carbon fibers Material Data," https://www.sglcarbon.com/en/markets-solutions/material/sigrafil-short-carbon-fibers/

26. West System ®, "G/flex® Epoxies Technical Data Sheet," October 2014, https://www.westsystem.com/wp-content/uploads/G-flex-tds.pdf

27. General Plastics Manufacturing Company, "Dielectric Foam Material," https://www.generalplastics.com/products/rf-2200

28. Slic3r - Open source 3D printing toolbox, "About Slic3r," https://slic3r.org/about/

29. D. Chakravorty, "3D Printer G-code Commands List & Tutorial," *All3DP*, January 22, 2020 [Online]. Available: https://all3dp.com/g-code-tutorial-3d-printer-gcode-commands/ [Accessed: 06-June-2020]

30. Zaber Console, "Manuals/ASCII Protcol Manual," https://www.zaber.com/wiki/Manuals/ASCII_Protocol_Manual#stream

31. E. Miller, "What is numerical simulation? And why should I care?" *Phoenix Business Journal*, April 19, 2016 [Online]. Available: https://www.bizjournals.com/phoenix/blog/techflash/2016/04/what-is-numerical-simulation-and-why-should-i.html [Accessed: 19-May-2020]

32. PRE Technologies, "Advantages of finite element analysis (FEA)," [Online]. Available: http://www.pretechnologies.com/services/finite-element-analysis/advantages [Accessed: 19-May-2020]

33. S. Anandan, G. Dhaliwal, S. Ganguly, and K. Chandrashekhara, "Investigation of sandwich composite failure under three-point bending: Simulation and experimental validation," *Journal of Sandwich Structures & Materials*, 2018: p. 1099636218791162.

34. M. Saras Chandra, M. Ramya, E. Suresh, and K. Padmanabhan, "Finite Element Analysis of Glass/Epoxy Skin and Rigid Foam Core Sandwich Composites – Simulation of Shear Modes and Flexural Modes of Failure," *Materials Today: Proceedings*, 2017. **4**(8): p. 8856-8865.

35. M. Hussain, R. Khan, and N. Abbas, "Experimental and computational studies on honeycomb sandwich structures under static and fatigue bending load," *Journal of King Saud University - Science*, 2019. **31**(2): p. 222-229.

36. V.N. Burlayenko and T. Sadowski, "Effective elastic properties of foam-filled honeycomb cores of sandwich panels," *Composite Structures*, 2010. **92**(12): p. 2890-2900.

37. L. Czechowski, J. Jankowski, and M. Kotełko, "Experimental and numerical three-point bending test for sandwich beams," *Journal of KONES*, 2017. **24**.

38. J. Arbaoui, Y. Schmitt, J.L. Pierrot, and F.-X. Royer, "NUMERICAL SIMULATION AND EXPERIMENTAL BENDING BEHAVIOUR OF MULTI-LAYER SANDWICH STRUCTURES," *Journal of Theoretical and Applied Mechanics*, 2014. **52**(2): p. 431-442.

39. L.J. Gibson and M.F. Ashby, *Cellular Solids: Structure and Properties*, Cambridge University Press, 1999.

40. L. Zhu, N. Li, and P.R.N. Childs, "Light-weighting in aerospace component and system design," *Propulsion and Power Research*, 2018. **7**.

41. D. Savic, "Single-objective vs. multiobjective optimization for integrated decision support," *Proceedings of the First Biennial Meeting of the International Environmental Modelling and Software Society*, 2002. **1**: p. 7-12.

42. M. Alteyeb and M. Jolgaf, "Optimization of Cantilever Beam for Minimum Weight Using Finite Element Analysis". 2017.

43. A. Nandi and H. Mishra, "Weight Optimization of Rectangular Core Sandwich Panel using ANSYS,″ *IOSR Journal of Mechanical and Civil Engineering*, 2017. **14**: p. 22-27.

44. A.I Salem, "Weight and cost multi-objective optimization of hybrid composite sandwich structures," 2016, *ProQuest Dissertations Publishing*.

45. F.S. Almeida and A.M. Awruch, "Design optimization of composite laminated structures using genetic algorithms and finite element analysis," *Composite Structures*, 2009. **88**(3): p. 443-454.

46. A. Khalkhali, S. Khakshournia, and N. Nariman-Zadeh, "A hybrid method of FEM, modified NSGAII and TOPSIS for structural optimization of sandwich panels with corrugated core," *Journal of Sandwich Structures & Materials*, 2014. **16**(4): p. 398-417.

47. T. Kellner, "3D-Printed 'Bionic' Parts Could Revolutionize Aerospace Design," *General Electric (GE)*, June 20, 2017 [Online]. Available: https://www.ge.com/news/reports/3d-printed-bionic-parts-revolutionize-aerospace-design [Accessed: 11-May-2020]

48. Everyone is Number One, "Meshing Methods (ANSYS Meshing)," https://deust.wordpress.com/2013/04/23/meshing-methods-ansys-meshing/

49. ANSYS Support, "Optimization in ANSYS Workbench," https://support.ansys.com/staticassets/ANSYS/Conference/Confidence/Houston/Downloads/optimization-in-ansys-workbench.pdf

50. OSprey, " FPV Frame Materials: Will Carbon Fibre Be Replaced?", *GetFPV Learn*, June 6, 2019 [Online]. Available: https://www.getfpv.com/learn/fpv-essentials/fpv-frame-materials/ [Accessed: 23-May-2020]

51. K. Hodicky, S. Hansen, T. Hulin, J.W. Schmidt, and H. Stang, "Cost optimization of load carrying thin-walled precast high performance concrete sandwich panels," *Structural and Multidisciplinary Optimization*, 2015. **52**(6): p. 1089-1106.

52. G. Rathnakar and H.K. Shivanand, "Experimental Evaluation of Strength and Stiffness of Fibre Reinforced Composites under Flexural loading," 2013.

53. C. Soares, V. Novais, P. Quagliatto, A. Bona, and L. Correr-Sobrinho, "Flexural modulus, flexural strength, and stiffness of fiber-reinforced posts," *Indian journal of dental research*, 2009. **20**(3): p. 277-281.

54. M.F. Ashby, *Materials selection in mechanical design*, Amsterdam: Butterworth-Heinemann, 2005

55. Mathworks, "fmincon", https://www.mathworks.com/help/optim/ug/fmincon.html

56. Mathworks, "Constrained Nonlinear Optimization Algorithms - fmincon Interior Point Algorithm", https://www.mathworks.com/help/optim/ug/constrained-nonlinear-optimization-algorithms.html#brnpd5f

57. J.S. Thompson, S. Walton, O. Hassan, S.A. Rolland, and J. Sienz, "The use of CFD and multi-objective optimization techniques to customise an industrial pre-mixer," *Structural and Multidisciplinary Optimization*, 2017. **55**(6): p. 2339-2351.